



UNIVERSIDAD NACIONAL AUTÓNOMA DE MÉXICO
POSGRADO EN CIENCIAS FÍSICAS

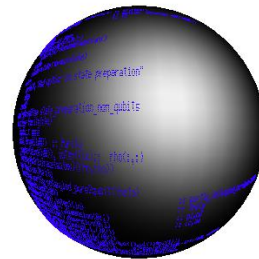
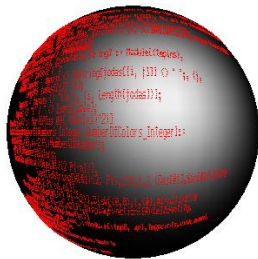
One, Two, and n Qubit Decoherence

TESIS

Que para obtener el grado de: Doctor en Ciencias (Física)
Presenta: Carlos Francisco Pineda Zorrilla
Directores de tesis: Dr. Tomaž Prosen
Dr. Thomas H. Seligman

Miembros del Comité Tutorial:

Dr. Jorge Flores, Dr. Tomaž Prosen, y Dr. Thomas H. Seligman



México D. F., 2007



posgrado en ciencias físicas
u n a m

UNIVERSIDAD NACIONAL AUTÓNOMA DE MÉXICO
POSGRADO EN CIENCIAS FÍSICAS

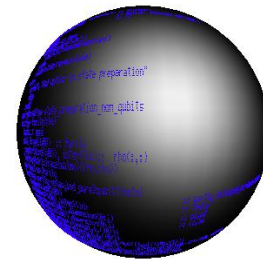
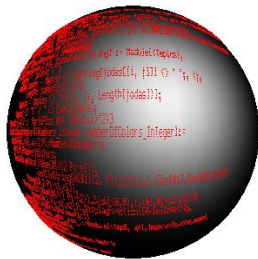
One, Two, and n Qubit Decoherence

THESIS

To obtain the degree: Doctor en Ciencias (Física)
Presents: Carlos Francisco Pineda Zorrilla
Directors: Dr. Tomaž Prosen
Dr. Thomas H. Seligman

Members of the Tutorial Committee:

Dr. Jorge Flores, Dr. Tomaž Prosen, and Dr. Thomas H. Seligman



México D. F., 2007

¡No contaban con mi astucia!
El Chapulín Colorado

Gracias

A Thomas por su paciencia. A Tomaž y François por su invaluable ayuda para crecer profesionalmente y también por brindarme su amistad. Carolina Spinel, Pier M., Thomas G., Chrisomalis, Rolando C., Carlos B., Rocío J., Ivette F. y Manuel T. influyeron (positivamente) en mi desarrollo profesional durante mi doctorado.

Desde un punto de vista personal debo agradecer a demasiadas personas. A mis padres, Thomas Seligman (de nuevo), Edna (por darme todo su amor), mis hermanas Maca y Nena, Emi y a toda la familia paterna y materna.

A los amigos atemporales: Alf, Jose, Betty, Camilo, Mi Perro, Ignacio F., Ceci L.M. y Sapoiguanacaimán (seguro alguien se me olvido acá).

En México agradezco a mis primeros amigos: Horacio, Eduardo, Félix, Fico, Emilio, Yanalté, Luz Alliete, Rebescua y Mírimix. A los compas del Gato Macho en especial a Giovanni, Holbert y John Jairo. A Jose Nicolás, MariaC, Yari (más Javo, Aleja, SICME y Julián) y rv_k292. A Elisa, Angie y Fabiola. A Angelina y Guillermina. A Caro Af., dagato, Evelin, Karen.

A varios amigos de la uni, en particular a Elías, Enrique, Belinka, Olivia U., gay_thama, Verónica, Reyes, Blas y Carlos Natorro. Al grupo de investigación: Luis, Mau, Rakel, David, Marc, Olivier, Sergey, Gursoy, Pablo, Choker, Rafael M., Claudia, Steffan, Luqi y Jorge Flores. A la gente de los eventos en Cuernavaca, DF, Dresden, París, Les Houches y Buzios. A los que me han brindado hospitalidad en Los Alamos, Ljubljana, Freiburg, Brecia, New York, Innsbruck y Bratislava.

A algunos amigos en Bogotá: Ana María, Vieja tal, Maryory, Cayita, Marta Gu, Katherine, Chocho, Maryory, Ernestina, Katherine, Carlos F. M., y Olga Lu. En París: Veronique, Luisa S., Caroline y Julian. En Taxco, Luisa F. En Melgar: Melguistas. En Ljubljana: Sneza, Amir, Osi, Marko (+ all the group) and Nade. En BsAs: Nacho, Ceci(s) y Angeles. En Montevideo: Turca y Capelanes. En otras partes: Rashnia, Rudi, Hartmut, Orus, Mario Z., V. Buzek, Sole (y Emi), Luca Bastardo, Juan Diego U. y Walter S.

A los amigos virtuales, como maracacol, juanita, lawawis, terepoeta, cecibl89, 987aw0s89duf, marcoandue, mzd_78, Audrey, terepoeta. A los nuevos amigos Camilo Cardona, Sonia, Aurora, Sayab, Tzolkin, Christian, Fernando y Yenni.

Finalmente, gracias a la música por acompañarme en momentos de alegría soledad, tristeza, rumba y trabajo.

SYNOPSIS

We study decoherence of one, two, and n non-interacting qubits. Decoherence, measured in terms of purity, is calculated in linear response approximation, making use of the spectator configuration. Monte Carlo simulations illustrate the validity of this approximation and of its extension by exponentiation. Initially, the environment and its interaction with the qubits are modelled by random matrices. Purity decay of entangled and product states are qualitatively similar though for the latter case it is slower.

For two qubits, numerical studies reveal a one to one correspondence between its decoherence and its internal entanglement decay. For strong and intermediate coupling to the environment this correspondence agrees with the one for Werner states, for initial Bell pairs. Using this relation we are able to give a formula for concurrence decay. In the limit of a large environment the evolution induces a unital channel in the two qubits, providing a partial explanation for the relation above.

Using a kicked Ising spin network, we study the exact evolution of two non-interacting qubits in the presence of a spin bath. Dynamics of this model range from integrable to chaotic and we can handle numerics for a large number of qubits. We find that the entanglement (as measured by concurrence) of the two qubits has a close relation to the purity of the pair, and closely follows an analytic relation derived for Werner states. As a collateral result we find that an integrable environment causes quadratic decay of concurrence as well as of purity, while a chaotic environment causes linear decay. Both quantities display recurrences in an integrable environment. Good agreement with the results found using random matrix theory is obtained.

Finally, we analyze decoherence of a quantum register in the absence of non-local operations *i.e.* n non-interacting qubits coupled to an environment. The problem is solved in terms of a sum rule which implies linear scaling in the number of qubits. Each term involves a single qubit and its entanglement with the remaining ones. Two conditions are essential: first decoherence must be small and second the coupling of different qubits must be uncorrelated in the interaction picture. We apply the result to the random matrix model, and illustrate its reach considering a GHZ state coupled to a spin bath.

PACS numbers: 03.65.Yz, 03.65.-w, 03.65.Ud, 05.40.-a

Keywords: entanglement, random matrix theory, purity, decoherence, concurrence, quantum memory, quantum register, GHZ.

RESUMEN

La decoherencia de 1, 2 y n qubits no interactuantes y posiblemente enlazados, medida en términos de la pureza, es calculada usando respuesta lineal y el concepto de configuración de espectador. A través de simulaciones de Monte Carlo exploramos la validez de la aproximación y su extensión mediante exponenciación. Inicialmente, modelamos la interacción y el medio ambiente con matrices aleatorias (MA).

Para 2 qubits, en el modelo MA, el enlazamiento interno y la decoherencia tienen una relación uno a uno. Esta relación, para acoplamientos moderados y fuertes, coincide con la relación correspondiente para estados de Werner, si la condición inicial es un par de Bell. Mediante ésta, obtenemos una fórmula explícita para el decaimiento del enlazamiento interno.

Introducimos un modelo de Ising pateado (MIP) para estudiar un grupo de espines, acoplado débilmente a un baño de espines. Este modelo presenta dinámicas integrable, mixta y caótica para diferentes parámetros. Observamos nuevamente la relación entre la decoherencia y el enlazamiento interno, obtenida con el modelo MA. Inicialmente, tanto el enlazamiento como la decoherencia decrecen cuadráticamente/linealmente para el caso integrable/caótico. En el caso integrable, si el acoplamiento es a un extremo de una cadena, ambas cantidades presentan comportamientos periódicos. Comparamos cuantitativamente el decaimiento de pureza en el modelo MA con nuestro sistema dinámico. Los resultados positivos demuestran la validez del modelo estocástico.

Finalmente, analizamos una memoria cuántica expuesta a decoherencia. Nuestro resultado, que asume altas purzas e independencia de los acoplamientos en la imagen de interacción, permite expresar la decoherencia como una suma de términos que involucran un solo qubit y su enlazamiento con el resto de la memoria. Aplicamos el resultado al modelo MA, generalizando nuestros hallazgos. En el MIP, observamos que incluso en situaciones integrables, los requerimientos se pueden cumplir.

Números PACS: 03.65.Yz, 03.65.-w, 03.65.Ud, 05.40.-a

Palabras clave: enlazamiento, enmarañamiento, RMT, pureza, decoherencia, concurrencia, memoria cuántica, GHZ, Bell.

Contents

1	Introduction and fundamental tools	1
1.1	Entanglement	5
1.2	The spectator configuration	10
1.3	Random matrix theory: a tool	12
2	One qubit decoherence	15
2.1	The model	16
2.2	Echo dynamics and linear response theory	17
2.3	The solution	18
2.4	The GUE case	19
2.5	The GOE case	23
3	Two qubit decoherence	27
3.1	The models	28
3.2	The spectator Hamiltonian	30
3.3	The separate environment Hamiltonian	37
3.4	The joint environment configuration	39
4	Entanglement decay	41
4.1	The CP plane	42
4.2	Entanglement decay	48
5	An example, the KI chain	53
5.1	Introduction	53
5.2	The kicked Ising spin chain	55
5.3	A generalized kicked Ising model	57
5.4	The evolution of concurrence and purity	60
5.5	A relation between concurrence and purity	63
5.6	Comparison with RMT predicted behavior	66

6	Quantum memories	71
6.1	The calculation	73
6.2	A RMT example	75
6.3	A dynamical model	75
7	Conclusions	81
Appendices		
A	One-qubit purity decay for pure and mixed states	85
A.1	General calculation	86
A.2	The GUE case	88
A.3	The GOE case	90
A.4	The general solution	92
A.5	Some particular correlation functions	92
B	Implementing the evolution of the KI models	97
C	The exponentiation	101
D	Entanglement	103
D.1	Quantifying two qubit entanglement	104
D.2	Some generalizations	105
E	RMT: various aspects	107
F	On the numerics of RMT and quantum information	113
F.1	Random matrices	113
F.2	Quantum information	115
G	Two minor technicalities	121
G.1	The Form Factor	121
G.2	A small proof of the Born expansion	122
	Bibliography	122

Chapter 1

Introduction and fundamental tools

Studying decoherence of one, two, and n qubits has a wide scope of applications due to the huge interest in implementing “quantum technology”. *The* limiting factor for building this technology is the sensitivity of quantum systems to undesired perturbations/coupling. Moreover, coupling to external degrees of freedom is *fundamentally* inevitable. Understanding its behavior is crucial to tame its effects.

Since a long time the coupling of quantum systems to external degrees of freedom has been studied (see e.g. [vN55, Eve57, Alb92, Alb93]). Philosophical aspects of quantum mechanics (the measurement process and the emergence of the classical world) are deeply connected with the problem. Some particular models designed for specific applications have been developed, but the favorite for general purposes (by far) is the Caldeira-Leggett model [CL83] in which the external degrees of freedom are modeled by a set of harmonic oscillators. Good agreement with the experiment has been observed, e.g. [KD98, WFL02, ZCP⁺07].

Regarding applications to quantum information some progress has been made. A big amount of literature exists and some aspects have been demonstrated experimentally. Most theoretical studies use Caldeira-Leggett like models; others explore the consequences of using/dropping the usual Markovian approximations. Some use very particular models either to obtain explicit analytical results or to study specific experimental situations. A more general picture is thus desirable to gain a deeper

understanding of the physics governing decoherence of quantum information systems. A few comments on some relevant papers on the field are useful to have an idea of the situation in the literature. This list of papers is not meant to be complete, it is just intended to give a brief overview of what people are currently working on, in relation to this topic.

- In a series of papers [YE02, YE03, YE04] Yu and Eberly explore how two qubits (in particular their entanglement properties) are affected by broadband bosonic reservoirs that induce vacuum noise, phase noise, etc. They find that entanglement after a finite time goes identically to zero.
- In [Bra06] a more complicated study is done using again a traditional harmonic oscillator bath. There, the off diagonal elements of the reduced density matrix (sometimes called “coherences”) are analyzed. Interestingly, the author discovers that decoherence is determined by a generalized Hamming distance. He introduces some primitive spectator (see sec. 3.1).
- In [Ged06] the author uses a spin bath as an environment. He studies concurrence of some Bell pairs. The results, though interesting, are quite model dependent. In [LDK⁺05] the relation between integrability and decoherence is studied for a spin bath environment, very much in the spirit of our results [PS06]. Studies of specific spin-bath environments, aiming to understand decoherence in experimental qubit realizations are [dSDS03b, dSDS03a] and [SLH⁺04].
- In another interesting article [GMCMB07], Garcia-Mata *et al.* use semi-classical considerations to study multi-particle qubit entanglement. They analyze how entanglement is affected both by the phase space structure and by the kind of noise applied.
- In [FFP04] the authors propose two measures for decoherence. These measures are additive, a property that is important to express the total decoherence in terms of the decoherence of each qubit.
- Some efforts to understand the implications of the Markovian approximation are made in [ALKH02, LKA⁺04], where it is shown that under certain circumstances that approximation leads to very inaccurate results.
- In [MCKB05] the authors use random Hamiltonians (though not with the minimum information properties of the classical ensembles [Bal68]) to study entanglement decay of n qubits. Using Markovian approxi-

mations, they arrive to time independent Lindblad equations. They obtain multi-exponential decay. They are able to analyze the differences between W and GHZ states.

- An isolated and possibly premature (due to the interests of the community) study is worth mentioning. In [MPK88] Mello *et al.* analyze the relaxation rates of a single $1/2$ spin particle using a random matrix model.

We are pioneering the use of Random Matrix Theory in the field of quantum information theory. Some previous work has influenced considerably our research namely [GPS04, GS03], where random matrices were used to analyze decoherence and fidelity in general quantum systems.

Joseph Emerson has developed methods to create random unitary operators (in the spirit of the CUE) using random gates (ironically a non-trivial task to implement efficiently) [EWS⁺03]. He has also explored the utilities of such random unitary operators in fidelity and local density of states estimation [ELPC04]. Other uses of randomization in quantum protocols, like diminishing the effects of static perturbations, have been introduced in [KAS05, PZ01] and further explored in [KA06]. Some people have also used random matrices to study fidelity decay [GPSŽ06, FFS04].

This thesis is based mainly on four publications [PS07, PGS07, PS06, GPS07]. We shall not follow the chronological order as the logical order will result in almost opposite. The reasons are clear. As you gain insight in the field, things become clearer, concepts become more elaborate and distilled and thus more suitable for understanding.

On the structure of the thesis –

In the remaining part of the introduction we explain some concepts and tools used along the thesis. Some material is not new, and is not appropriate for publication in a journal as it only contains a review of known things. However, for the reader a coherent presentation is always handy. A main concept used and studied during this thesis is entanglement. It is understood here both as a resource (to perform quantum information tasks) and as a cause of decoherence. We shall define it and discuss the two ways that we understand it. Next we explain the spectator configuration, which is an original tool exploited during most of this work. Finally we introduce Random Matrix Theory (RMT).

We next proceed to analyze decoherence of quantum systems. We first explore the single qubit case (sec. 2). The detailed mathematical derivation of the formulae used is given in appendix A. Both the time reversal invariant (TRI) case and the non-TRI case are analyzed in detail. We then consider the two qubit case (sec. 3). Different configurations corresponding to different physical situations are analyzed. Again TRI and non-TRI cases are also studied. The effect of internal entanglement proves important and provides interesting effects. In sec. 4 the relation between decoherence and entanglement is studied. Sections 2, 3, and 4 are based on [PGS07], though the basic idea was introduced in [PS07].

In sec. 5 we give an example of how some of the concepts can be applied to a simple model: the kicked Ising spin chain. Though this chapter is based on [PS06], major modifications have been introduced with the aim of getting closer to the RMT models.

Finally in sec. 6 we use some of the results obtained during the thesis to analyze decoherence of an n qubit register. We shall use both the RMT model and the KI spin chain to discover and understand the reach of the results. This chapter is based on [GPS07].

In appendix A we perform the main RMT calculation, for a single qubit in the spectator configuration. In appendix B we explain how to implement numerically the kicked Ising model in an efficient manner. The next appendix (C) explains a way of extending some analytical results via exponentiation. This heuristic result is tested throughout the thesis for most Monte Carlo simulations. We then discuss some technical aspects of both entanglement (appendix D) and random matrix theory (appendix E). Regarding entanglement, we discuss the definition of entanglement in more general systems than the ones discussed in this introduction, and the physical meaning of concurrence. For random matrix theory we mention the physical justification of the ensembles, relations among their matrix elements, and other formulae used during the thesis. In the last appendix we give the double integral of the form factor for a particular ensemble and a simple proof of the Born expansion for the echo operator.

I do hope you enjoy and have a nice time with this piece of work.

1.1 Entanglement

Though in mathematical terms entanglement is trivial to define (once the basic tools of quantum mechanics are introduced), its consequences challenge many deeply rooted (mis)conceptions about reality. Here we do not wish to discuss how the existence of entanglement affects our understanding of reality; this is a difficult topic outside the scope of this work, and even Einstein was puzzled by its consequences. We limit our selves to define and discuss briefly entanglement and how to quantify it.

A pure state of a quantum composite system is said to be entangled when it is not the “sum” of its parts (technically we mean tensor product). To be more precise, let our Hilbert space \mathcal{H} be composed of two parts: $\mathcal{H} = \mathcal{H}_A \otimes \mathcal{H}_B$. If, given a state $|\psi\rangle \in \mathcal{H}$, there exist $|\psi_A\rangle \in \mathcal{H}_A$ and $|\psi_B\rangle \in \mathcal{H}_B$ such that

$$|\psi\rangle = |\psi_A\rangle \otimes |\psi_B\rangle \quad (1.1)$$

it is said that $|\psi\rangle$ is separable or unentangled. Conversely, if

$$|\psi\rangle \neq |\psi_A\rangle \otimes |\psi_B\rangle, \forall (|\psi_A\rangle \in \mathcal{H}_A, |\psi_B\rangle \in \mathcal{H}_B) \quad (1.2)$$

it is said that $|\psi\rangle$ is entangled. In other words $|\psi\rangle$ is entangled if and only if

$$|\psi\rangle\langle\psi| \neq \text{tr}_A |\psi\rangle\langle\psi| \otimes \text{tr}_B |\psi\rangle\langle\psi|. \quad (1.3)$$

It is quite easy to show the existence of entangled states. The simplest case can be constructed when $\dim \mathcal{H}_A = \dim \mathcal{H}_B = 2$, *i.e.* when \mathcal{H}_A and \mathcal{H}_B represent qubits. Let $\{|0\rangle, |1\rangle\}$ be an orthonormal basis in each space. The Bell state

$$|\text{Bell}\rangle = \frac{|0\rangle \otimes |0\rangle + |1\rangle \otimes |1\rangle}{\sqrt{2}} \in \mathcal{H} \quad (1.4)$$

is entangled. Assuming the existence of $\alpha_A, \beta_A, \alpha_B, \beta_B \in \mathbb{C}$, such that $|\text{Bell}\rangle = (\alpha_A|0\rangle + \beta_A|1\rangle) \otimes (\alpha_B|0\rangle + \beta_B|1\rangle)$ results in a contradiction. For multipartite mixed systems a generalization of the definition of entanglement is straightforward. See appendix D for details.

In order to get deeper insight in the entanglement properties of pure bipartite states it is convenient to use the Schmidt decomposition [Sch07, NC00]. Given a state $|\psi\rangle$ in a bipartite space $\mathcal{H}_A \otimes \mathcal{H}_B$, there exist orthonormal states $\{|i_A\rangle\}$ in \mathcal{H}_A and $\{|i_B\rangle\}$ in \mathcal{H}_B such that

$$|\psi\rangle = \sum_{i=1}^{\min\{\dim \mathcal{H}_A, \dim \mathcal{H}_B\}} \lambda_i |i_A\rangle \otimes |i_B\rangle \quad (1.5)$$

and $0 \leq \lambda_i \leq 1$, with $\sum_i \lambda_i^2 = 1$. The numbers λ_i are called Schmidt coefficients and play an important role in entanglement theory. Consider an orthonormal (and complete) basis that diagonalizes $\rho_A = \text{tr}_B |\psi\rangle\langle\psi|$. We choose that basis to be $|i_A\rangle$; its existence is guaranteed by the spectral theorem. We can then write $|\psi\rangle = \sum_i |i_A\rangle \otimes |\tilde{i}_B\rangle$, but since $\rho_A = \sum_i |i_A\rangle\langle j_A| \langle \tilde{i}_B | \tilde{j}_B \rangle$ must be in fact diagonal, then $\langle \tilde{i}_B | \tilde{j}_B \rangle \propto \delta_{ij}$. Using some $|i_B\rangle \propto |\tilde{i}_B\rangle$ such that $\langle i_B | i_B \rangle = 1$ and suitably choosing its phases we can write eq. (1.5). The sharp reader will notice that the Schmidt coefficients are the square roots of the eigenvalues of the reduced density matrix of any of the two subsystems.

The Schmidt coefficients are unique for each pure state. From the argumentation we can see that ρ_A and ρ_B have the same eigenvalues (and with the same degeneracy) except for $|\dim \mathcal{H}_A - \dim \mathcal{H}_B|$ zeros. Determining whether a pure state is entangled or not is an easy task. From the previous paragraph one can see that a state is not entangled if and only if one of the Schmidt coefficients is one (implying that the others are zero).

1.1.1 Decoherence as entanglement

Decoherence can be seen as entanglement with the environment [Zur03, Zur91].

Quantum correlations [in our language, entanglement] can also disperse information throughout the degrees of freedom that are, in effect, inaccessible to the observer [Zur91].

Though a big debate has been issued since the formulation of that paradigm, it is now generally accepted.

We now discuss an example to explain the previous statement. To present the key idea it is enough to consider a central system, composed of a single qubit, and an environment alone; in the original formulation a measurement apparatus was also involved to allow the analysis of the “collapse” of the wave function after a measurement process. In this example the environment has three characteristics: large dimension, uncontrollable dynamics, and no possibility of being observed. We assume some interaction between the central system and the environment. Consider an initial state which is (i) separable with respect to the environment and (ii)

a superposition in the central system. *I.e.*

$$|\psi(t=0)\rangle = (\alpha|0\rangle + \beta|1\rangle) \otimes |\phi\rangle \quad (1.6)$$

where $|0\rangle$ and $|1\rangle$ form an orthonormal basis for the qubit, α and β are complex numbers, and $|\phi\rangle$ is the initial state of the environment. Assume that the interaction depends on the state of the qubit, e. g. a controlled- U . After some time, due to the interaction, the state will be

$$|\psi(\text{big } t)\rangle = \alpha|0\rangle|\phi_0\rangle + \beta|1\rangle|\phi_1\rangle. \quad (1.7)$$

As the dimension of the environment is big, the states of the environment, after some time scale, will be approximately orthogonal: $\langle\phi_i|\phi_j\rangle \approx \delta_{ij}$. Of course this last statement is not fulfilled for an arbitrary interaction, but precisely the basis (regarding the qubit) in which this condition is fulfilled will determine the preferred basis which determines the pointer states.

To quantify the degree of entanglement of a bipartite system, in a pure state, we make use of the Schmidt coefficients. Adding any convex function of these coefficients is enough. We use the sum of their squares, as it induces a very simple formula (other common choice, instead of x^2 , is $x \log x$ which induces the von Neumann entropy). This measure we call *purity*. Thus, for a given density matrix ρ , its purity is defined by

$$P(\rho) = \text{tr} \rho^2. \quad (1.8)$$

This quantity is 1 for pure states ($\rho = |\psi\rangle\langle\psi|$), less than one for mixed states, and reaches a minimum of $1/N$ (where N is the dimension of ρ) for the completely mixed state $\mathbf{1}/N$. If the partial trace with respect to an environment is represented by tr_e , a measure of decoherence is then $P(\rho = \text{tr}_e |\psi\rangle\langle\psi|)$. An important practical advantage of this measure is that one does not need to evaluate the Schmidt coefficients of the density matrix ρ .

Other views of decoherence are common in the literature. Consider a qubit in an initial state $|\psi\rangle = (|0\rangle + |1\rangle)/\sqrt{2}$. Its corresponding density matrix is

$$\rho = \frac{1}{2} \begin{pmatrix} 1 & 1 \\ 1 & 1 \end{pmatrix} \quad (1.9)$$

Assume we have pure dephasing (no amplitude damping). Typically, what will happen is that the off diagonal elements will decay exponentially. That is, its time evolution will be

$$\rho(t) = \frac{1}{2} \begin{pmatrix} 1 & e^{-\gamma t} \\ e^{-\gamma t} & 1 \end{pmatrix}. \quad (1.10)$$

Inspired in this behavior one can relate decoherence to the norm of the off diagonal term. We define

$$D(\rho) = 4 |\rho_{1,2}|^2. \quad (1.11)$$

For states of the form eq. (1.10) we obtain the formula $D(\rho) = P(\rho)$. However, in the general case, information about one only gives partial information about the other; for an arbitrary one qubit density matrix, $0 \leq D(\rho) \leq P(\rho)$, and thus one can have a completely pure state with $D = 0$. This quantity is used frequently as is easy to calculate and is related to the interference fringes shown in the very popular cat states in phase space, see e.g. [Zur03] page 742. A big disadvantage of using D is that it is a basis dependent quantity. Internal dynamics may produce a decay of the off diagonal elements of ρ and thus of D . Moreover, if one studies an ($n > 2$)-level system the situation becomes more complicated. Purity on the other hand works for a much wider class of systems.

1.1.2 Entanglement as a resource

It is not difficult to understand that entanglement is a (quantum) resource, since already classical correlations are an important (classical) resource used extensively in classical cryptography. Entanglement, as the quantum correlation, brings up richer possibilities. In general, controlled entanglement can be used for the following:

- Teleportation: It is the most celebrated application, due to its spectacularity and simplicity [BBC⁺93]. The transfer of an unknown quantum state can be achieved using an entangled state, local operations, and classical communication.
- Quantum computation: It is a controversial subject whether entanglement is *essential* for quantum computation, but so far it has been demonstrated that for an exponential speedup in pure state schemes, entanglement is necessary (see [JL03]).
- Communication: Both quantum and classical communication can benefit from entanglement. In particular, quantum key distribution extensively uses this resource [NC00].
- Quantum-Enhanced Metrology: It is shown that the signal/noise ratio can be increased qualitatively [GLM06, GLM04] if one uses

entangled states. Thus the use of highly entangled states shall be mandatory for precise measurements. Generalizations of the ideas developed in this area can be used to build quantum positioning systems (in analogy to GPS), enhanced radars, and for clock synchronization.

Still the field is quite young and ideas for exploiting entanglement are emerging at this point. New technology is arising: some quantum random number generators are already available as USB gadgets. In the near future many expected, and unexpected, technologies are going to be proposed and, no doubt, realized. Thus it is a major concern to be able to understand, quantify, and control internal entanglement.

One of the first tasks of quantum information theory was to quantify the degree of entanglement. It was soon realized that, in general, this was a complex task. We now know, for example, that for general systems, entanglement induces only a partial ordering.

We now focus on the simplest possible scenario that allows entanglement, a two qubit system. Four conditions must be fulfilled by an entanglement measure: (i) It must have a value between zero and one. It is zero for separable states and one for Bell states. (ii) Any local unitary operation leaves entanglement unchanged. This condition can be seen as an invariance of the measure under a *local* change of basis. (iii) Local operations plus classical communication cannot increase entanglement. *I.e.* to create entanglement we need genuine non-local quantum operations (say interaction, skew measurements, etc). (iv) The entanglement measure must be a convex function. This condition says that entanglement will not increase when mixing ensembles. These four conditions can be generalized to more complex systems (multipartite or higher dimensional systems).

Several measures of two qubit entanglement fulfill these conditions, however these measures do not provide exactly the same ordering of states [VADM01]. In this work we shall use the concurrence. The first reason being that it is straightforward to compute. Some measures of 2 qubit mixed state entanglement require explicit maximization over high dimensional continuous sets. Though in the definition of concurrence (via the entanglement of formation) a maximization is required, the problem is solved in a general fashion, and a closed formula is given. See appendix D for details. The second reason being that it is used widely in the community of quantum information, both by theoreticians and experimentalists.

Concurrence C of a two qubit density matrix ρ is

$$C(\rho) = \max\{0, \Lambda_1 - \Lambda_2 - \Lambda_3 - \Lambda_4\} \quad (1.12)$$

where Λ_i are the eigenvalues of the matrix $\sqrt{\rho(\sigma_y \otimes \sigma_y)\rho^*(\sigma_y \otimes \sigma_y)}$ in non-increasing order. The superscript $*$ denotes complex conjugation in the computational basis and σ_y is a Pauli matrix. Furthermore, concurrence fulfills all conditions of a legitimate entanglement measure discussed at the beginning of this section.

1.2 The spectator configuration

One of the important contributions of this work is the concept of spectator configuration. During the development of the thesis the concept was discovered, and its potential is exploited here. On one hand, it allows to enclose all the calculations in a single one, thus simplifying greatly the technical details. On the other, it enables to extend easily our results from one and two qubits to n qubits. Its full potential has not yet been exploited, but we hope that the community will take advantage of this concept.

The concept involves the following Hilbert spaces:

- The spectator space \mathcal{H}_s . The spectator is not coupled to the other spaces. However, it can be correlated initially via entanglement with the interacting space.
- The interacting space \mathcal{H}_i . This subspace is dynamically coupled to the environment and is initially entangled with the spectator subspace.
- The environment space \mathcal{H}_e . This space typically has a large dimension (though this is not essential at this point). It is initially decoupled (in the sense of entanglement) to the rest of the system.
- The central system \mathcal{H}_c . It is the tensor product of the spectator and the interacting space: $\mathcal{H}_c = \mathcal{H}_s \otimes \mathcal{H}_i$.

The whole Hilbert space \mathcal{H} is the tensor product of all spaces, namely

$$\mathcal{H} = \mathcal{H}_e \otimes \mathcal{H}_c = \mathcal{H}_e \otimes \mathcal{H}_s \otimes \mathcal{H}_i. \quad (1.13)$$

Additional to the Hilbert space structure, the spectator configuration, as explained above, has a characteristic Hamiltonian:

$$\begin{aligned} H &= H_e \otimes \mathbb{1}_{i,s} + H_s \otimes \mathbb{1}_{e,i} + H_i \otimes \mathbb{1}_{s,e} + \mathbb{1}_s \otimes W_{e,i} \\ &= H_e + H_s + H_i + W_{e,i}. \end{aligned} \quad (1.14)$$

The indices indicate the spaces in which the operators act. Where there is no danger of confusion, the identities are dropped as in the last equality of eq. (1.14). The first three terms represent local Hamiltonians in each proper subspace, and the last term is an interaction between the interacting subspace and the environment. The different parts of the Hamiltonian need not to be time independent; in this work the parts devoted to random matrix theory deal with time independent Hamiltonians. The parts studying the kicked Ising model and the n -qubit chapter use a time dependent Hamiltonian example of (1.14).

The initial condition is always separable with respect to the environment:

$$|\psi(t=0)\rangle = |\psi_e\rangle \otimes |\psi_c\rangle, \quad |\psi_e\rangle \in \mathcal{H}_e, \quad |\psi_c\rangle \in \mathcal{H}_c, \quad (1.15)$$

but not necessarily with respect to the spectator space. If there is separability between the interacting and the spectator spaces, the problem trivially separates and we can consider then 2 completely decoupled problems, one in \mathcal{H}_s and another in $\mathcal{H}_e \otimes \mathcal{H}_i$. The condition of the environment being pure in eq. (1.15) is technical. Some calculations have been done with mixed states in the environment(s) yielding similar results. At this point we could formulate, with no problem whatsoever, the model with a mixed environment, but since for further considerations it is convenient to have a pure state we keep it that way.

The Hamiltonians that are going to be analyzed during the thesis are not always of the form eq. (1.14), but do have a particular structure due to the structure of the underlying Hilbert space. This structure is of the form given in eq. (1.13), but with the interacting space being composed of different independent non-interacting groups. For this configuration, the environment will be coupled to all groups independently. Under some general conditions we shall be able to decouple this complicated problem into many spectator problems.

Two explicit examples of a simplification of the problem using the spectator configuration are given when we have 2 qubits as the central system in the context of random matrix theory (sec. 3.3 and sec. 3.4). Section 6

separates the decoherence problem in spectator configurations in a general fashion, and exemplifies the results with both random matrix theory and the kicked Ising spin chain. As the reader can notice, we shall follow a line of argumentation that will build step by step the general case. During the thesis we shall first study the simplest case (one qubit), then the next in complexity (two qubits) and finally explain a possible way to use the tools developed in a more general way.

1.3 Random matrix theory: a tool

All I know is I know nothing.
Socrates

Some people in the field consider the start of Random Matrix Theory as being the paper by John Wishart [Wis28] (who, incidentally, died in Acapulco). There he introduces random matrices with invariant measure under basis transformation. His objective was to analyze multivariate data. Others say that the landmark was placed by Élie Cartan in an old (and often forgotten) paper [Car35]. He introduces explicitly the circular ensembles, with invariance properties with respect to (usually) group operations, to generalize the integral theorem of Cauchy. Mehta [Meh91] was the first to calculate many of the mathematical properties of the classical ensembles [Car35].

There was not much development of RMT outside mathematics, until Wigner published his famous papers [Wig51, Wig55] pioneering its use in physics. These papers contain two important aspects. The first one is the idea to study *statistical* properties of the resonances of complex nuclei instead of studying its *particular* properties. This is in perfect analogy with statistical mechanics: One does not care about the particular position of the system in its phase space but rather about its thermodynamical (statistical) properties. The other idea was to use an ensemble of matrices to describe the system. This is again done in analogy with statistics mechanical, but it is conceptually quite different. Instead of performing averages over the phase space, one does averages over the space of systems. Wigner was successful in describing some experimental findings, and later evidence showed the wide scope of applicability of his idea [BFF⁺81, GMGW98, JPA].

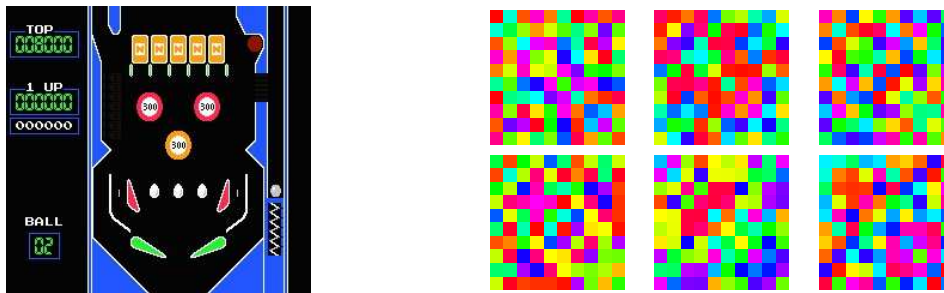


Figure 1.1: Cartoon of an idea exploited in this thesis. The statistical properties of particular system (on the left, say a complicated billiard) are studied using the properties of an ensemble of random matrices (on the right).

A next revolutionary step was marked by the papers by Casati *et al.* [CGVG80] and Bohigas *et al.* [BGS84]. There they conjectured that quantum systems whose classical counterparts are chaotic have a spectrum whose fluctuations resemble those of the appropriate classical ensembles. The revolutionary aspect of this conjecture is that it does not require a complex composition of the system (*i.e.* many bodies), but only complexity in its *dynamics*. Vast numerical evidence favoring this conjecture is available [GMGW98, JPA], but a precise understanding (*i.e.* a globally accepted proof) is yet outstanding. What about systems with no classical correspondence? Defining chaoticity in this case is cumbersome. We shall keep an oversimplified definition: quantum chaotic systems are those that exhibit fluctuations in its spectrum similar to those observed in the appropriate RMT ensemble. Alternatively one could say that quantum chaotic systems are those for which the correlations of most pair of observables decay to zero at large times.

In recent experiments [SKK⁺00, ZCZ⁺04, HSKH⁺05, HHR⁺05], it has been demonstrated that it is possible to protect ever larger entangled quantum systems, often arrays of qubits, ever more efficiently from decoherence. A close connection between the dynamics of fidelity decay and decoherence has been shown in some instances [CPW02, KJZ02, CDPZ03, GPSS04], which suggests to apply methods successful in one field to the other. In that context, a random matrix description [GPS04, GPS \check{Z} 06] is accessible and very effective in describing experiments [SSGS05, SGSS05, GSW06]. Based on this success of random matrix theory, we shall use it to model decoherence [GPS \check{Z} 06, GS02] of qubit systems [PS07], assuming

complicated dynamics in the environment, and a complicated coupling (in the interaction picture).

Three perspectives make such a random matrix treatment particularly attractive. First, reduction of decoherence may, in some instances, be achieved by isolating some “far” environment (including spontaneous decay) to a degree that it can, to first approximation, be neglected. Then it can happen that the Heisenberg time of the relevant “near” environment is finite on the time scale of decoherence. In such a case it becomes relevant that RMT shows, in linear response approximation, a transition from linear to quadratic decay at times of the order of the Heisenberg time. This behavior is seen with spin chain environments [see sec. 5], and is essential for the success of the theory in describing the above mentioned experiments of fidelity decay. Note also that the concept of a two stage environment has been used for basic considerations [Zur03]. Second, the long term goal must be to describe in one theory the decay of fidelity that includes undesirable deviations of the internal Hamiltonian of the central system (already done), together with decoherence (done in this thesis). Third, random matrix descriptions include some aspects of chaos or mixing that are essential in the above experiments and may be useful for application to quantum computing [PZ01, FFS04, CPŽ05].

For some technical aspects of random matrix theory, including Heisenberg time, GOE and GUE ensembles, form factor and density of states, please go to appendix E.

Chapter 2

One qubit decoherence

In this chapter we analyze decoherence of a single qubit. We focus on weak coupling of the qubit to an environment. We shall use the correlation function approach proposed for purity decay in echo-dynamics [PS02], treating the coupling as the perturbation. The linear response approximation will be sufficient. In this approximation the ensemble averages, which we have to take in any RMT model, are feasible though somewhat tedious. Exact solutions, which exist in some instances for the decay of the fidelity amplitude [SS05, GKP⁺06], seem to be out of reach at present, because they require the evaluation of four-point functions.

The general program is as follows. Assume that the qubit is initially in a pure state, and evolves under its own local Hamiltonian. The qubit is coupled via a random matrix to a large environment in turn described by another random matrix. The coupling to the environment gives rise to decoherence. Averaging both the coupling and the environment Hamiltonian over the RMT ensembles yields the generic behavior of decoherence of the qubit.

We present a detailed analysis using both the Gaussian unitary (GUE) and the Gaussian orthogonal (GOE) ensembles [Car35, Meh91] for the description of the environment and the coupling. The two ensembles correspond to time reversal invariance (TRI) breaking and conserving dynamics respectively.

In sec. 2.1 we shall state the model, recall the linear response formalism for echo dynamics, and show how it can be adapted to forward evolu-

tion. In sec. 2.2 we discuss how to express the problem in terms of echo dynamics. In sec. 2.3 we give the general solution, arising from the calculations done in the appendix A. The analysis for the GUE case is given in 2.4, whereas the one for the GOE is given in 2.5.

2.1 The model

We describe decoherence by considering explicitly additional degrees of freedom (henceforth called “environment”) which are interacting with the qubit. The Hilbert space studied in this section is

$$\mathcal{H} = \mathcal{H}_1 \otimes \mathcal{H}_e, \quad (2.1)$$

where \mathcal{H}_1 (of dimension two) and \mathcal{H}_e (of dimension N_e) denote the Hilbert spaces of the qubit and the environment, respectively. The Hamiltonian is of the following form

$$H_\lambda = H_1 \otimes \mathbf{1}_e + \mathbf{1}_1 \otimes H_e + \lambda V_{1,e} \quad (2.2)$$

$$\equiv H_1 + H_e + \lambda V_{1,e}. \quad (2.3)$$

Here, H_1 represents the Hamiltonian acting on the qubit, H_e the Hamiltonian of the environment, and $V_{1,e}$ the coupling between the qubit and the environment. Notice how the indices in the operators indicate the spaces in which they act. The real parameter λ controls the strength of the coupling. We shall study the time evolution of an initially pure and separable state

$$|\psi(t=0)\rangle = |\psi_1\rangle \otimes |\psi_e\rangle, \quad (2.4)$$

where $|\psi_1\rangle \in \mathcal{H}_1$ and $|\psi_e\rangle \in \mathcal{H}_e$. At any time t , the state of the whole system is thus $|\psi(t)\rangle = \exp(-itH_\lambda)|\psi(0)\rangle$, and the state of the single qubit is $\text{tr}_e |\psi(t)\rangle\langle\psi(t)|$. As time evolves, the qubit and the environment get entangled, which means that after tracing out the environmental degrees of freedom, the state of the qubit becomes mixed.

At this point we wish to compare this model with the spectator model. We can arrive to the one studied in this chapter from two different directions. One is if we eliminate the spectator. The other is if we consider a separable (with respect to the spectator) situation [*i.e.* if in eq. (1.15) we let $|\psi_c\rangle = |\psi_s\rangle \otimes |\psi_i\rangle$].

We describe both the coupling and the dynamics in the environment within random matrix theory. To this end, H_e and $V_{e,1}$ are chosen both

from either the GUE or the GOE, depending on whether we wish to describe a TRI breaking or TRI conserving situation. The Hamiltonian H_1 implies another free parameter of the model, namely the level splitting Δ of the two level system representing the qubit. While the state of the qubit $|\psi_1\rangle$ implies more free parameters in our model, we assume the state of the environment $|\psi_e\rangle$ to be random. This means that the state is chosen from an ensemble which is invariant under unitary transformations, and is fully consistent with our minimum information assumption. In practice, this means that the coefficients are chosen as complex random Gaussian variables, and subsequently the state is normalized.

2.2 Echo dynamics and linear response theory

We shall calculate the value of purity as a function of time analytically, in a perturbative approximation. As we want to use the tools developed in the appendix A for a linear response formalism in echo dynamics, we must state the problem in this language. To perform this task it is useful to consider the above Hamiltonian [eq. (2.2)], as composed by an unperturbed part H_0 and a perturbation λV . The unperturbed part corresponds to the operators that act on each individual subspace alone whereas the perturbation corresponds to the coupling among the different subspaces; *i.e.* $H_0 = H_e + H_1$ and $V = V_{e,1}$.

We write the Hamiltonian as

$$H_\lambda = H_0 + \lambda V, \quad (2.5)$$

and introduce the evolution operator and the echo operator defined by

$$U_\lambda(t) = e^{-iH_\lambda t}, \quad M_\lambda(t) = U_0(t)^\dagger U_\lambda(t), \quad (2.6)$$

respectively ($\hbar = 1$ during all the thesis). The echo operator receives its name because it evolves a state forward in time with a perturbed operator and backwards with an unperturbed one. For the calculation of purity at a given time t , we replace the forward evolution operator U_λ by the corresponding echo operator M_λ . Even though the resulting states are different, *i.e.*

$$\rho(t) = \text{tr}_{e,e'} U_\lambda(t) \rho U_\lambda^\dagger(t) \neq \rho^M(t) = \text{tr}_{e,e'} M_\lambda(t) \rho M_\lambda^\dagger(t), \quad (2.7)$$

they are still related by the local (in the qubit and the environment) unitary transformation $U_0(t)$. Since local transformations do not change the entanglement properties, it holds (exactly!) that

$$P(t) = P[\rho(t)] = P[\rho^M(t)]. \quad (2.8)$$

This step is crucial, since the echo operator admits a series expansion with much larger range of validity (both, in time and perturbation strength). However the numerical simulations are all done with forward evolution alone as they require less computational effort.

The Born expansion of the echo operator up to second order reads

$$M_\lambda(t) = \mathbf{1} - i\lambda I(t) - \lambda^2 J(t) + \mathcal{O}(\lambda^3), \quad (2.9)$$

with

$$I(t) = \int_0^t d\tau \tilde{V}(\tau), \quad J(t) = \int_0^t d\tau \int_0^\tau d\tau' \tilde{V}(\tau) \tilde{V}(\tau') \quad (2.10)$$

and $\tilde{V}(t) = U_0(t)^\dagger V U_0(t)$ being the coupling in the interaction picture. Using this expansion we calculate the purity of the central system, averaged over the coupling and the Hamiltonian of the environment.

The reader must notice that at no point we used that the dimension of the central system is 2. In fact, we only required the locality of the operator U_0 and the fact that $M_\lambda(t) \approx \mathbf{1}$. Thus, all this reasoning (in particular eqs. 2.8, 2.9, and 2.10) is equally valid for a completely general spectator configuration or even more general configurations to be introduced later.

2.3 The solution

In appendix A, we compute the average purity $\langle P(t) \rangle$ as a function of time in the linear response approximation eq. (2.9), following the steps outlined in sec. 2.2. The average is taken with respect to the coupling $V_{1,e}$ [using eqs. E.4 and E.5], the random initial state $|\psi_e\rangle$, and the spectrum of H_e . In the limit of $N_e \rightarrow \infty$, we obtain [eq. (A.8), eq. (A.36)]

$$\langle P(t) \rangle = 1 - 2\lambda^2 \int_0^t d\tau \int_0^t d\tau' \operatorname{Re} A_{\text{II}}(\tau, \tau') + \mathcal{O}(\lambda^4), \quad (2.11)$$

with

$$A_{\text{II}}(\tau, \tau') = [C_1(|\tau - \tau'|) - S_1(\tau - \tau')] \bar{C}(|\tau - \tau'|) + \chi_{\text{GOE}} [1 - S'_1(-\tau - \tau')], \quad (2.12)$$

where $\chi_{\text{GOE}} = 1$ for the TRI case, and $\chi_{\text{GOE}} = 0$ for the non-TRI case. The correlation functions $C_1(\tau)$, $S_1(\tau)$, $S'_1(\tau)$, and $\bar{C}(\tau)$ are defined in appendix A.5. The first three depend on the state of the central system. Note that $S'_1(\tau)$ is only relevant in the case of a GOE, and curiously is not strictly a correlation function as it contains a dependence on the *sum* of both times. The last one, $\bar{C}(\tau)$ deserves special attention, since it depends on the spectral properties of the environment determined by the function

$$\frac{1}{N_e} \left\langle \left| \sum_{j=1}^{N_e} e^{-iE_j t} \right|^2 \right\rangle = \bar{C}(t) = 1 + \delta(t/\tau_H) - b_2^{(\beta)}(t/\tau_H), \quad (2.13)$$

(recall eq. (E.8) and subsequent equations). Here the E_j 's are the eigenenergies of H_e and τ_H is the corresponding Heisenberg time. Actually the validity of eq. (2.11) is not dependent on the environment being represented by a GOE ($\beta = 1$) or GUE ($\beta = 2$). For these the two-point form factor $b_2^{(\beta)}$ is well known [Meh91] but any ensemble with the corresponding invariance properties will do, for example the POE or PUE [DRS91].

We first study the GUE case with and without an internal Hamiltonian governing the qubit. The next step is to work out the GOE case. There we concentrate on the case with no internal Hamiltonian governing in the qubit since we want to keep the discussion as simple as possible to focus on the consequences of the weaker invariance properties of the ensemble.

2.4 The GUE case

We are now in the position to give an explicit formula for $\langle P(t) \rangle$ in the GUE case. This formula will generally depend on some properties of the initial condition $|\psi_1\rangle$. We wish to write it in the most general way. However the symmetries involved in the problem reduce the number of parameters needed to describe the initial state $|\psi_1\rangle$.

Recall that $H = H_e + H_1 + \lambda V$ represents an ensemble of Hamiltonians in which H_e and V are chosen from GUEs of dimension N_e and $2N_e$ respectively, whereas H_1 together with the initial condition $|\psi_1\rangle$ remain fixed throughout the calculation. The operations under which the ensemble is invariant are local (with respect to the partitioning of the Hilbert space into \mathcal{H}_1 and \mathcal{H}_e), unitary (due to the invariance properties of the GUE), and leave H_1 invariant. Hence the transformation matrices must be of the

form

$$U \otimes \exp(i\alpha H_1) \quad (2.14)$$

with α a real number and U a unitary operator acting on \mathcal{H}_e . The solution must also be invariant under that transformation.

This freedom allows to choose a convenient basis to solve the problem. On the one hand, it allows to write H_0 in diagonal form (as done during the discussion of appendix A), and on the other hand, we can use it to represent the initial state of the qubit in such a way that there is no phase shift between the two components of the qubit. This can be achieved by appropriately choosing α in eq. (2.14). We thus write, without loosing generality

$$|\psi_1\rangle = \cos \phi |0\rangle + \sin \phi |1\rangle, \quad (2.15)$$

where $|0\rangle$ and $|1\rangle$ are eigenstates of H_1 . Notice that if $\phi \in \{0, \pi/2\}$, $|\psi_1\rangle$ is an eigenstate of H_1 . Finally, we choose the origin of the energy scale in such a way that the Hamiltonian of the qubit can be written as $H_1 = (\Delta/2)|0\rangle\langle 0| - (\Delta/2)|1\rangle\langle 1|$.

We obtain the average purity from the general expression in eq. (2.11) and eq. (2.12). For a pure initial state $\rho_1 = |\psi_1\rangle\langle\psi_1|$ the relevant correlation functions $\text{Re } C_1(\tau)$, $S_1(\tau)$, and $\bar{C}(\tau)$ are given in eq. (A.46), eq. (A.48), and eq. (A.41), respectively. Using the symmetry of the resulting integrand with respect to the exchange of τ and τ' , we find

$$\langle P(t) \rangle = 1 - 4\lambda^2 \int_0^t d\tau \int_0^\tau d\tau' \bar{C}(\tau') [1 - g_\phi (1 - \cos \Delta\tau')] + O(\lambda^4, N_e^{-1}) \quad (2.16)$$

with

$$g_\phi = \cos^4 \phi + \sin^4 \phi = \frac{3 + \cos(4\phi)}{4} \quad (2.17)$$

quantifying the “distance” between $|\psi\rangle$ and an eigenbasis of H_1 .

Let us consider the following two limits for H_1 . The “degenerate limit”, where the level splitting Δ is much smaller than the mean level spacing $d_e = 2\pi/\tau_H$ of the environmental Hamiltonian, and the “fast limit”, where the level splitting is much larger. In the latter case, the internal evolution of the qubit is fast compared with the evolution in the environment. (We shall refer to these limits also in later sections.)

The degenerate limit leads to the known formula [PS07]

$$P_D(t) = 1 - \lambda^2 f_{\tau_H}(t), \quad (2.18)$$

with

$$f_{\tau_{\text{H}}}(t) = 2t \max\{t, \tau_{\text{H}}\} + \frac{2}{3\tau_{\text{H}}}(\min\{t, \tau_{\text{H}}\})^3. \quad (2.19)$$

The result does not depend on the initial state of the qubit. Due to the degeneracy all states are eigenstates of H_1 and thus equivalent. The leading term of the purity decay is linear before the Heisenberg time and quadratic after the Heisenberg time. Similar features were already observed in fidelity decay and purity decay in other contexts [GPSŽ06].

In the fast limit ($\Delta \gg d_e$), purity is obtained from eq. (2.16) by replacing $\cos \Delta\tau'$ by 1 when it is multiplied with the δ function [see eq. (2.13)], and by zero everywhere else. For finite N_e care must be taken, since we are assuming Zeno time (which is given by the “width of the δ -function”) to be much smaller than all other time scales, such that $\Delta \ll N_e d_e$. The resulting expression is

$$P_{\text{F}}(t) = 1 - \lambda^2[(1 - g_\phi)f_{\tau_{\text{H}}}(t) + 2g_\phi t\tau_{\text{H}}]. \quad (2.20)$$

Typically (unless $|\psi_1\rangle$ is an eigenstate), this formula displays a dominantly linear decay below the Heisenberg time, and a dominantly quadratic decay above, similar to eq. (2.18).

In fig. 2.1 we compare numerical simulations of the average purity $\langle P(t) \rangle$ (symbols) with the corresponding linear response result (dashed lines) based on eqs. eq. (2.18) and eq. (2.20). The numerical results are obtained from Monte Carlo simulations with 15 different Hamiltonians and 15 different initial conditions for each Hamiltonian. We wish to underline two aspects. First, the energy splitting in general leads to an attenuation of purity decay. Even though a strict inequality only holds for the limiting cases, $P_{\text{F}}(t) > P_{\text{D}}(t)$ (for $t \neq 0$), we may still say that increasing Δ tends to slow down purity decay. This result is in agreement with earlier findings on the stability of quantum dynamics [PŽ02]. Second, for the fast limit and an eigenstate of H_1 ($g_\phi = 1$) we find linear decay even beyond the Heisenberg time. A similar behaviour has been obtained in [GPSŽ06], but there an eigenstate of the whole Hamiltonian was required.

In [PS07] it was shown that exponentiation of the linear response result leads to very good agreement beyond the validity of the original approximation. We use the formula eq. (C.1)

$$P_{\text{ELR}}(t) = P_\infty + (1 - P_\infty) \exp \left[-\frac{1 - P_{\text{LR}}(t)}{1 - P_\infty} \right]. \quad (2.21)$$

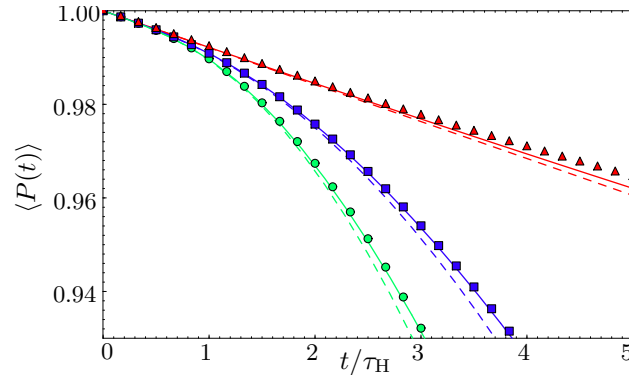


Figure 2.1: Numerical simulations for the average purity of one qubit using non-TRI Hamiltonians, as a function of time in units of the Heisenberg time τ_H of the environment. For the coupling strength $\lambda = 0.01$ and $N_e = 2048$, we show the dependence of $\langle P(t) \rangle$ on Δ (the level splitting) and ϕ (characterizing the initial state) of the internal qubit: $\Delta = 0$ (green circles), $\Delta = 8$, $\phi = \pi/4$ (blue squares), and $\Delta = 8$, $\phi = 0$ (red triangles). The corresponding linear response results (dashed lines) and exponentiated linear response results (solid lines) are based on eq. (2.16) and eq. (2.21), where P_∞ is given in C. Note that the level splitting Δ tends to slow down decoherence.

where $P_{\text{LR}}(t)$ is truncation to second order in λ of the expansion eq. (2.16), and $P_\infty = 1/2$ the estimated asymptotic value of purity for $t \rightarrow \infty$, see appendix C. From fig. 2.1 we see that the exponentiation indeed increases the accuracy of the bare linear response approximation.

2.5 The GOE case

We drop H_1 for a moment, leaving $H_0 = H_e$, resulting in

$$H_\lambda = H_e + \lambda V. \quad (2.22)$$

H_e is chosen from a GOE of dimension N_e and acts on \mathcal{H}_e ; V is chosen from a GOE of dimension $2N_e$ and acts on $\mathcal{H}_e \otimes \mathcal{H}_1$. The resulting ensemble of Hamiltonians is invariant under local orthogonal transformations. In the qubit this invariance allows rotations of the kind $\exp(i\alpha\sigma_y) \in \mathcal{O}(2)$. If such transformations are represented on the Bloch sphere, they become rotations around the y axis. Hence, they can take any point on the Bloch sphere onto the xy -plane. Supposing this point represents the initial state, it shows that we may assume the initial state in the qubit to be of the form

$$|\psi_1\rangle = \frac{|0\rangle + e^{i\gamma}|1\rangle}{\sqrt{2}}. \quad (2.23)$$

In this expression, $\gamma \in [-\pi/2, \pi/2]$ denotes the angle of the vector representing the initial state with the xz -plane (see fig. 2.2).

In order to obtain the linear response expression for $\langle P(t) \rangle$ we again make use of eq. (2.11) and eq. (2.12). However, apart from the correlation functions used in the GUE case, we have now to consider in addition $S'_1(\tau)$, as given in eq. (A.53). The special case $H_1 = 0$ can be simply obtained by setting $\Delta = 0$. This yields

$$A_{\text{II}}(\tau, \tau') = \bar{C}(|\tau - \tau'|) + \sin^2 \gamma. \quad (2.24)$$

After evaluating the double integral in eq. (2.11), we obtain

$$\langle P(t) \rangle = 1 - \lambda^2 \left\{ t^2 [3 - \cos(2\gamma)] + 2t\tau_H - 2B_2^{(1)}(t) \right\}, \quad (2.25)$$

where

$$B_2^{(1)}(t) = 2 \int_0^t d\tau \int_0^\tau d\tau' b_2^{(1)}(\tau'/\tau_H) \quad (2.26)$$

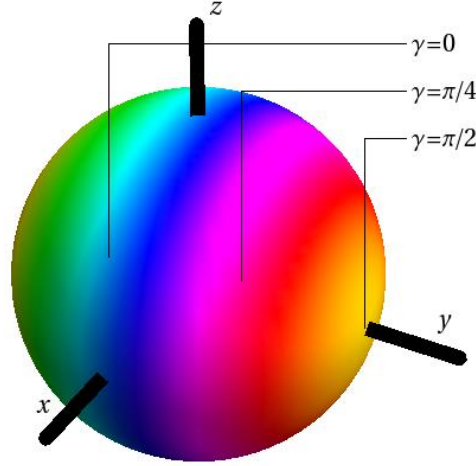


Figure 2.2: Any pure initial state of the qubit can be mapped onto the Bloch sphere. Here, we show the angle γ defined in eq. (2.23) in color code. Regions of a given color represent subspaces which are invariant under the transformation $\exp(i\alpha\sigma_y)$.

is the double integral of the form factor. It can be computed analytically, but the resulting expression is very involved [GPS04]. For our purpose it is sufficient to note that for $t \ll \tau_H$, $B_2^{(1)}(t) \propto t^3$ (as in the GUE case), whereas for $t \gg \tau_H$, $t - B_2^{(1)}(t)$ grows only logarithmically. Thus it has a similar behavior as in the GUE case, eq. (G.6).

In fig. 2.3 we show $\langle P(t) \rangle$ for $\gamma = 0$ (green squares), for $\gamma = \pi/2$ (blue circles), and for random values in the whole Bloch sphere (red triangles). In contrast to the GUE case in the degenerate limit, the average purity depends on the initial state (via the angle γ). The fastest decay of purity is observed for $\gamma = \pi/2$, where the image under the time reversal operation becomes orthogonal to the initial state. The slowest decay is observed for $\gamma = 0$, which characterizes states which remain unchanged under the time reversal symmetry operation. In the lower panel we show numerical results for the standard deviation of the purity as a function of N_e , the dimension of the Hilbert space of the environment. We consider the same cases as on the upper panel: random initial states $|\psi_1\rangle$ with fixed $\gamma = 0$ (green squares), with fixed $\gamma = \pi/2$ (blue circles) and random states $|\psi_1\rangle$ uniformly distributed on the Bloch sphere (red triangles). Note that along with the random choice of $|\psi_1\rangle$, also H_e , $V_{1,e}$, and $|\psi_e\rangle$ are randomly chosen from their respective ensembles. We clearly see that for those

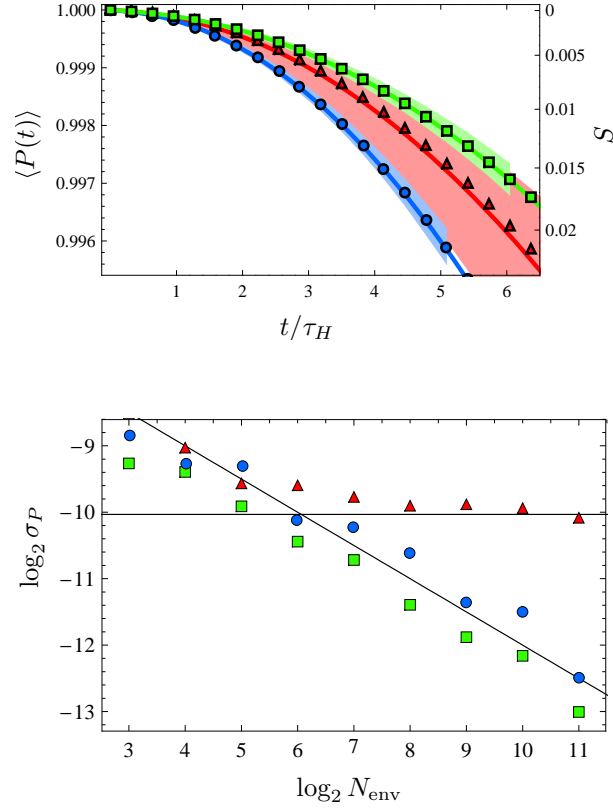


Figure 2.3: We display the behavior of purity and von Neumann entropy, in different regions in the Bloch sphere connected by orthogonal transformations, characterized by γ in eq. (2.23). On the top figure we see the enveloping curve after running 100 initial conditions (thick regions), their average (symbols) and the predicted behavior (solid curves) by eq. (2.25). If $\gamma = 0$ we use color green; if $\gamma = \pi/2$ we use blue; and if we allow arbitrary γ we use red. In the lower panel σ is plotted for $t = 40$. We use the same coding as the upper figure. For a fixed value of γ (blue and green) there is asymptotic self averaging whereas for an arbitrary initial condition (red) the standard deviation reaches the finite value predicted in eq. (2.28), plotted as a horizontal line. We fixed $\lambda = 10^{-3}$. A line $\propto 1/\sqrt{N_e}$ is also included.

cases where γ is kept fixed, the standard deviation falls off like $N_e^{-1/2}$. By contrast, the standard deviation converges to a finite value, when $|\psi_1\rangle$ chosen with no restriction. That value can be estimated from the standard deviation of the function $\cos 2\gamma$, which yields:

$$\int_{-\pi/2}^{\pi/2} \left[\overline{\cos(2\gamma)} - \cos(2\gamma) \right]^2 \frac{\cos(2\gamma)}{2} d\gamma = \frac{16}{45}. \quad (2.27)$$

Assuming that for $N_e \rightarrow \infty$, the fluctuations of $\cos 2\gamma$, is the only source for the fluctuations of purity, the standard deviation of the purity is

$$\sigma_P = \frac{4}{3\sqrt{5}} \lambda^2 t^2 + \mathcal{O}(\lambda^4, N_e^{-1}). \quad (2.28)$$

The statements of the last two paragraphs can be directly translated to the von Neumann entropy S . For one qubit it has a one to one relation with purity

$$S(P) = h\left(\frac{1 + \sqrt{2P-1}}{2}\right) + h\left(\frac{1 - \sqrt{2P-1}}{2}\right), \quad h(x) = -x \log_2 x. \quad (2.29)$$

Observe the entropy scale on the upper panel of fig. 2.3. The consequences of the weaker invariance properties of the GOE, and the relation to the states will be analyzed in detail in a general framework in a later paper.

Chapter 3

Two qubit decoherence

In this chapter, we address the question whether entanglement within a given system affects its decoherence rate. In particular, as the name suggests, we are going to study two qubit decoherence. We will use the spectator model described in sec. 1.2. Moreover we shall consider the first nontrivial example thereof, in the sense that the spectator space plays a nontrivial roll. However it is still the simplest example allowing this possibility as both the spectator and the interacting space are qubits. We shall study two other configurations, namely when both qubits are coupled to one or two environments. There, we shall start appreciating the power of the spectator model; we are going to be able to express there decoherence in terms of the decoherence in the spectator configuration.

We will base our arguments on the calculations made in appendix A and the results discussed in the previous chapter. Again we are going to study the linear response regime, and test with Monte Carlo simulations the validity of a heuristic exponentiation. The symmetries of the classical ensembles will continue to play an important role to simplify the problem. Moreover we shall find that entanglement has the property of transporting the symmetry from one qubit to the other.

We first describe the models (configurations) we are going to study, sec. 3.1. Next we analyze in detail the results for the simplest configuration, the spectator model for two qubits, sec. 3.2. There we consider both the GUE and GOE cases. We then generalize the result to the other configurations in sec. 3.3 and sec. 3.4.

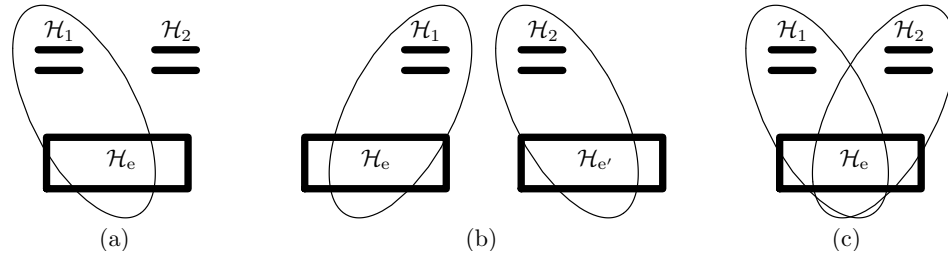


Figure 3.1: Schematic representations of the different dynamical configurations studied in this article: (a) the 2 qubit spectator Hamiltonian, (b) the separate, and (c) the joint environment Hamiltonian.

3.1 The models

For the two qubit case, the Hilbert space structure must be slightly more complicated than eq. (2.1). We need at least to provide the Hilbert space for a second qubit, and, in one of the models, we shall need an additional Hilbert space for a second environment. In all cases the initial condition is pure in the central system, but the two qubits can share some entanglement. We shall consider three different dynamical scenarios, all explicitly excluding any interaction between the two qubits:

- (a) *The 2 qubit spectator Hamiltonian:*
The Hilbert space structure is

$$\mathcal{H} = \mathcal{H}_1 \otimes \mathcal{H}_2 \otimes \mathcal{H}_e. \quad (3.1)$$

Both \mathcal{H}_1 and \mathcal{H}_2 are the state spaces of the qubits ($\dim \mathcal{H}_1 = \dim \mathcal{H}_2 = 2$) and \mathcal{H}_e (of dimension N_e) is the state space of an environment. The central system is, obviously,

$$\mathcal{H}_c = \mathcal{H}_1 \otimes \mathcal{H}_2. \quad (3.2)$$

Only the first qubit is coupled to an environment, and we allow for local dynamics. The total Hamiltonian reads

$$H_\lambda = H_1 + H_2 + H_e + \lambda V_{1,e}, \quad (3.3)$$

where λ is again a real number modulating the strength of the coupling. We recall the remark in sec. 1.2, namely that the sub-indices

of the operators indicate the space on which they act. This situation is shown schematically in fig. 3.1(a). Notice that if we choose an initial state where the two qubits are already entangled, this provides the *simplest* situation which allows to study entanglement decay. If the two qubits are initially not entangled, the process reduces effectively to the one-qubit case, described previously sec. 2.1. The special case $H_1 = H_2 = 0$ has been considered in Ref. [PS07].

The reader must notice that this situation is an example of the spectator configuration, discussed in sec. 1.2. In this case the interacting subspace is \mathcal{H}_1 and the spectator is played by \mathcal{H}_2 .

(b) *The separate environment Hamiltonian:*

The Hilbert space structure is

$$\mathcal{H} = \mathcal{H}_1 \otimes \mathcal{H}_2 \otimes \mathcal{H}_e \otimes \mathcal{H}_{e'}. \quad (3.4)$$

Besides the subspaces in eq. (3.1) (which keep their meaning), we have an additional space $\mathcal{H}_{e'}$ which represents a new environment. We again allow for similar dynamics except that we allow the second qubit to interact with the new environment. The two environments are assumed to be non-interacting and uncorrelated:

$$|\psi(0)\rangle = |\psi_{12}\rangle|\psi_e\rangle|\psi_{e'}\rangle, \quad |\psi_{12}\rangle \in \mathcal{H}_1 \otimes \mathcal{H}_2, |\psi_e\rangle \in \mathcal{H}_e, \text{ and } |\psi_{e'}\rangle \in \mathcal{H}_{e'}. \quad (3.5)$$

Thus, the Hamiltonian of this model reads

$$H_{\lambda_1, \lambda_2} = H_1 + H_2 + H_e + H_{e'} + \lambda_1 V_{1,e} + \lambda_2 V_{2,e'}, \quad (3.6)$$

where $V_{2,e'}$ and $H_{e'}$ describe the coupling to – and the dynamics in the additional environment. Both quantities are chosen independently from the respective random matrix ensembles, in perfect analogy with $V_{1,e}$ and H_e . The real parameters λ_1 and λ_2 fix the coupling strengths to either environment. This model, see fig. 3.1(b), may describe two qubits that are ready to perform a distant teleportation, where each of them is interacting only with its immediate surroundings. It can also represent a pair of qubits that, although close to each other, interact with different and independent degrees of freedom.

(c) *The joint environment Hamiltonian:*

The third case, shown in fig. 3.1(c), describes a situation in which both qubits are coupled to the same environment, even though the

coupling matrices are still independent. The Hilbert space is identical to the one for the 2 qubit spectator configuration. The total Hamiltonian reads

$$H_{\lambda_1, \lambda_2} = H_1 + H_2 + H_e + \lambda_1 V_{1,e} + \lambda_2 V_{2,e}, \quad (3.7)$$

where $V_{2,e}$ describes the coupling of the second qubit to the environment. It is chosen independently from the same random matrix ensemble as $V_{1,e}$.

3.2 The spectator Hamiltonian

The first step to calculate the decoherence of the initial state

$$\varrho_0 = |\psi_{12}\rangle\langle\psi_{12}| \otimes |\psi_e\rangle\langle\psi_e|, \quad (3.8)$$

evolved with the Hamiltonian (3.3), is to realize that the echo operator does not contain H_2 . The quantum echo of ϱ_0 after time t is

$$\varrho^M(t) = [\mathbb{1}_2 \otimes M_\lambda(t)] \varrho_0 [\mathbb{1}_2 \otimes M_\lambda^\dagger(t)]. \quad (3.9)$$

Since $\varrho^M(t)$ remains a pure state in $\mathcal{H}_1 \otimes \mathcal{H}_2 \otimes \mathcal{H}_e$,

$$P(t) = \text{tr} \rho_c(t)^2 = \text{tr} \rho_e(t)^2 \quad (3.10)$$

with $\rho_c(t) = \text{tr}_e \varrho^M(t)$ and $\rho_e(t) = \text{tr}_c \varrho^M(t)$. This simply means that, as a formality, we can calculate purity of the central system, calculating purity of the environment. As the echo operator acts as the identity on the second qubit,

$$\begin{aligned} \rho_e(t) &= \text{tr}_1 M_\lambda(t) (\text{tr}_2 \varrho_0) M_\lambda^\dagger(t) \\ &= \text{tr}_1 M_\lambda(t) (\rho_1 \otimes |\psi_e\rangle\langle\psi_e|) M_\lambda^\dagger(t), \end{aligned} \quad (3.11)$$

where $\rho_1 = \text{tr}_2 |\psi_{12}\rangle\langle\psi_{12}|$.

We may therefore compute the purity of the spectator model, without ever referring explicitly to the second qubit! Any dependence of the decay of purity on the central system as a whole is encoded into the initial density matrix ρ_1 . This also implies that we can use the results obtained in A, and hence eq. (2.11) and eq. (2.12) remain valid. The only difference is that for the correlation functions $C_1(\tau)$, $S_1(\tau)$, and $S'_1(\tau)$, we now have

to insert the respective expressions which apply for mixed initial states of the first qubit. These expressions are given in A.5. We stress, for later reference, that this line of reasoning is not limited by the fact that the interacting and spectator systems are qubits.

3.2.1 The GUE case

We wish to write the initial condition in its simplest form. We must respect the structure of the Hamiltonian (3.3). However we can still take advantage of all its invariance properties, when seen as an ensemble. Given a fixed H_1 , that ensemble of Hamiltonians is invariant under local operations of the form

$$U_{N_e} \otimes \exp i\alpha H_1 \otimes U_2 \quad (3.12)$$

where $U_{N_e} \in \mathcal{U}(N_e)$ is any unitary operator acting on the environment, α a real number, and $U_2 \in \mathcal{U}(2)$ is any unitary operator acting on the second qubit.

The freedom within the qubits allows to choose a basis $\{|0\rangle, |1\rangle\} \otimes \{|0\rangle, |1\rangle\}$ in which the initial state [see eq. (3.8)] can be written as

$$|\psi_{12}\rangle = \cos\theta(\cos\phi|0\rangle + \sin\phi|1\rangle)|0\rangle + \sin\theta(\sin\phi|0\rangle - \cos\phi|1\rangle)|1\rangle, \quad (3.13)$$

and still, $H_1 = \frac{\Delta}{2}|0\rangle\langle 0| - \frac{\Delta}{2}|1\rangle\langle 1|$ is diagonal. Let us prove it in a constructive manner. To find this basis we start using the Schmidt decomposition to write

$$|\psi_{12}\rangle = \cos\theta|\tilde{0}_1\tilde{0}_2\rangle + \sin\theta|\tilde{1}_1\tilde{1}_2\rangle \quad (3.14)$$

with $\{|\tilde{0}_i\rangle, |\tilde{1}_i\rangle\}$ being an orthonormal basis of particle i . For the first qubit, we fix the z axis of the Bloch sphere (containing both $|0\rangle$ and $|1\rangle$) parallel to the eigenvectors of H_1 , and the y axis perpendicular (in the Bloch sphere) to both the z axis and $|\tilde{0}_1\rangle$. The states contained in the xz plane are then real superpositions of $|0\rangle$ and $|1\rangle$, which implies that

$$|\tilde{0}_1\rangle = \cos\phi|0\rangle + \sin\phi|1\rangle, \quad (3.15)$$

$$|\tilde{1}_1\rangle = \sin\phi|0\rangle - \cos\phi|1\rangle, \quad (3.16)$$

for some ϕ . In the second qubit it is enough to set

$$|\tilde{0}_2\rangle = |0\rangle, \quad (3.17)$$

$$|\tilde{1}_2\rangle = |1\rangle. \quad (3.18)$$

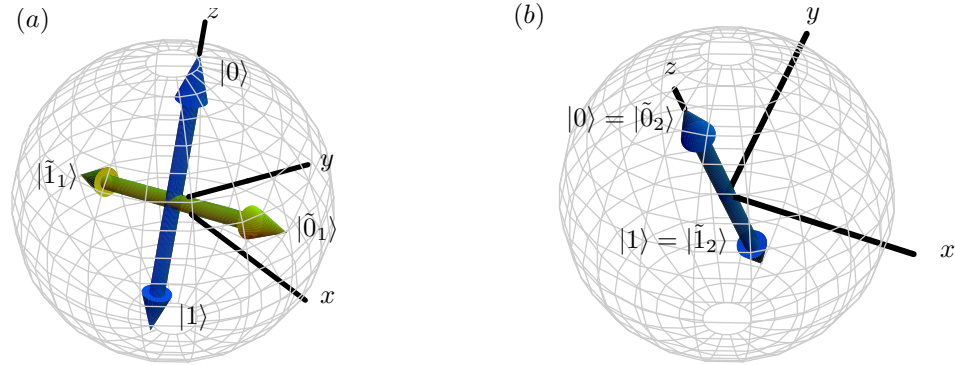


Figure 3.2: A figure to visualize the way the initial condition is parametrized, using the Bloch sphere, is presented. On the left, qubit one has an internal Hamiltonian. Its eigenvectors ($|0\rangle$ and $|1\rangle$) are represented in blue. The z axis is chosen parallel to $|0\rangle$. The x axis is chosen so that both $|\tilde{0}_1\rangle$ and $|\tilde{1}_1\rangle$ have real coefficients; *i.e.* such that the xz plane contains $|\tilde{0}_1\rangle$ and $|\tilde{1}_1\rangle$. On the right we represent the second qubit. We have absolute freedom to choose the basis (even if an internal Hamiltonian is present), and thus we choose it according to the natural Schmidt decomposition.

This freedom is also related to the fact that purity only depends on $\text{tr}_2 |\psi_{12}\rangle\langle\psi_{12}|$. A visualization of this argumentation is found in fig. 3.2. The angle $\theta \in [0, \pi/4]$ measures the entanglement

$$C(|\psi_{12}\rangle\langle\psi_{12}|) = \sin 2\theta \quad (3.19)$$

whereas the angle $\phi \in [0, \pi/2]$ is related to an initial magnetization.

The general solution for purity using this parametrization is

$$P(t) = 1 - 4\lambda^2 \int_0^t d\tau \int_0^\tau d\tau' \bar{C}(\tau') [g_{\theta,\phi}^{(1)} + g_{\theta,\phi}^{(2)} \cos \Delta\tau'] + \mathcal{O}(\lambda^4, N_e^{-1}), \quad (3.20)$$

where the geometric factors $g_{\theta,\phi}^{(1)} \in [0, 1/2]$, and $g_{\theta,\phi}^{(2)} \in [1/2, 1]$ are expressed as

$$g_{\theta,\phi}^{(1)} = g_\theta(1 - g_\phi) + g_\phi(1 - g_\theta) \quad (3.21)$$

$$g_{\theta,\phi}^{(2)} = 2(1 - g_\theta) - g_\phi(1 - 2g_\theta), \quad (3.22)$$

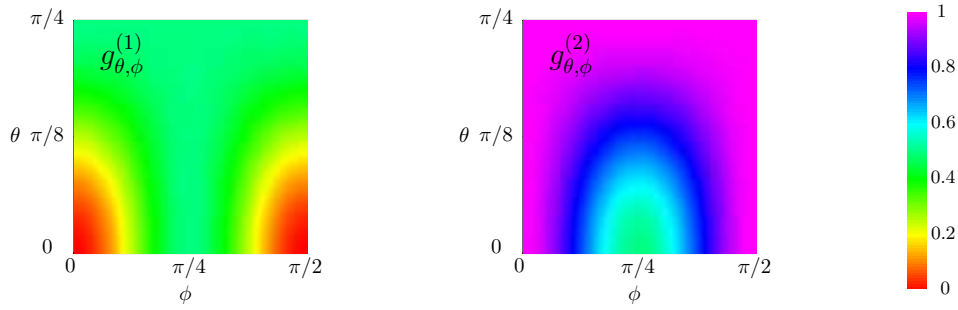


Figure 3.3: Visualization of the geometric factors $g_{\theta,\phi}^{(1)}$ and $g_{\theta,\phi}^{(2)}$ from left to right respectively. For $g_{\theta,\phi}^{(1)}$ we see that for pure eigenstates of H_1 its value is zero. This leads to a higher qualitative stability of this kind of states.

in terms of the functions g_ϕ and g_θ , defined in eq. (2.17). Both geometric factors are shown in fig. 3.3. Eq. (3.20) is obtained from eq. (2.11) and eq. (2.12) by insertion of the eq. (A.46) and eq. (A.52) for $\text{Re } C_1(\tau)$ and $S_1(\tau)$, respectively.

We consider again two limits for Δ . In the degenerate limit ($\Delta \ll 1/\tau_H$) purity decay is given by

$$P_D(t) = 1 - \lambda^2(2 - g_\theta)f_{\tau_H}(t), \quad (3.23)$$

where $f_{\tau_H}(t)$ is defined in eq. (2.19). The result is independent of ϕ since a degenerate Hamiltonian is, in this context, equivalent to no Hamiltonian at all. The θ -dependence in this formula shows that an entangled qubit pair is more susceptible to decoherence than a separable one.

In the fast limit ($\Delta \gg 1/\tau_H$) we get

$$P_F(t) = 1 - \lambda^2 \left[g_{\theta,\phi}^{(1)} f_{\tau_H}(t) + 2\tau_H g_{\theta,\phi}^{(2)} t \right]. \quad (3.24)$$

For initial states chosen as eigenstates of H_1 we find linear decay of purity both below and above Heisenberg time. In order for ρ_1 to be an eigenstate of H_1 it must, first of all, be a pure state (in \mathcal{H}_1). Therefore this behavior can only occur if $\theta = 0$ or $\theta = \pi/2$. Apart from that particular case, we observe in both limits, the fast as well as the degenerate limit, the characteristic linear/quadratic behavior before/after the Heisenberg time similar to the one qubit case.

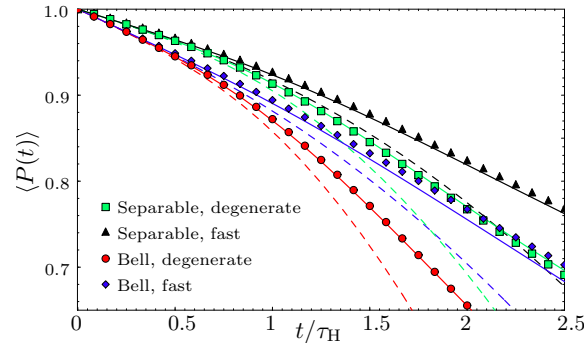


Figure 3.4: Numerical simulations for the average purity as a function of time in units of the Heisenberg time of the environment (spectator configuration, GUE case). For the coupling strength $\lambda = 0.03$ we show the dependence of $\langle P(t) \rangle$ on the level splitting Δ in H_1 and on the initial degree of entanglement between the two qubits (in all cases $\phi = \pi/4$). For separable state ($\theta = 0$) and a degenerate limit we use \blacksquare whereas for the fast limit, with $\Delta = 8$, we use \blacktriangle ; For Bell states, the corresponding limits are encoded as \bullet in the degenerate limit and \blacklozenge in the fast limit ($\Delta = 0.8$). The corresponding linear response results (dashed lines) are based on eq. (3.23), eq. (3.24) and eq. (2.21). The exponentiated linear response results (solid lines) are obtained based on the results of appendix C. The theoretical curves are plotted with the same color, as the respective numerical data. In all cases $N_e = 1024$.

In fig. 3.4 we show numerical simulations for $\langle P(t) \rangle$. We average over 30 different Hamiltonians each probed with 45 different initial conditions. We contrast Bell states ($\phi = \pi/4, \theta = \pi/4$) with separable states ($\phi = \pi/4, \theta = 0$), and also systems with a large level splitting ($N_e \gg \Delta = 8 \gg 1/\tau_H$) with systems having a degenerate Hamiltonian ($\Delta = 0$). The results presented in this figure show that entanglement generally enhances decoherence. This can be anticipated from fig. 3.3, since for fixed ϕ , increasing the value of θ (and hence entanglement) increases both $g_{\theta,\phi}^{(1)}$ and $g_{\theta,\phi}^{(2)}$. At the same time we find again that increasing Δ tends to reduce the rate of decoherence. A strict inequality only holds among the two limiting cases (just as in the one qubit case): From $g_{\theta,\phi}^{(2)} = 2 - g_{\theta,\phi}^{(1)} - g_{\theta}$, it follows that $(P_F - P_D)/\lambda^2 = g_{\theta,\phi}^{(2)}[f_{\tau_H}(t) - 2t\tau_H] \geq 0$. Therefore, for fixed

initial conditions and t greater than 0, $P_F(t) > P_D(t)$. This is the second aspect illustrated in fig. 3.4.

In order to extend the formulae to longer times/smaller purities we exponentiate them using the results of appendix C. The numerical simulations (see fig. 3.4) agree very well with that heuristic exponentiated linear response formula. In one case (blue rhombus) where the agreement is not as good, we found that it is the inaccurate estimate $P_\infty = 1/4$ of the asymptotic value of purity, which leads to the deviations.

3.2.2 The GOE case

Let us consider the GOE average of both H_e and $V_{1,e}$. When averaging H_e and $V_{1,e}$ over the GOE, we are again confronted with the fact that the invariance group is considerably smaller than in the GUE case. In this context the initial entanglement between the two qubits has a crucial importance since it “transports” the invariance properties from the spectator to the coupled qubit.

For the sake of simplicity, we focus on the degenerate limit setting $H_1 = 0$. Note that on the basis of the results in appendix A, the general case can be treated similarly and the corresponding result will be presented at the end of this subsection.

We first specify the operations under which the spectator Hamiltonian eq. (3.3), considered as a random matrix ensemble, is invariant. As both, the internal Hamiltonian of the environment and the coupling, are selected from the GOE the invariance operations form the group

$$\mathcal{O}(N_e) \times \mathcal{O}(2) \times \mathcal{U}(2), \quad (3.25)$$

and have the structure $O_{N_e} \otimes \exp(i\alpha\sigma_y) \otimes U_2$, with O_{N_e} being an orthogonal matrix (acting in \mathcal{H}_e), α a real number, and U_2 a unitary operator acting on the spectator qubit. The direct product structure of the invariance group obliges us to respect the identity of each particle, but allows to analyze each qubit separately. For instance, if we replace the random coupling matrix $V_{1,e}$ with one which involves both qubits, the invariance group would be $\mathcal{O}(N_e) \times \mathcal{O}(4)$. As a consequence, purity decay would become independent of the entanglement within the qubit pair: for any entangled state one can find an orthogonal matrix which maps the state

onto a separable one ¹.

We write the initial condition $|\psi_{12}\rangle$ as in eq. (3.14). For the coupled particle follows the same analysis made in sec. 2.5. We can thus write $|\tilde{0}_1\rangle = 2^{-1/2} [|0\rangle + \exp(i\gamma)|1\rangle]$ and, in order to respect orthogonality, $|\tilde{1}_1\rangle = 2^{-1/2} \exp(i\zeta) [|0\rangle - \exp(i\gamma)|1\rangle]$. For the second qubit we have the same complete freedom as in eq. (3.2.1). We thus select $|\tilde{0}_2\rangle = |0\rangle$ and $|\tilde{1}_2\rangle = \exp(-i\zeta)|1\rangle$ to erase the relative phase in the first qubit and finally write the initial state as

$$|\psi_{12}\rangle = \frac{\cos\theta(|0\rangle + e^{i\gamma}|1\rangle)|0\rangle + \sin\theta(|0\rangle - e^{i\gamma}|1\rangle)|1\rangle}{\sqrt{2}}. \quad (3.26)$$

The average purity is still given by the double integral expression in eq. (2.11). However, in the present case the mixed initial state $\rho_1 = \text{tr}_2 |\psi_{12}\rangle\langle\psi_{12}|$ must be used. For $\Delta = 0$, the resulting integrand reads

$$A_{\text{II}}(\tau, \tau') = (2 - g_\theta)\bar{C}(|\tau - \tau'|) + 1 - g_\theta + (2g_\theta - 1)\sin^2\gamma, \quad (3.27)$$

where $\bar{C}(|\tau - \tau'|)$ is given in eq. (2.13). Evaluating the double integral, we obtain

$$\langle P(t) \rangle = 1 - \lambda^2 \left\{ t^2 [4 - 2\cos^2(2\theta)\cos^2\gamma] + (4 - 2g_\theta) \left[t\tau_{\text{H}} - B_2^{(1)}(t) \right] \right\}, \quad (3.28)$$

where $B_2^{(1)}(t)$ is given in eq. (2.26). As in the GUE case, this result depends on the entanglement of the initial state and, as in the one-qubit GOE case, it also depends on γ . Again it turns out that Bell states are more susceptible to decoherence than separable states. Note however, that purity as a function of θ is not monotonous. Hence, a finite increase of entanglement does not guarantee that the purity decreases everywhere in time. For separable states, $g_\theta = 1$, we retrieve formula eq. (2.25). However, for completely entangled states, $\theta = \pi/4$ the dependence on γ is lost. This is understood from a physical point of view, noticing that any local unitary operation on a Bell state can be reduced to a single

¹One can see a general state $|\psi_{12}\rangle = \sum_{i=0}^3 (a_i + ib_i)|i\rangle$, $a_i, b_i \in \mathbb{R}$ as characterized by 2 real vectors $\vec{a} = (a_0, a_1, a_2, a_3)$, $\vec{b} = O(b_0, b_1, b_2, b_3) \in \mathbb{R}^4$. We can rotate \vec{a} to a vector having only the first component $\vec{a}' = (a'_0, 0, 0, 0)$ using an orthogonal matrix O . Consider the vector $\vec{b}' = O\vec{b}$ rotated by the same transformation. We next repeat the procedure on the last 3 axes (for \vec{b}') with an orthogonal transformation O' , to obtain a vector having only the first two components. We thus have, an orthogonal transformation that takes $|\psi_{12}\rangle$ to $O'O|\psi_{12}\rangle = \sum_{i=0}^1 (a''_i + ib''_i)|i\rangle = |\alpha\rangle|\alpha\rangle + |\beta\rangle|\beta\rangle$, a separable state.

local unitary operation acting on a single qubit. In other words, given $U_{1,2} = U_1 \otimes U_2$, there exists a unitary U'_1 such that

$$U_1 \otimes U_2 |\text{Bell}\rangle = U'_1 \otimes \mathbf{1} |\text{Bell}\rangle \quad (3.29)$$

($|\text{Bell}\rangle$ is any 2 qubit pure state with $C = 1$, e.g. $|00\rangle + |11\rangle$). We can then say that the invariance properties in the coupled qubit are inherited from the spectator qubit via entanglement.

Let us obtain the standard deviation for the different possible initial conditions in the qubits. We want to analyze the situation separately for a fixed value of concurrence. Then, as the invariant measure of the ensemble of initial conditions, and fixing the amount of entanglement, we shall use the tensor product of the invariant measures in each of the qubits. Since there is no dependence of eq. (3.28) on the second qubit, the appropriate invariant measure is trivially inherited from the invariant measure for a single qubit. The resulting value for the standard deviation is

$$\sigma_P = \frac{4\lambda^2 t^2 \cos^2(2\theta)}{3\sqrt{5}}. \quad (3.30)$$

Based on the appendix A we can also obtain the average purity for $\Delta \neq 0$. The parametrization of the initial states is more complicated since two preferred directions arise, one from the eigenvectors of the internal Hamiltonian and the other from the invariance group. The result can be expressed in the form given in eq. (2.11), with

$$\begin{aligned} \text{Re } A_{\text{II}}(\tau, \tau') &= \bar{C}(|\tau - \tau'|) \left[g_{\theta,\phi}^{(1)} + g_{\theta,\phi}^{(2)} \cos \Delta(\tau - \tau') \right] \\ &\quad + g_{\theta,\phi}^{(1)} - (1 - g_{\theta,\phi}^{(2)}) \cos[\Delta(\tau + \tau') - 2\eta] + \mathcal{O}(\lambda^4, N_e^{-1}). \end{aligned}$$

The angle η is related to a phase shift between the components of any of the eigenvectors of the initial density matrix ρ_1 . Here we can again see the term containing a sum of times, *i.e.* a term that is not a correlation function. However, this term is small, and adequate values must be chosen to see its effect. Still it is observable in numerical simulations, with moderate effort.

3.3 The separate environment Hamiltonian

We proceed to study purity decay with other configurations of the environment. Consider the separate environment configuration, pictured in

fig. 3.1(b). The corresponding uncoupled Hamiltonian is

$$H_0 = H_1 + H_2 + H_e + H_{e'} \quad (3.31)$$

and the coupling is

$$\lambda V = \lambda_1 V_{e,1} + \lambda_2 V_{e',2}. \quad (3.32)$$

From now on we assume that the internal Hamiltonians of the environment and the couplings are chosen from the GUE. The generalization for the GOE can be obtained along the same lines using the corresponding results of sec. 3.2.2. The initial condition has a separable structure with respect to both environments, see eq. (3.5). The coupling in the interaction picture separates into two parts acting on different subspaces $\lambda \tilde{V} = \lambda_1 \tilde{V}^{(1)} + \lambda_2 \tilde{V}^{(2)}$, where

$$\tilde{V}^{(1)} = e^{i(H_1+H_e)} V_{e,1} e^{-i(H_1+H_e)}, \quad \tilde{V}^{(2)} = e^{i(H_2+H_{e'})} V_{e',2} e^{-i(H_2+H_{e'})}. \quad (3.33)$$

Notice that $\tilde{V}^{(1)}$ ($\tilde{V}^{(2)}$) does not depend on $H_{e'}$ (H_e). Since $V^{(1)}$ and $V^{(2)}$ are uncorrelated, quadratic averages separate as

$$\lambda^2 \langle \tilde{V}_{ij} \tilde{V}_{kl} \rangle = \lambda_1^2 \langle \tilde{V}_{ij}^{(1)} \tilde{V}_{kl}^{(1)} \rangle + \lambda_2^2 \langle \tilde{V}_{ij}^{(2)} \tilde{V}_{kl}^{(2)} \rangle. \quad (3.34)$$

This leads to a natural separation of each of the contributions to purity

$$1 - \langle P(t) \rangle = 1 - P_{\text{spec}}^{(1)}(t) + 1 - P_{\text{spec}}^{(2)}(t), \quad (3.35)$$

where $P_{\text{spec}}^{(i)}(t)$ denotes the average purity with particle i being a spectator, as given in sec. 3.2. In this way, the problem formally reduces to that of the spectator model. The respective expressions in sec. 3.2 may be used. For instance, if we assume broken TRI, we obtain from eq. (3.20)

$$\langle P(t) \rangle = 1 - 4 \sum_{i=1}^2 \lambda_i^2 \int_0^t d\tau \int_0^\tau d\tau' \left[g_{\theta, \phi_i}^{(1)} + g_{\theta, \phi_i}^{(2)} \cos \Delta_i \tau' \right] \bar{C}_i(\tau') + \mathcal{O}(\lambda^4, N_e^{-1}), \quad (3.36)$$

where \bar{C}_1 and \bar{C}_2 are the correlation functions of the corresponding environments defined in exact correspondence with eq. (2.13), for H_e and $H_{e'}$ respectively. If in one or both of the qubits, the level splitting in the internal Hamiltonians is very large/small compared to the Heisenberg time in the corresponding environment (denoted by τ_e and $\tau_{e'}$ for H_e and $H_{e'}$, respectively) the degenerate and/or fast approximations may be used. As an example, if $\Delta_1 \ll 1/\tau_e$ and $\Delta_2 \ll 1/\tau_{e'}$ we find

$$P_D(t) = 1 - (2 - g_\theta)(\lambda_1^2 f_{\tau_e}(t) + \lambda_2^2 f_{\tau_{e'}}(t)), \quad (3.37)$$

whereas if $\Delta_1 \gg 1/\tau_e$ and $\Delta_2 \gg 1/\tau_{e'}$

$$P_F(t) = 1 - \lambda_1^2 \left[g_{\theta, \phi_1}^{(1)} f_{\tau_e}(t) + 2\tau_e g_{\theta, \phi_1}^{(2)} t \right] - \lambda_2^2 \left[g_{\theta, \phi_2}^{(1)} f_{\tau_{e'}}(t) + 2\tau_{e'} g_{\theta, \phi_2}^{(2)} t \right]. \quad (3.38)$$

It is interesting to note that if we have two separate but equivalent environments (*i.e.* both Heisenberg times are equal), we get exactly the same result as for a single environment. Also notice that the Hamiltonian of the entire system separates and thus the total entanglement of the two subsystems ($\mathcal{H}_1 \otimes \mathcal{H}_e$ and $\mathcal{H}_2 \otimes \mathcal{H}_{e'}$) becomes time independent.

3.4 The joint environment configuration

The last configuration we shall consider is the one of joint environment; see fig. 3.1(c). Its uncoupled Hamiltonian is

$$H_0 = H_1 + H_2 + H_e \quad (3.39)$$

whereas the coupling is given by

$$\lambda V = \lambda_1 V_{e,1} + \lambda_2 V_{e,2}. \quad (3.40)$$

Notice the similarity with eq. (3.31) and eq. (3.32). However, as discussed in the introduction, they represent very different physical situations. The coupling in the interaction picture can again be split $\lambda \tilde{V} = \lambda_1 \tilde{V}^{(1)} + \lambda_2 \tilde{V}^{(2)}$, where

$$\tilde{V}^{(1)} = e^{i(H_1+H_e)} V_{e,1} e^{-i(H_1+H_e)}, \quad \tilde{V}^{(2)} = e^{i(H_2+H_e)} V_{e,2} e^{-i(H_2+H_e)}. \quad (3.41)$$

Note the slight difference with eq. (3.33). However $V^{(1)}$ and $V^{(2)}$ are still uncorrelated, enabling us to write again eq. (3.34).

From now on, the calculation is formally the same as in the separate environment case. Hence we can inherit the result eq. (3.36) directly, taking into account that since they come from the same environmental Hamiltonian, the two correlation functions are the same. In case any of the Hamiltonians fulfills the fast or degenerate limit conditions, the corresponding expressions to eq. (3.37) and eq. (3.38) can be written. As an example, if the first qubit has no internal Hamiltonian, and the second one has a big energy difference, the resulting expression for purity decay is

$$\langle P(t) \rangle = 1 - \lambda_1^2 (2 - g_\theta) f_{\tau_H}(t) - \lambda_2^2 \left[g_{\theta, \phi_2}^{(1)} f_{\tau_H}(t) + 2\tau_H g_{\theta, \phi_2}^{(2)} t \right] + \mathcal{O}(\lambda^4, N_e^{-1}), \quad (3.42)$$

where τ_H is the Heisenberg time of the joint environment. Monte Carlo simulations showing the validity of the result were done with satisfactory results, comparable to those obtained in fig. 3.4. The parameter range checked was similar to that in the figure.

Chapter 4

Entanglement decay

In the previous chapter we studied purity decay of two qubits. Purity measures entanglement with the environment, but we can wonder how decoherence affects the internal quantum mechanical properties of the central system. Possibly the most important quantum mechanical property of a multi-particle system is its internal entanglement. As discussed in appendix D, a simple and meaningful measure of two qubit entanglement is concurrence (C). Since concurrence is defined in terms of the eigenvalues of a Hermitian 4×4 -matrix, an analytical treatment, even in linear response approximation, is much more involved than in the case of purity. A study along the same lines followed in the last chapters, is out of reach for the time being.

We shall first explore a relation (first found in [PS06], partly explained in [ZB05], and further studied in [PS07]) between concurrence and purity. We show that this relation is valid in a wide parameter range (sec. 4.1). Combining it with an appropriate formula for purity decay, we obtain an analytic prediction for concurrence decay in sec. 4.2. We compare our prediction with Monte Carlo simulations. It is essential that the two qubits do not interact; otherwise the coupling between the qubits would act as an additional sink (or source) for internal entanglement – a complication we wish to avoid. In the last part of the section we extend our ideas to non-Bell states.

4.1 The CP plane

We study the relation between concurrence and purity using the CP -plane, where we plot concurrence against purity with time as a parameter. This plane is plotted in fig. 4.1. The gray area indicates the region of physically admissible states [MJWK01]. The upper boundary of this region is given by the maximally entangled mixed states. This set depends on the entanglement measures chosen [WNG⁺03]. Large purity, *i.e.* low entanglement with the environment, is required in order to have large concurrence, *i.e.* entanglement within the pair. This is a consequence of the monogamy of entanglement. Note also that concurrence becomes identically zero before purity reaches its minimum at $1/4$. Another region of interest, plotted in red in fig. 4.1(a), corresponds to those states (density matrices), which form the image of a Bell state under the set of local (*i.e.* acting separately on each qubit) unital operations [ZB05]. Unital operations are those which preserve the identity [Key02]. Single qubit unital operations include bit flip and phase flip, whereas an example of a non-unital operation is amplitude damping [NC00]. Finally, the Werner states $\rho_W = \alpha \frac{\mathbb{1}}{4} + (1 - \alpha)|\text{Bell}\rangle\langle\text{Bell}|$, $0 \leq \alpha \leq 1$, define a smooth curve on the CP -plane (black solid line). The analytic form of this curve is [PS07]

$$C_W(P) = \max \left\{ 0, \frac{\sqrt{12P - 3} - 1}{2} \right\}, \quad (4.1)$$

and will be referred to as the Werner curve. Note that states mapped to the Werner curve are not necessarily Werner states.

In fig. 4.1(b), we perform numerical simulations in the spectator configuration assuming broken time reversal symmetry (GUE case). We compute the average concurrence for a given interval of purity using 15 different Hamiltonians and 15 different initial states for each Hamiltonian. We fix the level splitting in the coupled qubit to $\Delta = 1$ and consider two different values $\lambda = 0.02$ and 0.14 for the coupling to the environment. Fig. 4.1(b) shows the resulting CP -curves for different dimensions of \mathcal{H}_e . Observe that for both values of λ , the curves converge to a certain limiting curve as $\dim(\mathcal{H}_e)$ tends to infinity. While for $\lambda = 0.02$, this curve is at a finite distance of the Werner curve, for $\lambda = 0.14$ it practically coincides with $C_W(P)$. Varying the configuration, the coupling strength, the level splitting, or the ensemble (GOE/GUE), gives the same qualitative results in the CP plane, for large dimensions. In some cases we have an accumu-

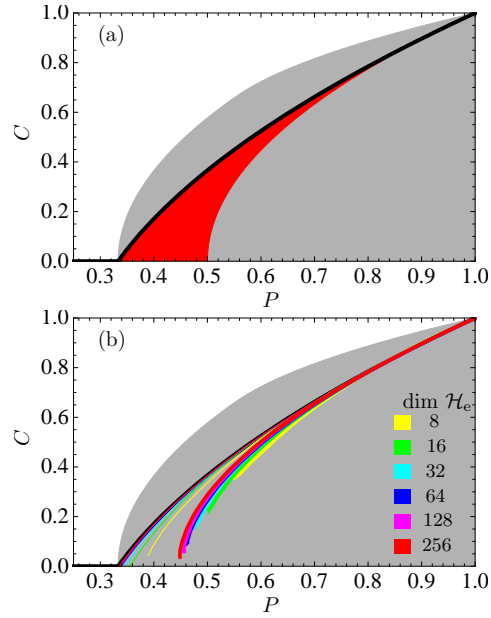


Figure 4.1: We present the CP plane. In (a) we show the area of concurrence-purity (CP) combinations which are allowed for physical states (gray area plus the set $\{(0, P), P \in [1/4, 1/3]\}$). The image of a Bell state under the set of local unital operations defines the red area. The Werner curve eq. (4.1) is shown as a thick black solid line. In (b) we show curves $(\langle C(t) \rangle, \langle P(t) \rangle)$ as obtained from numerical simulations of the spectator Hamiltonian. GUE matrices are used during all numerical experiments in this section. We choose $\Delta = 1$ and vary $\dim(\mathcal{H}_e)$ for two different coupling strengths $\lambda = 0.02$ (thick lines) and $\lambda = 0.14$ (thin lines). The resulting curves are plotted with different colors, according to $\dim(\mathcal{H}_e)$ as indicated in the figure legend.

lation towards the Werner curve, in others there is a small variation, but staying in the unital area.

Are the channels induced by our RMT model (RMT channels) typically unital? If so, we could use the results of [ZB05] to explain our numerical findings. The fact that our RMT channels map Bell states to the unital region only is not enough to ensure unitality. Non-unital channels can also map Bell states into the unital region. The amplitude damping channel acting on a single qubit provides the simplest example. We now examine the question in more detail.

For small dimensions the channels are clearly not unital as can be inferred from fig. 4.2. Bell states are mapped, after the action of our RMT channels, to the non unital region. The probability of these events, however, decrease rapidly with the environment size. Within numerical accuracy, the probability of being mapped outside the unital region, for $\delta = 0.2$ and a time range between 0 and 4000 is $\approx 10^{-5}$ already for $N_e = 32$. For larger dimensions a tighter test must be performed as virtually all points in the CP plane are in the unital region.

We want to test how close to unitality the RMT channels \mathcal{E}_{RMT} are. The channels depend on the particular Hamiltonian chosen from the ensemble, on time, and on the initial condition in the environment. As we want to test unitality of the channel on a single qubit, we can think of the spectator configuration, or the single qubit model. Since we want check how closely $\mathcal{E}_{\text{RMT}}(\mathbb{1}) = \mathbb{1}$, we prepare an initial pure condition (in the qubit plus environment) that leads to a completely mixed state in the qubit, *i.e.*

$$\frac{|0\psi_e^{(0)}\rangle + |1\psi_e^{(1)}\rangle}{\sqrt{2}} \quad (4.2)$$

with $\langle\psi_e^{(i)}|\psi_e^{(j)}\rangle = \delta_{ij}$. We let the state evolve with a particular member of the ensemble of Hamiltonians defined in eq. (2.2). Afterwards we evaluate the Euclidean distance $d(\cdot, \cdot)$ in the Bloch sphere, of the points corresponding to the resulting mixed state in the qubit and the fully mixed state. For unital channels this distance should be exactly zero. The average distance is plotted as a function of the size of the environment in fig. 4.3, for two coupling values, and various times. Instead of reporting the times, we report the approximate value of concurrence a Bell pair would have after the corresponding time, and thus the area to which it would be mapped in the CP plane. We conclude from the figure that the unitality condition is approached algebraically fast as the size of the

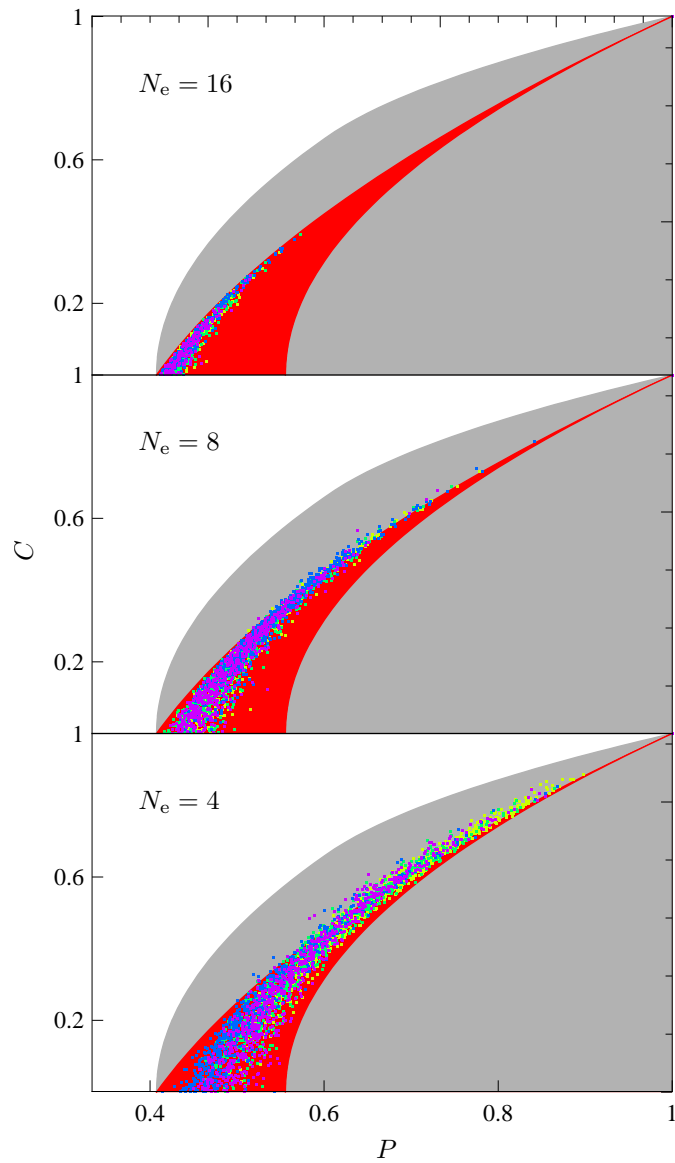


Figure 4.2: We show the points reached in the CP plane after the evolution with different sizes of the environment. Four initial conditions (with different colors) are studied per environment size. For very small environments the evolution can reach regions outside the unital region. Here we use the spectator configuration, $\delta = 0.2$, and $\Delta = 0$ with the GUE model.

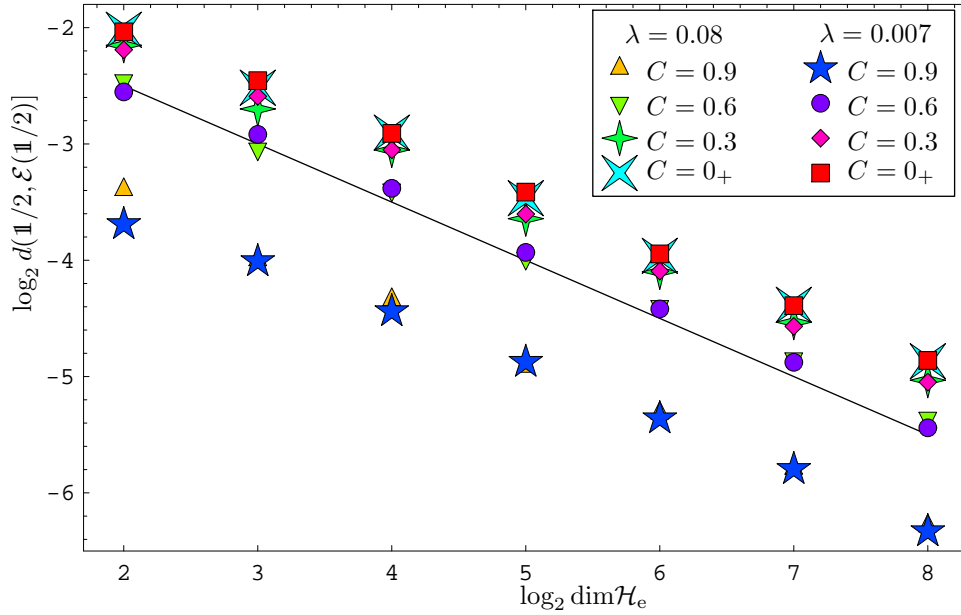


Figure 4.3: We evaluate the unitality condition for the spectator configuration (*i.e.* on one of the qubits). We vary the size of the environment and test different times, that would lead approximately to different values of concurrence as shown in the inset. See text for details. $C = 0_+$ refers to the value a time step immediately before $C = 0$. A line with slope $-1/2$ is included for comparison.

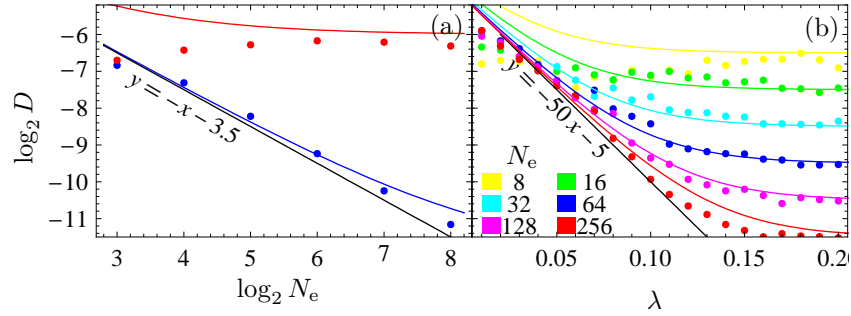


Figure 4.4: We show D [eq. (4.3)] which measures a “distance” in the CP plane between numerical curves for the RMT model and the Wigner curve. In (a) its dependence with the size of the environment is studied for two cases. For $\lambda = 0.02$ (red dots) a finite value is approached, whereas for $\lambda = 0.14$ algebraic decay is seen. The black solid line, which is proportional to N_e^{-1} , is meant as a guide to the eye. In (b) we plot D as a function of the coupling λ , for various values of N_e . In the large environment limit, and for $\lambda \ll 0.1$, we have a noticeable deviation from the Werner curve. In all cases $\Delta = 1$.

environment increases.

We have established convincingly that the RMT channels are nearly unital. For large purities this allows to establish a one to one relation between purity and concurrence, as the unital area converges rapidly to the line $C = P$. Another fact remains to be clarified. When/how do the curves approach the Werner curve?

To study this situation in more detail, consider a CP -curve $C_{\text{num}}(P)$, obtained from our numerical simulations, and define its “distance” D to the Werner curve as

$$D = \int_{P_{\min}}^1 dP |C_{\text{num}}(P) - C_W(P)|. \quad (4.3)$$

It is sensible to compare D with the unital area $D_u = 1/18$. The behavior of D as a function of the size of the system is shown in fig. 4.4(a). For $\lambda = 0.14$ (black dots), the error goes to zero in an algebraic fashion, at least in the range studied. In fact, from a comparison with the black solid line we may conclude that the deviation D is inversely proportional to the dimension of \mathcal{H}_e . By contrast, for $\lambda = 0.02$ (red dots), D tends to a finite value, in line with the assertion that the numerical results converge to a

different curve. In fig. 4.4(b) we plot the error D as a function of λ , for different dimensions of \mathcal{H}_e . The results suggest an exponential decay of D with the coupling strength. The simplest dependence of the deviation in agreement with these two observations is

$$D_{\Delta=1} = \frac{1}{2^{3.5}N_e} + \frac{1}{2^{5+50\lambda}}. \quad (4.4)$$

We also plot the curves corresponding to this ansatz in fig. 4.4. Good agreement is observed for $D \ll D_u$. Notice the exponential decay of D with respect to λ . One can thus, in an excellent approximation for large λ , say that for large dimensions the limiting curve is the Werner curve. For $\Delta = 0$, all studied couplings numerical convergence to the Werner curve was observed in the large N_e limit.

In the presence of TRI the CP -curves a similar behavior is observed whenever $\Delta > 0$. However, in contrast to the GUE case, no saturation of the deviation D was observed when $\Delta = 0$. In the other configurations considered (the joint and the separate environment), the behavior is similar. In those cases it is the largest (of the two) coupling strength which dominates the behavior in the CP plane (as well, naturally, as in time).

4.2 Entanglement decay

Sufficiently close to $P = 1$, the above arguments imply a one to one correspondence between purity and concurrence, which simply reads $C \approx P$. This allows to write an approximate expression for the behavior of concurrence as a function of time

$$C_{\text{lr}}(t) = P_{\text{LR}}(t), \quad (4.5)$$

using the appropriate linear response result for the purity decay. The corresponding expressions for purity decay have been discussed in detail in the previous chapters. Eq. (4.5) has similar limits of validity as the linear response result for the purity. As it follows from a linear response approximation for purity, we call it a linear response expression for concurrence decay.

In those cases where the deviation from the Werner curve [see eq. (4.1)] is small and where the exponentiated linear response expression eq. (2.21) holds for the average purity, we can write down a phenomenological

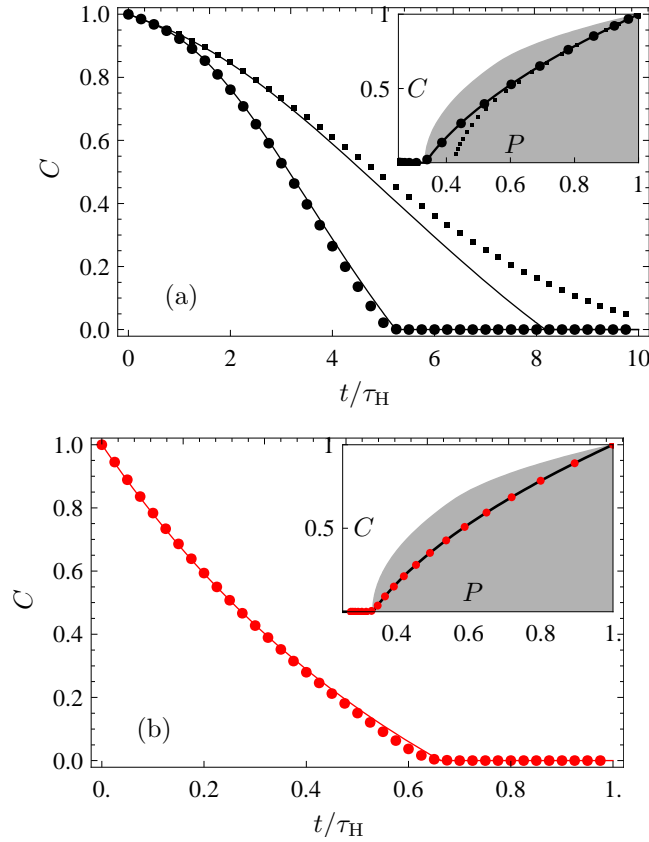


Figure 4.5: We show numerical simulations for the average concurrence as a function of time in the joint environment configuration (GUE case). In (a) we consider small couplings $\lambda_1 = \lambda_2 = 0.01$ which lead to the Gaussian regime for purity decay. The red symbols show the result without internal dynamics, whereas the black symbols are obtained for fast internal Rabi oscillations ($\Delta_1 = \Delta_2 = 10$). The theoretical expectation for concurrence decay based on eq. (4.6) and eq. (3.36) is plotted in the corresponding color. In (b) we consider stronger couplings, $\lambda_1 = \lambda_2 = 0.1$, such that purity decay becomes essentially exponential (Fermi golden rule regime), while the level splitting have been set to $\Delta_1 = \Delta_2 = 0.1$ (red symbols). The theoretical expectation (red solid line) is based on the same expressions as in (a). The insets display the corresponding evolution in the CP -plane with the same symbols as used in the main graph. In addition, the physically allowed region (gray area) and the Werner curve (black solid line) are shown. In all cases $N_e = 1024$

formula for concurrence decay, which is valid over the whole range of the decay

$$C_{\text{elr}}(t) = C_W(P_{\text{ELR}}(t)). \quad (4.6)$$

In fig. 4.5 we show random matrix simulations for concurrence decay in the joint environment configuration. We consider small couplings $\lambda_1 = \lambda_2 = 0.01$ which lead to the Gaussian regime for purity decay, as well as strong couplings $\lambda_1 = \lambda_2 = 0.1$ which lead to the Fermi golden rule regime. We find good agreement with the prediction of eq. (4.6), except for the Gaussian regime when we switch-on a fast internal dynamics in both qubits ($\Delta_1 = \Delta_2 = 10$) and consequently D is large. See the insets in fig. 4.5. Notice how in both the heuristic formula and the Monte Carlo simulations, we observe entanglement sudden death [YE04].

Note that, in the separate environment case, the entanglement of the two subsystems defined on the spaces $\mathcal{H}_1 \otimes \mathcal{H}_e$ and $\mathcal{H}_2 \otimes \mathcal{H}_{e'}$ is constant in time. For the initial conditions we use, the entanglement stems entirely from the two qubits. The concurrence of these two qubits decays because the constant entanglement spreads over all constituents of the two large subspaces.

We now investigated pure initial states of the qubits that are not Bell states. Consider the GUE case with no internal Hamiltonian, in the spectator configuration. As discussed in previous sections, thanks to the symmetry of the ensemble, we can write the state as

$$|\psi_{12}\rangle = \cos\theta|00\rangle + \sin\theta|11\rangle. \quad (4.7)$$

The initial concurrence is $C_0 = \sin 2\theta$; for $\theta = \pi/4$ we obtain initial Bell states. Applying the totally depolarizing channel to one or both qubits, results in Werner states. For $\theta \not\equiv \pi/4 \pmod{\pi/2}$, applying the channel to a single qubit or to both qubits results in different evolutions in the CP plane. Since we are considering the spectator configuration it is sensible to apply it to a single qubit. If we parametrize the depolarizing channel [NC00] using the Kraus operators $\{\sqrt{1-\gamma}\mathbb{1}, \sqrt{\gamma/3}\sigma_x, \sqrt{\gamma/3}\sigma_y, \sqrt{\gamma/3}\sigma_z\}$, we obtain the state

$$\rho = \begin{pmatrix} \frac{1}{3}(3-2\gamma)\lambda & 0 & 0 & \frac{1}{3}(3-4\gamma)\sqrt{(1-\lambda)\lambda} \\ 0 & \frac{2}{3}\gamma(1-\lambda) & 0 & 0 \\ 0 & 0 & \frac{2\gamma\lambda}{3} & 0 \\ \frac{1}{3}(3-4\gamma)\sqrt{(1-\lambda)\lambda} & 0 & 0 & \frac{1}{3}(3-2\gamma)(1-\lambda) \end{pmatrix}, \quad (4.8)$$

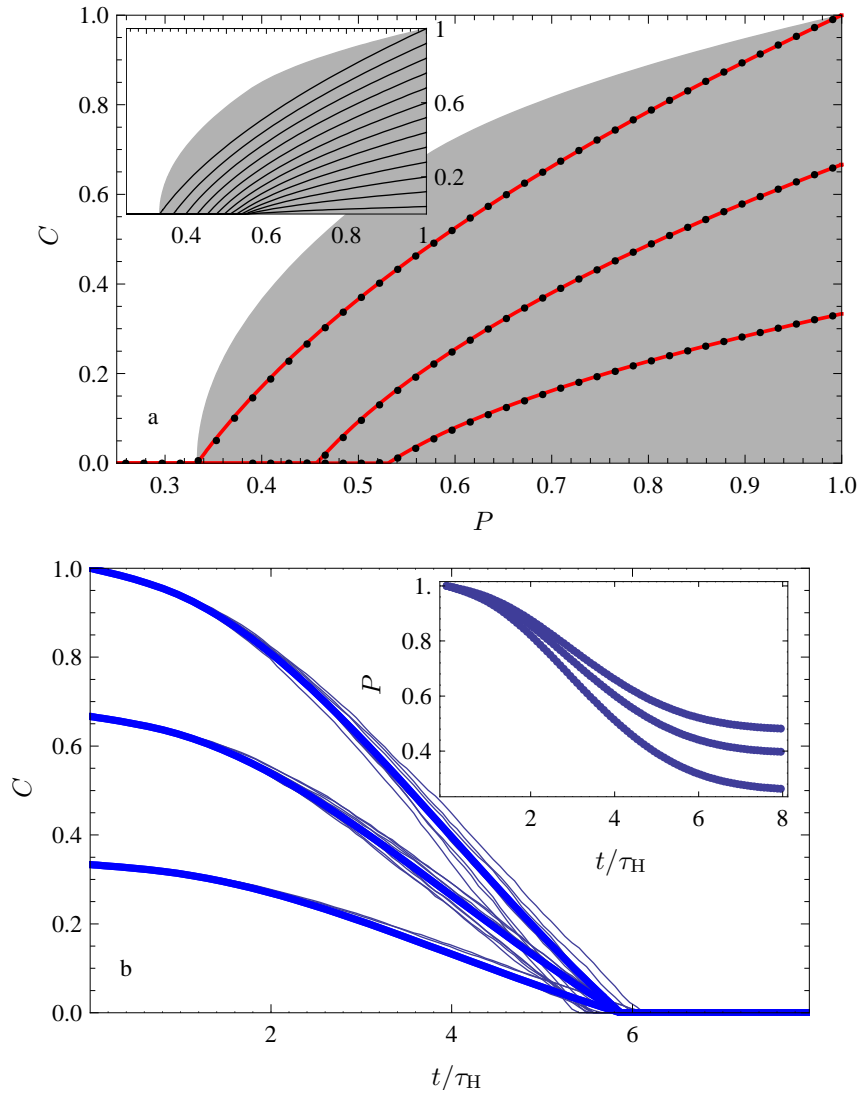


Figure 4.6: On the top panel the behavior in the CP plane for different pure states is shown. We let the initial states have $C = 1, 2/3$, or $1/3$. The red curves are the ones described by the states when a totally depolarizing channel acts on the first qubit, whereas the black dots correspond to Monte Carlo simulations. In the inset we see theoretical curves for other initial concurrences. On the lower panel in the inset, we see the exponentiated formula for purity decay (blue line) and the Monte Carlo averaged purity (black dots). On the main panel we see theoretical result (blue line) and 30 samples from the numerical ensemble (thin black lines). $\Delta = 0$, $\lambda = 0.01$, and $\dim \mathcal{H}_e = 256$.

with $C_0 = 2\sqrt{\lambda(1-\lambda)}$. Concurrence for this state is $\max\{C_0(1-2\gamma), 0\}$ and purity is $1 + [4\gamma^2(2+C_0) - 6\gamma(2+C_0^2)]/9$. Inverting gamma in terms of purity and the initial concurrence, we can insert it in the formula for concurrence to obtain the Werner-like relations

$$C_{W,C_0} = C_0 \begin{cases} \frac{3}{2} \sqrt{1 - \frac{4(1-P)}{2+C_0^2}} - \frac{1}{2} & \text{if } 9P > 5 - C_0^2, \\ 0 & \text{otherwise} \end{cases}. \quad (4.9)$$

The comparison between numerics and the ansatz is presented in fig. 4.6(a). The agreement is more than satisfactory. We also show in the inset a set of curves for more values of C_0 . The success of the description allows to give a heuristic concurrence decay formula for initial states, not being Bell states along the same lines as in the previous paragraphs and using eq. (4.9) instead of eq. (4.1). A comparison between our heuristic formula and Monte Carlo simulation is presented in fig. 4.6(b). Note that "sudden death" of entanglement [YE04] persists, though it happens at different purities. This is also visible for the individual members of the ensemble.

$$C_{W,C_0} = \max \left\{ 0, \frac{C_0 - 1}{3} + \frac{1 + 2C_0}{3} \operatorname{Re} \frac{-1 + \sqrt{1 - (1 + C_0^2)(3 - 6P - C_0^2)}}{1 + C_0^2} \right\} \quad (4.10)$$

is the analogous expression for concurrence in terms of purity, when both qubits are coupled with similar strength.

Chapter 5

An example, the KI chain

5.1 Introduction

In this chapter we continue studying decoherence and entanglement decay using two qubits as the central system. We pursue two main objectives. The first one is to test some of the qualitative and quantitative conclusions we have derived in the previous chapters, in a deterministic model. The second one is to explore dynamical regimes that, up to this point, we have ignored: integrable dynamics and intermediate dynamics (not integrable but with chaos not fully developed). We shall focus on three points. First we wish to study how dynamics of the environment, *i.e.* its integrability or chaoticity influence the behavior of decoherence and internal entanglement. Second, we shall analyze to what extent purity and concurrence may be related. In particular we want to test the reach of the relation discovered in sec. 4. Finally, we wish to relate quantitatively the behavior of purity, in the chaotic regime, with the results obtained with RMT in the previous chapters. To implement such a program we need a model with flexible dynamics, which allows efficient numerics for large Hilbert spaces.

The fact that the central system consists of two qubits, makes a spin system an attractive candidate. Indeed the kicked Ising spin chain, a model introduced by Prosen [Pro02], was used to study decay of fidelity and purity [PS02] in echo dynamics for integrable, chaotic (more precisely mixing [Pro00]) as well as for intermediate cases. Results for purity in echo dynamics can be used for purity decay in standard forward dynamics if

the perturbation is chosen as the coupling between the central system and the environment, sec. 2.2. The main advantage of this model is the high computational efficiency that allows to perform numerical calculations up to twenty qubits [PSPS06] and more on any good workstation. Yet the model in its original form does not allow for variable Ising interactions, and is thus not well suited outside of the field of echo dynamics. Experimental realizations of similar models have been proposed [BMM05] and related studies appeared in [LS05].

In the present chapter we shall generalize this model allowing arbitrary interactions between the spins, and site dependent kicks (this does not affect the numerical efficiency of the model, see appendix B). We then use the generalized model to study the evolution of purity and concurrence of central system (consisting of two spins) initially in a Bell state, evolving in environments with different dynamical properties. As we want concurrence to be affected solely by the coupling to the environment, we choose non-interacting spins for the selected pair. Some preliminary results were published in [PS06]. For the environment it is sensible to consider random states to emulate a bath at fairly high temperature. Using unitary time evolution of the total system and partial tracing over the environment we can then calculate concurrence and purity decay of the selected pair, and discuss their behavior.

To discuss the general model we first recall and discuss a particular case of the model which, in fact, will help to understand the properties of the environment (sec. 5.2). Then we state the general model and discuss the particular configurations to be studied (sec. 5.3). Next we proceed to discuss the behavior in time of both concurrence and purity for the different configurations and different dynamics, sec. 5.4. Afterwards, in sec. 5.5, we discuss the relation between concurrence and purity. Finally, we compare purity evolution with the corresponding RMT model in sec. 5.6.

This chapter is largely based on [PS06]; however, we have learned a lot since its publication. Further research and major rewriting were thus required to contextualize and discuss the results presented here. We added new configurations and discuss in detail the physical differences between the different models. The comparison with RMT is now possible as the theory is completed.

5.2 The kicked Ising spin chain

We first study the *kicked Ising chain* (KIC) [Pro02]: A ring of L spin $1/2$ particles which interact with their nearest neighbors via a homogeneous Ising interaction of dimensionless strength J , and are periodically kicked with a dimensionless homogeneous magnetic field \vec{b} . The Hamiltonian is thus

$$H = J \sum_{j=1}^L \sigma_j^z \sigma_{j+1}^z + \delta_1(t) \sum_{j=1}^L \vec{b} \cdot \vec{\sigma}_j \quad (5.1)$$

where $\delta_1(t) = \sum_{n \in \mathbb{Z}} \delta(t - n)$ represents an infinite train of Dirac delta functions with primitive period one; $\sigma_j^{x,y,z}$ are the Pauli matrices of particle j and $\vec{\sigma}_j = (\sigma_j^x, \sigma_j^y, \sigma_j^z)$. We must also impose periodic conditions in order to close the ring: $\vec{\sigma}_{L+1} \equiv \vec{\sigma}_1$. During the free evolution, *i.e.* between the kicks, the system evolves with the unitary propagator

$$U_{\text{Ising}}(J) = \exp \left(-iJ \sum_{j=1}^L \sigma_j^z \sigma_{j+1}^z \right), \quad (5.2)$$

and the action of the kick is described by the unitary operator

$$U_{\text{kick}}(\vec{b}) = \exp \left(-i \sum_{j=1}^L \vec{b} \cdot \vec{\sigma}_j \right). \quad (5.3)$$

The Floquet operator for one period is thus

$$U_{\text{KI}} = U_{\text{Ising}}(J) U_{\text{kick}}(\vec{b}). \quad (5.4)$$

A detailed discussion of the symmetries of the system can be found in [PP07]. We summarize the main observations here. Due to the homogeneity of the kick \vec{b} and the nearest neighbor interaction J , the system has a rotational symmetry $\vec{\sigma}_j \rightarrow \vec{\sigma}_{j+1}$. The dimension of each of the invariant subspaces (\mathcal{H}_k with $k = 1, \dots, L$) is close to $2^L/L$ for large L . Each of the invariant subspaces has an anti-unitary symmetry which, if we choose a base in which $\vec{b} \cdot \vec{\sigma}_j$ is real, is complex conjugation (*i.e.* not conventional time reversal symmetry). Since each minimal invariant subspace has an internal anti-unitary symmetry, it is reasonable to compare with the GOE or the COE to understand the properties of the system.

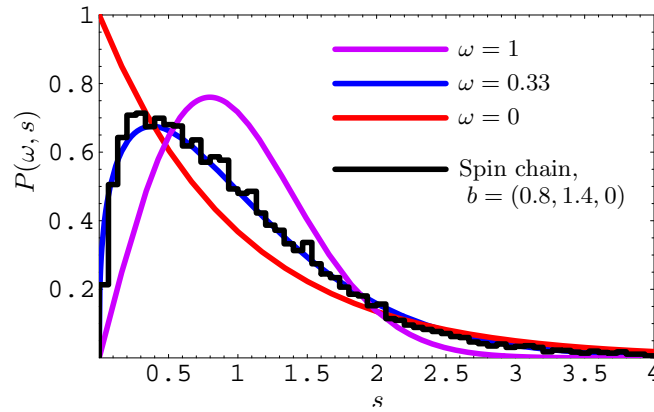


Figure 5.1: The nearest-neighbor spacing of the homogeneous spin ring (as a black curve) with a magnetic kick $b = (0.8, 1.4, 0)$. We compare with the Brody distribution $P(\omega, s)$. Its limiting values $\omega = 1$ and $\omega = 0$ yield GOE and Poissonian statistics respectively. Intermediate values suggest intermediate dynamics. Here we use 15 qubits.

As mentioned above the system is very rich regarding its dynamics. Various parameter combinations yield integrable (meaning analytically solvable) dynamics. In particular setting the magnetic kick parallel or perpendicular to the preferred direction of the Ising interaction implies integrability. However, using \vec{b} parallel to the Ising interaction yields trivial integrability (all σ_j^z commute with the Hamiltonian), so we shall use \vec{b} perpendicular to the z axis. In particular we shall set $\vec{b} = (0, 1.53, 0)$ since for this parameter some oscillations that we shall observe have a bigger amplitude and period. In order to obtain chaotic dynamics one cannot just choose parameters outside the set that yield integrable dynamics. One must be “far enough” from this set. We verified that for $J = 1$, $b = (1.4, 1.4, 0)$ (used in this chapter) and $J = 0.7$, $b = (0.9, 0.9, 0)$ (used in the following one) the system is chaotic (see [PSPS06, PP07]); many statistical tests like the nearest-neighbor spacing, the form factor, and the skewness, were applied. Except at extremely large energies, no significant deviations from RMT were observed. In order to obtain intermediate dynamics we wanted to be far enough from both integrability and completely mixing dynamics to have an appreciable compromise regarding spectral statistics. For $J = 1$ and $b = (0.8, 1.4, 0)$ we indeed find intermediate spectral statistics. Their nearest-neighbor spacing is characterized

by a Brody parameter [Bro73] of 0.33, see fig. 5.1. The nearest-neighbor spacing distribution in the Floquet spectrum shows a marked level repulsion, but it is still quite far from the distribution we expect and get for the chaotic case.

5.3 A generalized kicked Ising model

The Hamiltonian of the generalized kicked Ising model is

$$H = \sum_{j>k=1}^L J_{j,k} \sigma_j^z \sigma_k^z + \delta_1(t) \sum_{j=1}^L \vec{b}_j \cdot \vec{\sigma}_j. \quad (5.5)$$

The model thus consists of a set of L spin 1/2 particles coupled to all other spins by an Ising interaction (first term) and periodically kicked by a site dependent tilted magnetic field (second term).

Our model differs from the one stated in eq. (5.1) by the fact that the coupling $J_{j,k}$ is between any pair of particles and has an arbitrary strength. This freedom allows to build a variety of models with different topologies. Each of them will correspond to a well defined physical picture, and thus we show how the flexibility of the model can be exploited to study diverse physical situations in a common framework. We also allow site independent kicks to be able to have (or not) internal dynamics in our central system.

The central system is composed of two spins, say spins “1” and “2”. We are left with $q_e = L - 2$ spins which are going to be considered as the environment. We furthermore diminish the number of parameters by setting $\vec{b}_1 = \vec{b}_2 = \vec{b}_c$ and $\vec{b}_3 = \dots = \vec{b}_L = \vec{b}_e$. The fact that we keep the kick in the central system can represent local operations made by the “owners” of each of the qubits, and will not affect the values of concurrence and purity. We shall furthermore require weak coupling of the central system to the environment. Thus $J_{i,1}$ and $J_{i,2}$ must be much smaller than the typical Ising interaction within the environment. We set $J_{2,1} = 0$ in order to prevent any interaction between the spins in the central system.

We propose in particular six models. They are schematically drawn in fig. 5.2. The open circles represent qubits 1 and 2 (the central system) whereas the filled circles represent the other qubits (environment). The

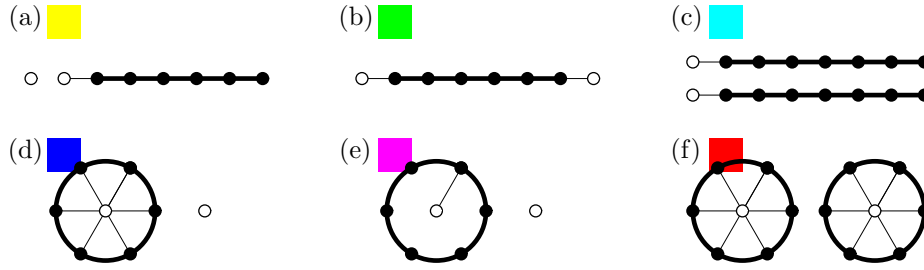


Figure 5.2: Different configurations of the coupling of the central system (represented as open circles) to the spins that act as environment (represented as filled circles). Thick/thin lines represent J'_{ce}/J_e respectively. The description for each model and its features is given in the main text.

thin lines represent a weak Ising interaction J'_{ce} of a particle in the central system with one in the environment. The thick lines represent an interaction J_e among particles in the bath; in all numerical results presented we fix $J_e = 1$. Finally we note that the dimension of the Hilbert space of the environment is $N_e = 2^{q_e}$. Writing the Hamiltonian for each of the models we propose is now a trivial task. As an example we write the Hamiltonian of the model (a) in fig. 5.2: Rewriting the Hamiltonian in terms of central system, environment and interaction as $H = H_c + H_e + H_{ce}$ the parts are given by

$$H_c = \delta_1(t) \sum_{j=1}^2 \vec{b}_c \cdot \vec{\sigma}_j, \quad (5.6)$$

$$H_e = J_e \sum_{j=3}^{L-1} \sigma_j^z \sigma_{j+1}^z + \delta_1(t) \sum_{j=3}^L \vec{b}_e \cdot \vec{\sigma}_j \quad (5.7)$$

$$H_{ce} = J'_{ce} \sigma_2^z \sigma_3^z. \quad (5.8)$$

Each of the models has a characteristic Heisenberg time τ_H . For a system with no symmetries the Heisenberg time is defined simply as $2\pi/d$, where d is the mean level spacing. If the system has symmetries, for each sector we have a Heisenberg time defined again as $2\pi/d$, but d is the mean level spacing in each sector. We shall stress the Heisenberg time of each model, as our RMT models show a strong dependence on it [e. g. eq. (3.23)]. We also use a normalized coupling J_{ce} , which gives a model independent coupling strength. Finally, we want to mention the

corresponding configuration (spectator, joint environment or separate environment), as in sec. 3.1.

Please refer to fig. 5.2 while reading the descriptions.

- Model (a) is in the spectator configuration. A single qubit is coupled to the extreme of an open chain. Due to the breaking of the symmetry of the coupling, the Heisenberg time of the environment is $\tau_H \approx N_e$. We use the normalized coupling $J_{ce} = J'_{ce}$.
- The second model is a variation of the previous one. In this the second qubit is coupled to the other extreme of the chain. It is an example of the joint environment configuration. Again $\tau_H \approx N_e$, however to have the same effective coupling we must scale $J_{ce} = \sqrt{2}J'_{ce}$.
- Model (c) is the last of this family of models in which the environment is an open chain. In this case $\tau_H \approx \sqrt{N_e} \ll N_e$. As we have two coupling spots, we must scale $J_{ce} = \sqrt{2}J'_{ce}$. This is a good example of a separate environment Hamiltonian. This, and the previous two models, were analyzed in [PS06].
- Model (d) is again in the spectator configuration, but here we have a ring (thus the translational symmetry is not broken) and the coupling is symmetric. The Heisenberg time is then related to each symmetry sector separately and is approximately equal to N_e/q_e . The coupling must be normalized to $J_{ce} = \sqrt{q_e}J'_{ce}$.
- The next model differs from the previous one only inasmuch that the coupling is not symmetric. This is enough to mix the invariant subspaces and thus the Heisenberg time is $\approx N_e$. There is a single coupling and thus it is enough to set $J_{ce} = J'_{ce}$.
- Model (f) is another example of a separate environment configuration. It has the smallest Heisenberg time, since the coupling does not break the symmetry of the ring. Thus, it is approximately $\sqrt{N_e}/q_e$. The coupling is normalized to $J_{ce} = \sqrt{q_e}J'_{ce}$.

It is pertinent to mention, that the degree of chaoticity was obtained for cyclic chains, while the chains representing some of our environments are open. Yet, for large number of spins, this is irrelevant.

The non-unitary evolution of the central system alone is calculated along the same lines as for the RMT models. We perform a unitary evolution of the whole system (yielding state $|\psi(t)\rangle\rangle$) and then we partial trace over the environment. That is

$$\rho(t) = \text{tr}_e |\psi(t)\rangle\rangle\langle\langle\psi(t)|. \quad (5.9)$$

We shall consider an initial condition

$$|\psi(t=0)\rangle\rangle = |\psi_{\text{Bell}}\rangle\rangle \otimes |\psi_{\text{env}}\rangle\rangle, \quad (5.10)$$

i.e. a general Bell state [any state such that $C(|\psi_{\text{Bell}}\rangle\rangle\langle\langle\psi_{\text{Bell}}|) = 1$] not entangled with the environment, which is in a pure random state [for models (a), (b), (d), and (e)] or in a tensor product of pure random states in each section of the environment [for models (c) and (f)].

5.4 The evolution of concurrence and purity

We now present the results of our numerical calculations of both concurrence and purity of the selected pair of spins as a function of time. We first concentrate on the short time behavior.

Fig. 5.3 shows the time evolution of purity of the selected pair of spins for the initial state consisting of a Bell pair in the central system and the appropriate random state in the environment. We choose the environment to be chaotic in one case and integrable in the other, using the corresponding parameters mentioned in sec. 5.2. The chaotic environment leads to linear decay for some time interval, while the integrable environment leads to a quadratic decay. The interval in which the linear decay can be observed depends on two things: the configuration and the dimension of the environment. Indeed, for configuration (f) we have the shortest linear decay but we also have the shortest Heisenberg time. The reader is encouraged to check table 5.4 to understand better our numerical results. Recall that in all our derived formulae, we predicted linear decay before Heisenberg time. The situation for the integrable case is different. We observed a marked quadratic decay, independent of the configuration and the size of the environment. We believe that one should be able to explain the results (for the integrable situation) with exact analytic calculations, however the aim of this chapter is not to explain the details, but to illustrate the qualitative differences between having a chaotic and regular environment.

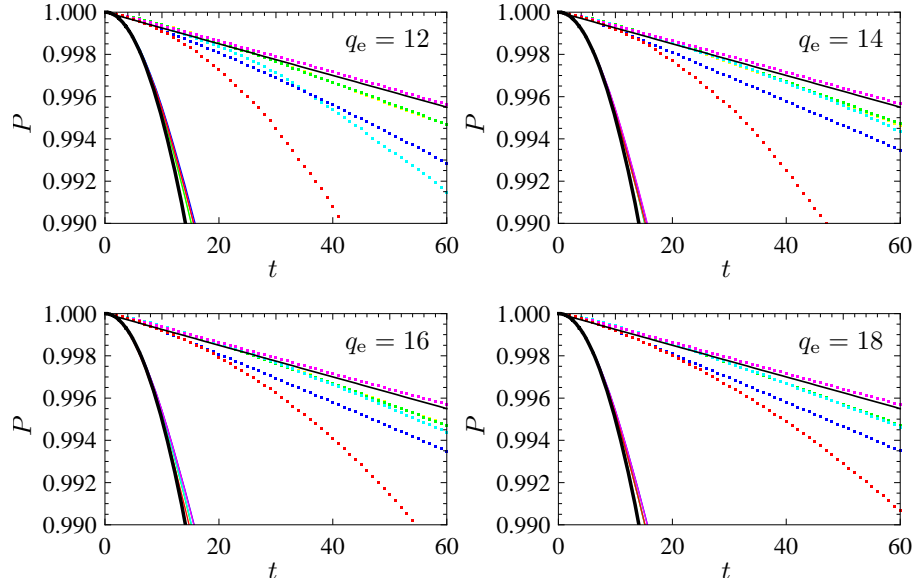


Figure 5.3: These figures show the evolution of purity for a single initial condition per configuration, for chaotic (points) and integrable (thin lines) dynamics. All different configurations from fig. 5.2 are tested (we keep the corresponding color coding). In the chaotic case, purity shows a linear dependence on time whereas in the integrable one, it exhibits a quadratic decay. We also plot the line $1 - 3J_c^2 t$ and the parabola $1 - 2J_c^2 t^2$ with thick black curves, as guides. We vary the size of the environment to understand the scaling with q_e . The corresponding plots for concurrence are indistinguishable from the ones presented here. We have set $J_c = 0.005$ and $\vec{b}_c = \vec{b}_e$.

	(a) ■	(b) ■	(c) ■	(d) ■	(e) ■	(f) ■
$q_e = 12$	4096	4096	64	341.3	4096	10.7
$q_e = 14$	16348	16348	128	1170.3	16348	18.3
$q_e = 16$	65536	65536	256	4096	65536	32
$q_e = 18$	262144	262144	512	14563	262144	56.9

Table 5.1: Numerical values of the Heisenberg times for the different configurations of the environment, and different sizes of it.

We now proceed to look at the long-time evolution of concurrence and purity again for all configurations. In Fig. 5.4 we show both concurrence and purity for integrable, intermediate and chaotic situations.

For the integrable case we see that for some configurations [(a), (b), and (c)] after the initial quadratic decay there is a full revival of both concurrence and purity. However the autocorrelation function of the full system (not shown) drops fast and reaches negligible values even after the first few kicks. It is also worthwhile to note that the oscillations of purity imply increase in some cross-correlation function [PSŽ03]. For the other configurations there is no such revival, and the decay seems Gaussian; this is in agreement with the quadratic decay observed for large purities. Notice that in all the configurations in which there is a revival the coupling is to one end of a chain. Notice how concurrence drops to exactly 0 after a finite time.

For the chaotic case we observe a monotonic decay of both purity and concurrence. The speed at which they decay, though initially the same, is quite different for the different configurations. This can be explained with the huge differences in the Heisenberg times of the environment.

For the mixed case, we observe a compromise among the behavior in the integrable case and the chaotic one. Interestingly in all cases we observed that concurrence drops identically to zero after some time, in contrast with purity which does not reach its minimum.

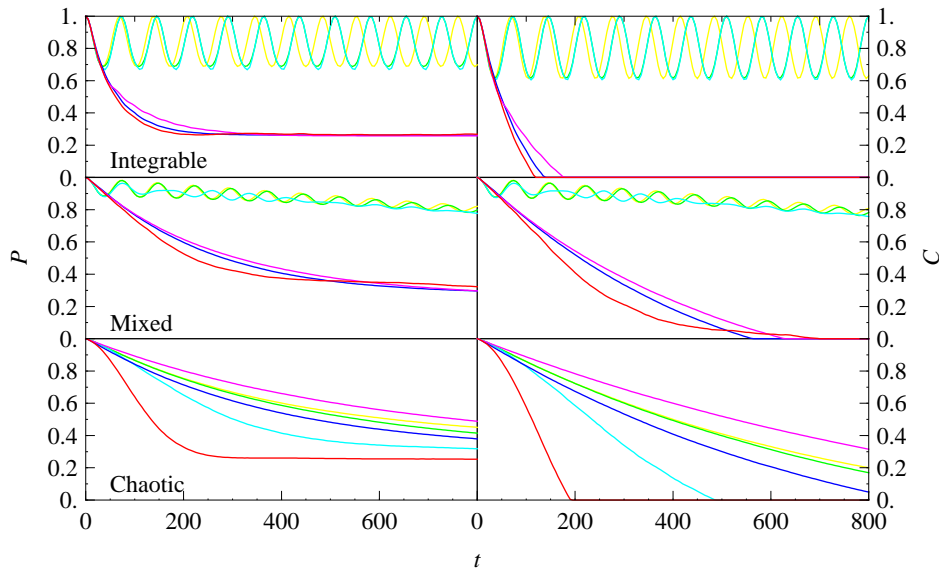


Figure 5.4: Long-time behavior of purity (left) and concurrence (right) for an arbitrary initial condition in integrable (top), non-ergodic and non-integrable (middle), and fully chaotic (bottom) regimes. For the integrable regimes we observe recurrences for the open environment configurations and fast, possibly Gaussian, decay in the others. For the intermediate case we observe in some instances the superposition of oscillations together with the exponential decay. For the chaotic case we observe exponential decay together with a marked dependence on the kind of environment. We have set $q_e = 16$, $J_c = 0.02$, and $\vec{b}_c = \vec{b}_e$.

5.5 A relation between concurrence and purity

The rather similar pictures emerging for concurrence and purity suggest that a simple relation between the two might emerge. Indeed, from the results of the previous chapter this could be expected for the chaotic case. Unfortunately we are not able to access such a big range of values of the coupling as in the previous section; too strong coupling leads to total concurrence decay after a single period (remember that we are dealing with Floquet operators). Too weak couplings imply too long runs as we have to integrate one step at a time. On the other hand, we are going to be able to test the relation not only on chaotic situations but also in other dynamical regimes such as integrable environments and intermediate environments.

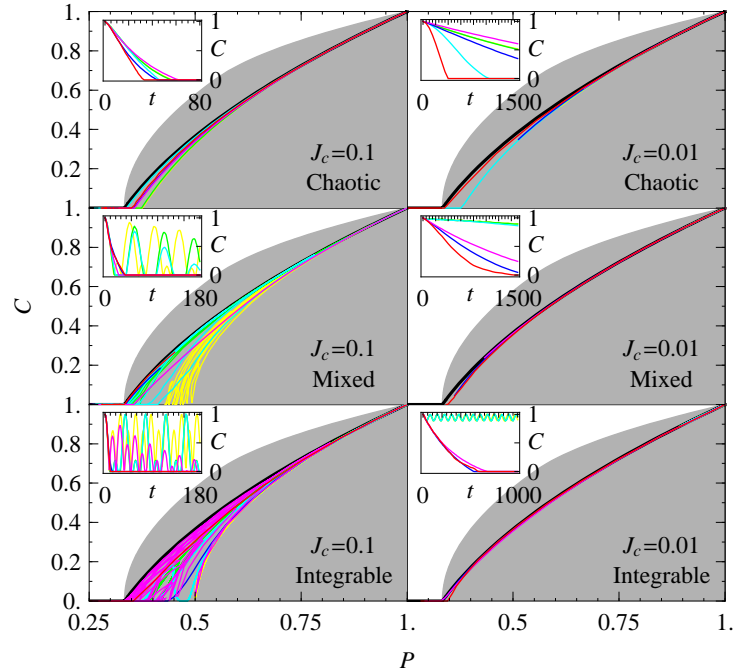


Figure 5.5: The evolution of a random initial condition, in the (C, P) plane, for different dynamical regimes: integrable, intermediate, and chaotic, for two different coupling strengths. All configurations are tested, the color indicates the configuration, as in fig. 5.3. In the thermodynamical limit all curves seem to fall in the unital region. For smaller couplings there is a tendency to stick to the Werner curve. For stronger couplings, in the integrable and intermediate regime, they seem to fill the unital area. We set here $q_e = 16$, and $\vec{b}_c = \vec{b}_e$. The gray region and the black thick line have the same meaning as in fig. 4.1.

We plot in fig. 5.5 concurrence against purity in all the dynamical regimes studied so far. We do so for two strengths of the perturbation, namely $J_c = 0.1$ and 0.01 . A wide variety of behaviors are observed. One thing that stands out is that all curves lie in the unital region. Indeed for $J = 0.1$, in the integrable and intermediate regime we observe a filling of the unital region [recall it from fig. 4.1]. This is not a finite dimension effect: we verified that the behavior remains for increasing dimension of the environment in both cases. For small dimensions, and in configuration (b) one observes that the curves do not lie in the unital region and explore a larger area. This can be explained: one has a common environment which, in fact, has memory (due to its small dimension). An example of this behavior can be found in figure 5 of [PS06].

For the other cases, where there is no filling of the unital region, one can suspect self averaging. This can be tested calculating the standard deviation of purity σ_P , one time step before concurrence is zero. This is equivalent to examining the width of the coloured curves in fig. 4.1. We numerically observed that for some set of parameters, $\sigma_P \propto 1/N_e$ whereas for other it approaches a finite value. Though a tendency to accumulate towards the Werner curve is clear from the pictures presented, in some cases it is not more than a tendency. Indeed, even in the chaotic case and when having self averaging, the limiting curve not always crosses the line $C = 0$ at $P = 1/3$ (like the Werner curve), but a slighter bigger value. Again our numerics show that this is not a finite size effect. However, all the limiting curves are similar to the Werner curve, and that still can be used for approximations, as long as we recall it is only an approximation. Though all six configurations are physically quite different and the individual behavior of purity and concurrence is quite affected, the relation between the two is entirely robust.

Cases (c) and (f) lead to an instructive lesson: Here we have two uncoupled environments, and we start with a pure state in each of these. The purity of the uncoupled subsystems will remain unchanged, but the purity and concurrence of the initial Bell pair will decay. Thus one might consider seeing a paradox, but this is not the case; the entanglement of the pair is simply spread over all the system with time.

Up to this point our results are in full qualitative agreement with the ones found in previous chapters. This leads us to make a tighter comparison with the RMT models developed before.

5.6 Comparison with RMT predicted behavior

Our KI model has some parameter ranges in which we can consider the system to be “quantum chaotic”. A quantitative comparison of purity decay for the dynamical system and the RMT model is sound. Statistical tests and analytical arguments, indicate that one can consider the homogeneous KI as a typical member of the GOE. Thus we shall compare with the results obtained in sec. 2.5 and sec. 3.2.2. We first list some differences between the two models.

- The most serious difference is the structure of the coupling. Relations of the form eqs. (E.4) and (E.5) used to define the coupling in the RMT model, generically yield non-separable operators, whereas the coupling for the KI model is indeed separable and of the form $\sigma_z \otimes V_e$. Dynamics involving separable operators have special properties. We must not be surprised that this particular structure of the coupling affects the behavior.
- The theory developed in earlier chapters is for an ensemble of systems. Here we are dealing with a single system. Self averaging takes care of this issue. Numerical tests indicate that as the size of the environment increases, the behavior for a typical Hamiltonian approaches rapidly the behavior of the ensemble average (see fig. 2.3). We can safely ignore this problem as long as we go to high enough dimensions. However, for very detailed discussions this must be taken into consideration (as in [PSPS06]).
- We are using environments with either exact rotational symmetries [(d), (e), and (f)] or with some approximate translational symmetry [(a), (b), and (c)]. But we have not developed a theory for chaotic environments with discrete unitary symmetries.

One might be tempted to assume that the overall result is an average of the results in the different sectors, as happens with fidelity f : Given an echo operator M with a discrete unitary symmetry, and a set of states $\{|\psi_s\rangle\}$ living in the different symmetry sectors,

$$f = \left(\sum_s \alpha_s^* \langle \psi_s | \right) M \left(\sum_{s'} \alpha_{s'} |\psi_{s'}\rangle \right) = \sum_s |\alpha_s|^2 \langle \psi_s | M | \psi_s \rangle.$$

For purity the situation is different,

$$P \left(\text{tr}_1 \sum_{s,s'} \alpha_s \alpha_{s'} |\psi_s\rangle \langle \psi_{s'}| \right) \neq \sum_s |\alpha_s|^2 P(\text{tr}_1 |\psi_s\rangle \langle \psi_s|). \quad (5.11)$$

Let $\alpha_1 = \alpha_2 = 1/\sqrt{2}$, $|\psi_{s=1}\rangle = |00\rangle$, and $|\psi_{s=2}\rangle = |11\rangle$. In this case purity of the reduced system is minimal (1/2) whereas the purity of the reduced state of each of the components is maximal (1).

However, a quantity that is affected immediately when superposing spectra is the form factor. The form factor of a superposition of many, say GOE, spectra approaches that of a Poissonian one. Thus, a simplified way to incorporate this effect is to replace in our formulae the GOE form factor $b_2^{(1)}(t)$ by the one of a random spectra $b_2(t) = 0$.

- During the first chapters we assumed time independent Hamiltonians. The KI Hamiltonian (5.5) depends explicitly on time. However, due to its periodic nature, one can construct its corresponding Floquet operator. The circular ensembles [Dys62] are used to model such operators [Haa01]. Circular and Gaussian ensembles share all the properties regarding its eigenvectors. The eigenphases of the former and the eigenvalues of the later share most properties but a precise mathematical relation among them is cumbersome to state. We can naively consider the circular ensembles as an exponentiated (and approximated) version of the Gaussian ensembles. We thus do not need to modify our theory to take into account this issue.

- With eq. (E.4) we are assuming certain normalization of the coupling. One can adjust the coupling constant λ so any V has the given normalization [see eq. (2.5)]. In our case, we can expect that for models (a) and (e) the decay, at least for short times, does not depend on the number of qubits. This can be achieved substituting $\lambda \rightarrow \alpha J_{ce}/\sqrt{\tau_H}$ with α an N_e independent number. The leading term (with respect to time) is now independent of τ_H and N_e .

For simplicity we eliminate the internal Hamiltonian in the dynamical model ($H_c = 0$) to use the RMT formulae with $\Delta = 0$. We use configuration (d) for the comparison to eliminate possible border effects. Its Heisenberg time is moderately small and thus we can access easily time regimes comparable with the Heisenberg time. The effective size of the environment is still large (2^{q_e}) [compared with separate environment configurations ($\sqrt{2^{q_e}}$)] so the large dimension limit is achieved faster.

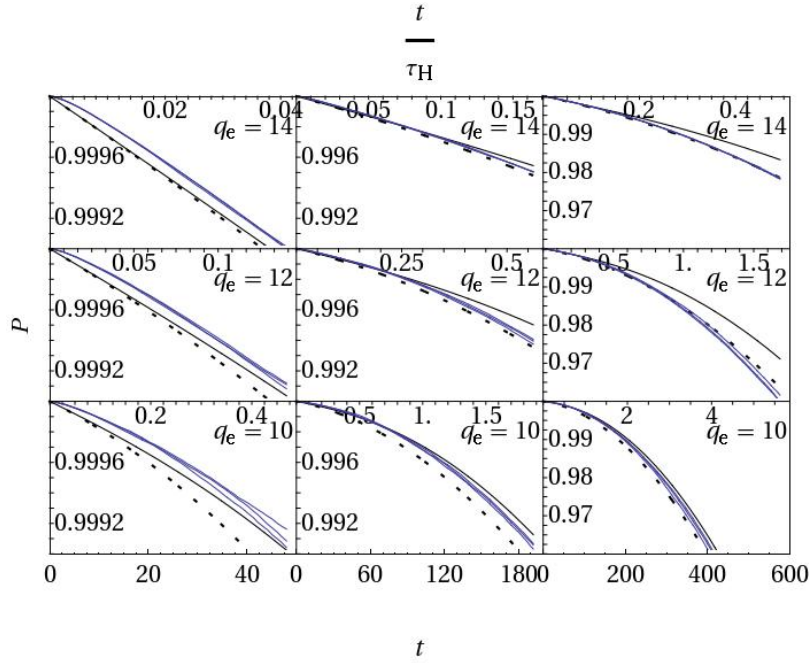


Figure 5.6: We plot, with blue thin lines, the evolution of purity for 10 initial condition in model (d). We vary the number of qubits vertically and the time ranges horizontally. The formula derived from our RMT model eq. (5.12) is plotted as a thin black line. The same formula, but assuming no correlations within the spectra, is plotted as a dashed line. We use $J'_{ce} = 0.0005$ to be in the linear response regime for all plots. See text for a complete description.

Our adapted RMT formula (using Bell states as initial conditions) reads

$$P(t) = 1 - \alpha \left(\frac{J'_{ce}}{\sqrt{q_e}} \right)^2 \left\{ 3t\tau_H + \frac{4}{\tau_H} t^2 - \frac{3}{\tau_H} B_2^{(1)}(t) \right\}. \quad (5.12)$$

The numerical results are summarized in fig. 5.6. There we find 9 plots for the evolution of purity in the KI chain. Each blue line corresponds to a different realization of the initial condition eq. (5.10). We include formula (5.12) with and without the correlation term $\frac{3}{\tau_H} B_2^{(1)}(t)$ as solid and dashed black lines respectively. We increase the size of the environment (from bottom to top) to appreciate how the large dimension limit is approached.

We also vary the plot range to examine different time regimes of the problem. In the plots, two time scales are available. The lower scale is the number of time steps (number of applications of the Floquet operator) while the upper one is time in units of the Heisenberg time.

We first encounter the Zeno regime, in which the discreteness of the spectrum induces deviations of the RMT formulae; for a finite spectrum, what we take as a δ function in eq. (2.13), has a finite width and height, causing an initial quadratic decay. Indeed we can see on the left most plots that the deviation lasts a few kicks. The effect is more visible for $q_e = 12$ and 14. The next regime is the linear one, sometimes called Fermi golden rule regime. We observe linear decay as predicted by RMT whenever $1 \ll t \ll \tau_H$. We use this regime to obtain the fitting parameter $\alpha = 0.21$. Next we observe a crossover in which deviations from the linear behavior are evident (starting at $t \approx \tau_H/4$). For $q_e = 10$ this regime overlaps slightly with the Zeno regime. After the crossover we find the Gaussian regime, in which a quadratic decay of purity is manifest. The clearest picture of this behavior is seen for $q_e = 10$ where the Heisenberg time is the smallest.

As we increase the size of the environment we observe better agreement between the dynamical model and the RMT formula with no correlation. For $q_e = 14$ the agreement is virtually perfect for all time regimes beyond the Zeno regime. Comparing the behavior for different environments, we can observe the dramatic effect of the Heisenberg time on decoherence: The denser the spectrum, the later we arrive to the Gaussian regime. Environments with tighter spectra cause less damage to the central system. Other configurations also show qualitative agreement with the RMT formula developed before.

The results of sec. 2.5 predict that for arbitrary separable conditions, on a TRI system (or with any other anti-unitary symmetry), we have a finite spreading of purity, even in the large dimension limit. This effect becomes important after the Heisenberg time. We argued why we expect self averaging (with respect to the initial conditions) for Bell states and indeed observed it in the large dimension limit.

We tested these two findings in our KI models. As expected, we found no self averaging for separable ones. However, we observed the same effect before and after the Heisenberg time. This anomaly can be due to the separable structure of the coupling, which implies a preferred base within the central system. From that point of view, this irregularity is analogous

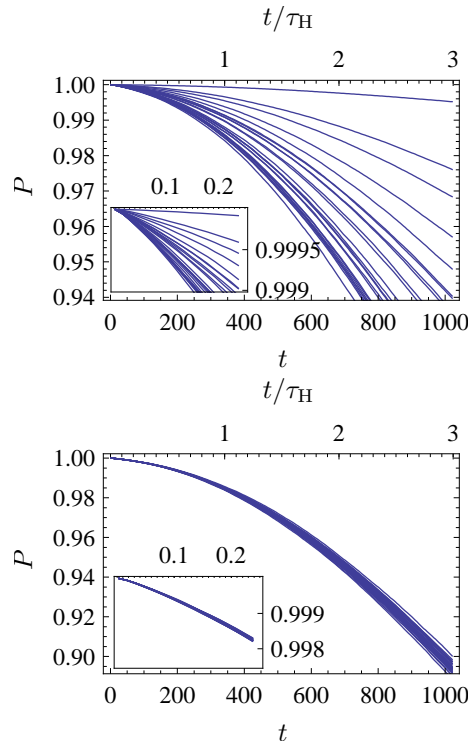


Figure 5.7: Evolution of 25 random initial conditions for configuration (d). In the top panel we prepare separable initial conditions, whereas in the lower panel entangled ones. We observe no self-averaging both for long times and short times (in the insets). This might be due to the separable structure of the coupling. $J_{ce} = 0.0005$ and $q_e = 12$.

to the effect of an internal Hamiltonian. Interestingly, we again observe that for entangled states we do have self averaging. This suggests that the “transport” of symmetries via entanglement is a general property that is not limited to the topics discussed during this thesis.

Chapter 6

Quantum memories

Divide et impera.

Physical devices capable of storing faithfully a quantum state, *i.e.* quantum memories, are crucial for any quantum information task. While different types of systems have been considered, most of the effort is concentrated in manipulating qubits as they are essential for most quantum information tasks [NC00]. For a general quantum memory (QM) it is necessary to record, store, and retrieve an arbitrary state. For quantum communication and quantum computation initialization in the base state, single qubit manipulations, a two qubit gate (e.g. control-not), and single qubit measurements are sufficient. For arbitrary quantum memories recording and retrieving the state is still an experimental challenge but initializing a qubit register and individual measurement is mostly mastered. Faithful realization of two qubit gates together with better isolation from the environment are the remaining obstacles for achieving fully operational quantum technology. However the huge effort done in the community has born some fruit [JSC⁺04, CdRF⁺05, CMJ⁺05, EAM⁺05, PF02, PFL⁺04].

Understanding decoherence of one, two, and n qubits has been of interest for some time. In [FFP04] the authors calculate decoherence of a QM for a spin-boson model using a measure designed for their purposes. In the limit of slight decoherence they obtain various results including additivity. Experimental results are also available [KS04, KS06]. In the previous chapters we have studied one and two qubit decoherence using both a random matrix formulation and a specific dynamical model. One would wish to encompass some of this progress in a general picture.

In the present chapter we address this problem using a standard measure of decoherence, namely purity. We obtain analytic expressions for the decoherence of a QM during the storage time. Specifically we discuss a QM composed of a set of individual qubits interacting with some environment. The expressions given are based on previous knowledge of the decoherence of a single qubit entangled with some non-interacting spectator. Their validity is limited to small decoherence, *i.e.* large purity of the QM. Note that the latter is not a significant restriction, within the context of quantum information processing, due to the high fidelity requirements of quantum error correction codes. We again assume that the entire system is subject to unitary time-evolution, and that decoherence comes about by entanglement between the central system (CS) and the environment. Spurious interactions inside the central system are neglected.

A further and critical assumption is the independence of the coupling of different qubits with the environment *in the interaction picture*. This is justified if the couplings are already independent in the Schrödinger picture or if we have rapidly decaying correlations due to mixing properties of the environment [PS02]. Physically, the first would be more likely if we talk about qubits realized in different systems or degrees of freedom, while the second seems plausible for many typical environments.

The central result is a decomposition of the decoherence of the full QM, coupled to a single or several environments into a sum of terms. Each of these describes the decoherence of a single qubit in a “spectator configuration” eq. (1.2). Recall, the CS consists of two non-interacting parts, one (the qubit) interacting with the environment and the other (the rest of the QM) not. This configuration is non-trivial if the two parts of the CS are entangled. Apart from the above assumptions, this result does not depend on any particular property of the environment or coupling. Thus, it can be applied to a variety of models.

The general relation is obtained in linear response approximation and leads to explicit analytic results if the spectral correlations of the environment are known, see sec. 6.1. We test successfully the results in our random matrix model (sec. 6.2). Finally, we perform numerical simulations for four qubits, interacting with the kicked Ising spin chain as an environment, in sec. 6.3.

6.1 The calculation

We now outline the calculation for n qubits. Since it just represents a variation in the indices of some calculations presented in appendix A, we skip some details and go through it pretty fast.

The central system (our QM) is composed of n qubits. Thus, its Hilbert space is $\mathcal{H}_{\text{qm}} = \bigotimes_{i=1}^n \mathcal{H}_i$, where \mathcal{H}_i are the Hilbert spaces of the qubits. The Hilbert space of the environment is again denoted by \mathcal{H}_e . The Hamiltonian reads

$$H = H_{\text{qm}} + H_e + \lambda V, \quad \lambda V = \sum_{i=1}^n \lambda_i V^{(i)}. \quad (6.1)$$

Here, $H_{\text{qm}} = \sum_{i=1}^n H_i$, where H_i acts on \mathcal{H}_i , whereas H_e describes the dynamics of the environment, and λV the coupling of the qubits to the environment. The strength of the coupling of qubit i is controlled by the parameter λ_i , while $\lambda = \max\{|\lambda_i|\}$. The (possibly time-dependent) Hamiltonian gives rise to the unitary evolution operator $U_\lambda(t)$.

We consider two different settings. In the first one $V^{(i)}$ acts on the space $\mathcal{H}_i \otimes \mathcal{H}_e$, *i.e.* all qubits interact with a single environment called *joint environment*. In the second one each qubit interacts with a *separate environment*. Thus the environment is split into n parts, $\mathcal{H}_e = \bigotimes_{i=1}^n \mathcal{H}_{e,i}$ and $V^{(i)}$, in eq. (6.1), acts only on $\mathcal{H}_i \otimes \mathcal{H}_{e,i}$. The first case would be typical for a quantum computer, where all qubits are close to each other, while the second would apply to a non-local quantum network. Both configurations are defined in perfect analogy with the ones, with corresponding names, considered in sec. 3.1.

Again we choose the initial state to be the product of a pure state of the central system (the QM) and a pure state of the environment

$$|\psi_0\rangle = |\psi_{\text{qm}}\rangle |\psi_e\rangle, \quad |\psi_{\text{qm}}\rangle \in \mathcal{H}_{\text{qm}}, \quad |\psi_e\rangle \in \mathcal{H}_e. \quad (6.2)$$

In the separate environment configuration we furthermore assume that $|\psi_e\rangle = \bigotimes_i |\psi_{e,i}\rangle$ with $|\psi_{e,i}\rangle \in \mathcal{H}_{e,i}$, which corresponds to the absence of quantum correlations among the different environments.

Purity evolves as $P(t) = \text{tr} \rho_{\text{qm}}^2(t)$, with $\rho_{\text{qm}}(t) = \text{tr}_e U_\lambda(t) |\psi_0\rangle \langle \psi_0| U_\lambda^\dagger(t)$. To calculate purity (or any other quantity that depends solely on the Schmidt coefficients) we replace the forward time evolution $U_\lambda(t)$ by the

echo operator $M(t) = U_0(t) U_\lambda(-t)$ where $U_0(t)$ gives the evolution without coupling, recall sec. 2.2. Using Born expansion for the echo operator and defining $\lambda \tilde{V}_t = U_0(t) \lambda V U_0^\dagger(t)$ (the coupling at time t in the interaction picture) purity is then given by

$$P(t) = 1 - 2\lambda^2 \int_0^t d\tau \int_0^t d\tau' \operatorname{Re} A(\tau, \tau') + \mathcal{O}(\lambda^4), \quad (6.3)$$

with

$$A(\tau, \tau') = p[\tilde{V}_\tau \tilde{V}_{\tau'} \varrho_0 \otimes \varrho_0] - p[\tilde{V}_{\tau'} \varrho_0 \tilde{V}_\tau \otimes \varrho_0] \\ + p[\tilde{V}_\tau \varrho_0 \otimes \tilde{V}_{\tau'} \varrho_0] - p[\tilde{V}_{\tau'} \varrho_0 \otimes \varrho_0 \tilde{V}_\tau], \quad (6.4)$$

and $\varrho_0 = |\psi_0\rangle\langle\psi_0|$ [recall that $p[\rho_1 \otimes \rho_2] = \operatorname{tr}(\operatorname{tr}_e \rho_1 \operatorname{tr}_e \rho_2)$]. Note that the linear terms vanish identically after tracing out the environment. Considering the form of the coupling in eq. (6.1) we can decompose $\lambda^2 A(\tau, \tau') = \sum_{i,j} \lambda_i \lambda_j A^{(i,j)}(\tau, \tau')$ with

$$A^{(i,j)}(\tau, \tau') = p[\tilde{V}_\tau^{(i)} \tilde{V}_{\tau'}^{(j)} \varrho_0 \otimes \varrho_0] - p[\tilde{V}_{\tau'}^{(i)} \varrho_0 \tilde{V}_\tau^{(j)} \otimes \varrho_i] \\ + p[\tilde{V}_\tau^{(i)} \varrho_0 \otimes \tilde{V}_{\tau'}^{(j)} \varrho_0] - p[\tilde{V}_{\tau'}^{(i)} \varrho_0 \otimes \varrho_0 \tilde{V}_\tau^{(j)}]. \quad (6.5)$$

$\tilde{V}_t^{(i)} = U_0^\dagger(t) V^{(i)} U_0(t)$ in analogy with \tilde{V}_t . Equation (6.3) is given as a double sum in the indices of the qubits. In a diagonal approximation ($i = j$), $P(t)$ is expressed in terms of the purities $P_{\text{sp}}^{(i)}(t)$ which correspond to the purity decay of the CS in a spectator configuration where only qubit i is interacting with the environment. Purity then reads as

$$P(t) = 1 - \sum_{i=1}^n \left(1 - P_{\text{sp}}^{(i)}(t)\right), \quad (6.6)$$

$$P_{\text{sp}}^{(i)}(t) = 1 - 2\lambda_i^2 \int_0^t d\tau \int_0^t d\tau' A^{(i,i)}(\tau, \tau') + \mathcal{O}(\lambda_i^4).$$

This is our central result of this chapter. The diagonal approximation is justified in two situations: First if the couplings $V^{(i)}$ of the individual qubits are independent from the outset, as would be typical for the separate environment configuration or for the random matrix model of decoherence. Second, if the couplings in the interaction picture become independent due to mixing properties of the environment, as would be typical for a “quantum chaotic” environment.

6.2 A RMT example

To illustrate the case of independent couplings mentioned above, random matrix theory provides a handy example. Such models were discussed in previous chapters and in [PS07, PGS07, GS02, AV07].

In chapter 3 purity decay was computed in linear response approximation for two qubits, one of them being the spectator. For the sake of simplicity we choose the joint environment configuration, no internal dynamics for the qubits, and H_e and $V^{(1)}$ as typical members of the Gaussian unitary ensemble. Purity is then given by

$$P_{\text{sp}}^{(1)}(t) = 1 - \lambda_1^2(2 - p_1)f(t); \quad (6.7)$$

$$f(t) = t \max\{t, \tau_H\} + \frac{2}{3\tau_H} \min\{t, \tau_H\}^3. \quad (6.8)$$

Here, τ_H is the Heisenberg time of the environment and p_1 is the *initial* purity of the first qubit alone, which measures its entanglement with the rest of the QM, see eq. (3.23). As we required a priori independence of the couplings, we can now insert eq. (6.7) in eq. (6.6) to obtain the simple expression

$$P(t) = 1 - f(t) \sum_{i=1}^n \lambda_i^2(2 - p_i), \quad (6.9)$$

where p_i is the initial purity of qubit i . In the presence of internal dynamics the spectator result is also known and can be inserted. As an example, we apply the above equation to an initial GHZ state ($(|0 \dots 0\rangle + |1 \dots 1\rangle)/\sqrt{2}$). Then all $p_i = 1/2$ and we obtain $P(t) = 1 - (3/2)f(t) \sum_i \lambda_i^2$. For a W state ($(|10 \dots 0\rangle + |01 \dots 0\rangle + \dots + |00 \dots 1\rangle)/\sqrt{n}$), purity for each qubit is $p_i = (n^2 - 2n + 2)/n^2 \approx 1$, in the large n limit, and purity decays as $P(t) = 1 - f(t) \sum_i \lambda_i^2$.

6.3 A dynamical model

We now use the homogeneous kicked spin (sec. 5.2) as an environment for n qubits. We consider its chaotic and integrable regimes. We shall thus use a particular realization of eq. (5.5) in the spirit of chapter 5.

The main assumption in eq. (6.6) is the fast decay of correlations for couplings of different qubits to the environment. For the random ma-

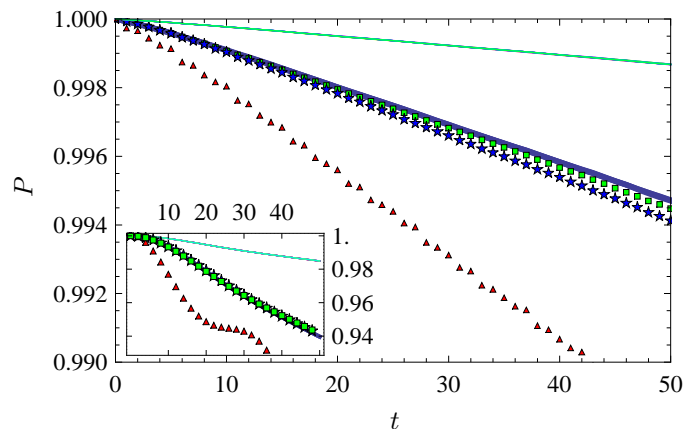


Figure 6.1: Purity decay for a GHZ state is shown for the environment described by eq. (6.10). The couplings are: all qubits to one spin (red triangles), nearby spins (blue stars), and maximally separated spins (green squares). The theoretical result (thick line) is calculated in terms of the $P_{(\text{sp})}^{(i)}(t)$ (thin lines). The main figure corresponds to the case of a mixing environment and the inset for an integrable one.

trix model discussed above this is trivially fulfilled. Yet, integrable environments are commonly used [CL83] and one may wonder whether eq. (6.6) can hold in such a context. We shall therefore study a dynamical model where a few qubits are coupled to an environment represented by a kicked Ising spin chain using identical coupling operators for all qubits. In this model, the variation of the angle of the external kicking field allows the transition from a “quantum chaotic” to an integrable Hamiltonian for the environment [Pro02, PP07](a). For convenience we separate it in the environment and the central system. The Hamiltonian of the environment, namely the homogeneous kicked Ising spin chain, recall, is given by

$$H^{(e)} = \sum_{i=0}^{L-1} \sigma_x^{(e,i)} \sigma_x^{(e,i+1)} + \delta(t) \sum_{i=0}^{L-1} b \cdot \sigma^{(e,i)} \quad (6.10)$$

where $\delta(t) = \sum_{n \in \mathbb{Z}} \delta(t - n)$ (*i.e.* time is measured in units of the kick period), L the number of spins in the environment, $\sigma^{(e,i)} = (\sigma_x^{(e,i)}, \sigma_y^{(e,i)}, \sigma_z^{(e,i)})$ the Pauli matrices of spin i , and b the dimensionless magnetic field with which the chain is kicked ($\hbar = 1$). We close the ring requiring $\sigma^{(e,L)} \equiv \sigma^{(e,0)}$. The Hamiltonian of the QM is

$$H^{(\text{qm})} = \delta(t) \sum_i b \cdot \sigma^{(\text{qm},i)}, \quad (6.11)$$

where $\sigma^{(\text{qm},i)}$ is defined similarly as for the environment. The coupling is given by

$$\lambda V = \lambda \sum_i \sigma_x^{(\text{qm},i)} \sigma_x^{(e,j_i)}. \quad (6.12)$$

The j_i 's define the positions where the qubits of the QM are coupled to the spin chain. Equivalently we could use kicked Ising couplings and a time-independent field [PSW01].

To implement a chaotic environment, we use here $b = (0.9, 0.9, 0)$. We use a ring consisting of $L = 12$ spins for the environment and 4 additional spins for the qubits of the QM. The coupling strength is $\lambda = 0.005$. In Fig. 6.1, we study purity decay when all four qubits are coupled to the same spin, to neighboring spins, and to maximally separated spins, $\vec{j} = (0, 3, 6, 9)$. The initial state is the product of a GHZ state in the QM and a random pure state in the environment. We compare the results with eq. (6.6) (thick line) obtained from simulations of the spectator configuration (thin solid line). Coupling the spectator to different positions

in the chain yields near identical results for $P(t)$, so we can see only one line. The figure demonstrates the validity of eq. (6.6) for well separated and hence independent couplings. For coupling to neighboring spins decay is slightly faster while the sum rule does not hold if all qubits are coupled to the same spin.

A similar calculation for integrable environments with $b = (0, 1.53, 0)$ yields faster purity decay than in the mixing case as expected from general considerations in [GPSŽ06]. Nevertheless the sum rule is again well fulfilled except if we couple all qubits to the same spin. This leads us to check the behavior of the correlation function

$$p[\tilde{V}_\tau^{(i)} \tilde{V}_{\tau'}^{(j)} \varrho_0 \otimes \varrho_0] = \langle \psi_0 | \tilde{V}_\tau^{(i)} \tilde{V}_{\tau'}^{(j)} | \psi_0 \rangle. \quad (6.13)$$

This is the simplest and usually largest term in $A^{(i,j)}$, eq. (6.5). Figure 6.2 shows this quantity for chaotic (*i.e.* mixing) and integrable environments in the first and second row, respectively. The first column shows the autocorrelation function ($i = j$). The second and third columns give the cross correlation function ($i \neq j$) when the qubits are coupled to the same or opposite spins, respectively. In the latter case, correlations are always small thus showing that also in integrable situations our condition can be met. Non-vanishing correlations, as in fig. 6.2(b) and fig. 6.2(e) lead to deviations from the sum rule. The pronounced structure for the integrable environment, fig. 6.2(e), may be associated to the oscillations of purity decay (inset of fig. 6.1).

Another example where the conditions of our derivation are not met is the following. A Bose-Einstein condensate in which the n atoms have two immiscible internal states [DDZ00] could be interpreted as a QM. The symmetry of the wave function reduces the dimension of the Hilbert space and causes high correlations among the couplings to the environment. It is not surprising then that decoherence scales differently (as n^2).

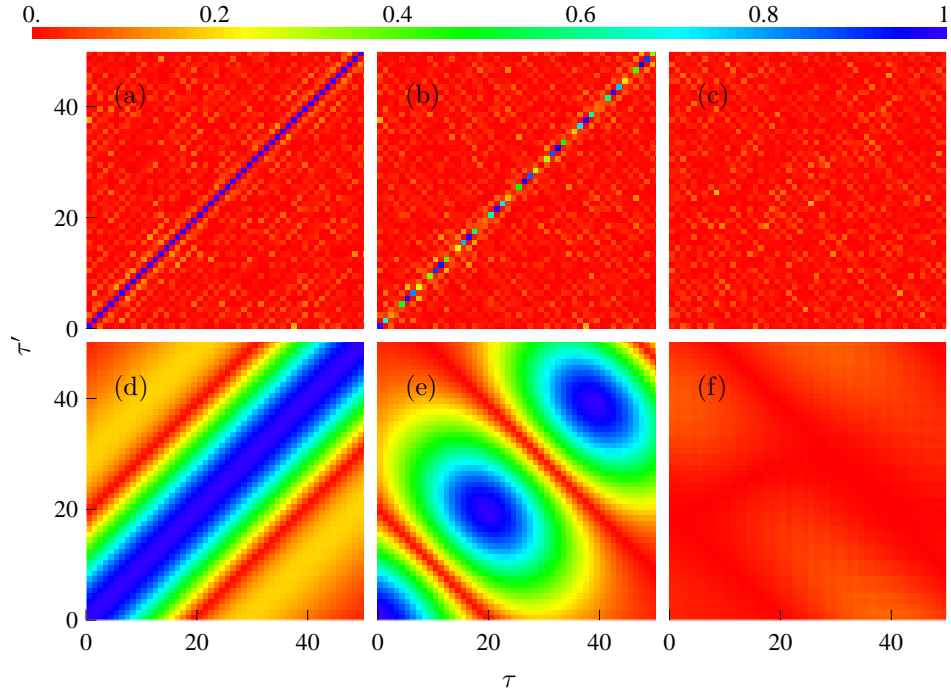


Figure 6.2: The color-coded absolute value of the real part of $\langle \psi_0 | \tilde{V}_\tau^{(i)} \tilde{V}_{\tau'}^{(j)} | \psi_0 \rangle$ given in eq. (6.13) as a function of τ and τ' for the chaotic [(a) (b) (c)] and the integrable [(d) (e) (f)] spin chain environment ($L = 8$). (a),(d) show the autocorrelation function ($i = j$); (b), (e) and (c) (f) the cross correlation function for couplings to the same spin or opposite spins in the ring respectively.

Chapter 7

Conclusions

We now proceed to formulate the conclusions of this work. We start by particular conclusions for each chapter, and afterwards to the general conclusions and perspectives.

In chapter 2 we analyzed the decoherence (measured by purity during all the thesis) of a single qubit immersed in an environment. For this purpose we introduced a model with unitary dynamics in the qubit plus environment space. Both the environment Hamiltonian and the interaction were chosen as random matrices from the classical ensembles. We solved purity decay in terms of correlation functions of the environment.

We obtained linear and quadratic decay before and after the Heisenberg time respectively. In general, purity of a superposition of eigenstates decays faster than an eigenstate. The presence of an internal Hamiltonian in the qubit was observed to contribute to stability. For the GOE case, different initial conditions in the Bloch sphere yield different behaviors of purity and von Neumann entropy, even in the large environment limit.

Monte Carlo simulations showed that exponentiating the analytical formulae, as explained in appendix C, allowed extending the analytical result outside the scope of linear response formalism.

In chapter 3 we used the spectator configuration (introduced in the introduction of the thesis), in which only a part (one qubit) of the central system (two qubits) is coupled to an environment. This constituted the first of three models analyzed. We solve it using extensively the symmetries of the ensembles. We found some elements in common with the

single qubit case: the same qualitative dependence on time (linear and quadratic before and after the Heisenberg time, respectively; a dependence on an internal Hamiltonian, namely having a big energy splitting in the qubit increases stability; finally, a reasonable agreement with a heuristic exponentiation. With the second qubit we added a new element, entanglement. We observed that entanglement allowed taking the invariance properties of one qubit into the other. We also observed that entanglement induces a faster decoherence. For the TRI breaking case we found that, due to entanglement, self averaging is expected when using Bell states.

The other two models (joint environment and separate environment), which possess a very different physical interpretation, were reduced to the spectator configuration using the independence of the couplings. Their behavior is similar, up to a scaling of the coupling constant.

In chapter 4 we studied, for two qubits coupled to an environment, the relation between purity and concurrence as both evolve in time. Both the environment and the coupling are chosen from the classical ensembles. In order to analyze their relation we introduce the CP plane. We found that in the large dimension limit of the environment, concurrence and purity are restricted to a small region defined using unital channels. In fact, in the large dimension limit, for all parameters studied, the channels induced by the random Hamiltonian approach rapidly the unitality condition. For large purities the allowed unital region is almost one dimensional, which allows to write a one to one relation for concurrence and purity. In some cases the curve described by the system in the CP plane coincides with the Werner curve. The deviation from it, for a particular level splitting in the coupled qubit, is given in an empirical formula which depends on the coupling strength and the size of the environment. This deviation goes rapidly to zero as the size of the environment and the coupling increase. Assuming that purity and concurrence are related via the Werner curve, it is possible to use our knowledge from the previous chapters to give a formula for concurrence decay.

In chapter 5 we studied the same problem as in previous chapters (one and two qubit decoherence), but using particular dynamical models. The models consists of n spins interacting pairwise with individually adjustable strengths, and kicked with a magnetic field. The dynamical system is flexible enough to allow different configurations and symmetries of the environment and coupling. Moreover, varying the parameters we

can have qualitatively different kinds of dynamics, namely chaotic, intermediate and integrable. In the chaotic regime of the environment we obtained quantitative agreement with the RMT formulae obtained earlier for purity decay. For the integrable case we observed quadratic decay, sometimes with strong revivals (when the coupling was to an open end of a chain). The intermediate case displays oscillations superimposed to a linear decay. In the chaotic case we observe that the effective Heisenberg time (determined, among other things, by the symmetry of both the environment and the coupling) plays an important roll in decoherence.

Purity and concurrence behave in a qualitatively similar way for all configurations. The relation between the two, for sufficiently large environments, follows an analytic expression we get for Werner states quite closely, although the specific dynamics does not produce Werner states.

Finally, in chapter 6 we calculated generic decoherence of a n -qubit quantum memory as represented by purity decay. For large purities it is globally given in linear response approximation by a sum rule in terms of the purities of the individual qubits entangled with the remaining register as spectator. This sum rule depends crucially on the absence or rapid decay of correlations between the couplings of different qubits in the interaction picture. We prove that this is fulfilled by sufficiently chaotic environments or couplings but, using a spin chain model as an environment, we find that even if the latter is integrable correlations can be absent and the sum rule holds. While exceptions can be constructed we have a very general tool to reduce the decoherence of a QM of n qubits to the problem of a single qubit entangled with the rest of the QM. Furthermore the result is equally valid if we perform local operations on the qubits.

Some possible extensions or generalizations of the thesis are now outlined.

- Several measures for entanglement of multi-qubit systems exist. Depending on the particular problem to be treated, one or the other might be useful. Preliminary results [ste] indicate that for multi-qubit systems a relation, like the one found for two qubits, might be used to obtain formulae for entanglement decay.
- In order to deepen our knowledge of the behavior of integrable and intermediate systems, one should study particular models.
- As many interactions are indeed separable, a RMT formulation for

separable interactions of the qubit(s) with the environment might prove useful to understand the similarities and differences with this “more realistic” coupling.

- The sum rule studied in chapter 6 also applies if the register is split into arbitrary sets of qubits. In fact, one and two qubit gates are known to be universal for quantum computation [NC00], so we lay the foundation for the computation of decoherence during the execution of a general algorithm. This extension only requires the knowledge of the decoherence of a pair suffering the gate operation while entangled with the rest of the register. As each gate is different, we will have to take a step by step approach, which at each step will only involve one and two qubit decoherence. The linear response approximation will be sufficient due to the high fidelity requirements of quantum computation.

Summarizing, we have developed a tool to study decoherence of qubits based on the spectator configuration and on random matrix theory. We have compared the results found with a kicked Ising model. We almost always observed linear/quadratic decay of purity before/after the Heisenberg time of the environment and self averaging both with respect to the Hamiltonian and to the initial conditions. The exceptions are: (i) In the presence of an internal Hamiltonian, the central system eigenstates decay linearly even after Heisenberg time. (ii) If we have a time reversal invariant Hamiltonian, no self averaging with respect to the initial conditions is observed after the Heisenberg time. (iii) In the KI model, and presumably due to the separable structure of the Hamiltonian, no self averaging, before the Heisenberg time, was observed. Entanglement enhances decoherence and may transport symmetry properties from one qubit to the other. When studying two qubits we also studied their internal entanglement, as quantified by concurrence. A one to one correspondence was often found, characterized by the Werner curve. Thus, formulae for entanglement decay are also available. For a larger number of qubits a sum rule can be applied in a wide range of circumstances to express purity decay of a group of particles in terms of purity decay of each particle in a spectator configuration. In all cases, heuristic exponentiation leads to good agreement beyond linear response scope.

Appendix A

One-qubit purity decay for pure and mixed states

Here, we consider the one-qubit decoherence in a more general context. One-qubit decoherence as described in sec. 2 deals with a separable initial state $\varrho_0 = \rho_1 \otimes |\psi_e\rangle\langle\psi_e|$, $\rho_1 = |\psi_1\rangle\langle\psi_1|$. Thus ϱ_0 is a pure state of a single qubit coupled to an environment in the pure state $|\psi_e\rangle$. We consider here arbitrary, finite dimensions of \mathcal{H}_1 and \mathcal{H}_e , and we allow ρ_1 to be mixed. The latter poses some problems on the physical interpretation of purity as a measure for decoherence. However, these can be avoided by taking the point of view of the environment, as it becomes entangled with the central system. That means we consider the purity of the state of the environment after tracing out the central-system's degrees of freedom; see eq. (3.10) and eq. (3.11). If we consider the entanglement with a spectator being responsible for the mixedness of ρ_1 , we can use the following results to describe purity decay in the spectator model.

We will derive explicit expressions for the average purity $\langle P(t) \rangle$ as a function of time, where the average is only over the random coupling. These expressions involve a few elemental spectral correlation functions, whose properties will be discussed in A.5. As detailed in sec. 2.2, we work with the echo operator $M(t)$ in the linear response approximation eq. (2.9). Note that $I(t)$ is Hermitian, while, due to time-order inversion, $J(t)$ is not.

This section is slightly boring, but since this is a Ph.D. thesis, the details must be incorporated. My thanks an admiration to the devoted reader

who reached this section.

A.1 General calculation

Let ϱ_1 and ϱ_2 be two operators acting on the Hilbert space $\mathcal{H}' = \mathcal{H}_1 \otimes \mathcal{H}_e$. We define the purity form $p[\cdot]$ as a function of pairs of such operators,

$$p[\varrho_1 \otimes \varrho_2] = \text{tr}_e[\text{tr}_1(\varrho_1) \text{tr}_1(\varrho_2)]. \quad (\text{A.1})$$

Since any linear operator acting on $\mathcal{H}' \otimes \mathcal{H}'$ can be expanded in terms of separable operators of the form $\varrho_1 \otimes \varrho_2$, linearity implicitly defines the purity form for arbitrary linear operators. For arbitrary operators A, B acting both on \mathcal{H}' , the purity form has the following property:

$$p[A \otimes B] = p[A^\dagger \otimes B^\dagger]^* = p[B \otimes A] = p[B^\dagger \otimes A^\dagger]^*. \quad (\text{A.2})$$

The purity defined in eq. (1.8) can be expressed in terms of the purity form as

$$P(\text{tr}_e \varrho) = p[\varrho \otimes \varrho]. \quad (\text{A.3})$$

Note that on the RHS of this equation, we first take the trace over the central system, *i.e.* we consider the purity of the state of the environment after tracing out the central degrees of freedom. With this little twist we can describe the one-qubit decoherence and the spectator model at the same time.

To average purity, we use eq. (2.9) to compute $\varrho^M(t) \otimes \varrho^M(t)$ in linear response approximation

$$\langle P(t) \rangle = \langle p[\varrho^M(t) \otimes \varrho^M(t)] \rangle = p[\langle \varrho^M(t) \otimes \varrho^M(t) \rangle]. \quad (\text{A.4})$$

Keeping terms only up to second order in λ :

$$\begin{aligned} \varrho^M(t) \otimes \varrho^M(t) &= \varrho_0 \otimes \varrho_0 \\ &- i\lambda \left[I\varrho_0 \otimes \varrho_0 - \varrho_0 I^\dagger \otimes \varrho_0 + \varrho_0 \otimes I\varrho_0 - \varrho_0 \otimes \varrho_0 I \right]^\dagger \\ &- \lambda^2 \left[J\varrho_0 \otimes \varrho_0 + \varrho_0 J^\dagger \otimes \varrho_0 + \varrho_0 \otimes J\varrho_0 + \varrho_0 \otimes \varrho_0 J \right]^\dagger \\ &+ \lambda^2 \left[I\varrho_0 I^\dagger \otimes \varrho_0 - I\varrho_0 \otimes I\varrho_0 + I\varrho_0 \otimes \varrho_0 I^\dagger \right. \\ &\quad \left. + \varrho_0 I^\dagger \otimes I\varrho_0 - \varrho_0 I^\dagger \otimes \varrho_0 I^\dagger + \varrho_0 \otimes I\varrho_0 I^\dagger \right]. \end{aligned} \quad (\text{A.5})$$

In the next step, we perform the ensemble average over the coupling. The odd terms in λ vanish as purity (even without averaging) must be real. For the remaining terms, we use the properties in eq. (A.2) and the fact that $I(t)$ is Hermitian, to obtain

$$\langle P(t) \rangle = P(0) - \lambda^2(A_J - A_I) \quad (\text{A.6})$$

with $P(0) = p[\varrho_0 \otimes \varrho_0]$ and

$$\begin{aligned} A_J &= 4 \text{Rep}[\langle J \rangle \varrho_0 \otimes \varrho_0] \\ A_I &= 2(p[\langle I \varrho_0 I \rangle \otimes \varrho_0] - \text{Rep}[\langle I \varrho_0 \otimes I \varrho_0 \rangle] + p[\langle I \varrho_0 \otimes \varrho_0 I \rangle]). \end{aligned} \quad (\text{A.7})$$

In order to pull out the same double integral of A_J and A_I , we use the time ordering symbol \mathcal{T} . It allows to write for the average purity as a function of time

$$\langle P(t) \rangle = P(0) - 2\lambda^2 \int_0^t d\tau \int_0^t d\tau' \text{Re } A_{\text{II}} \quad (\text{A.8})$$

with

$$\begin{aligned} A_{\text{II}} &= p[\mathcal{T} \langle \tilde{V} \tilde{V}' \rangle \varrho_0 \otimes \varrho_0] - p[\langle \tilde{V}' \varrho_0 \tilde{V} \rangle \otimes \varrho_0] \\ &\quad + p[\langle \tilde{V} \varrho_0 \otimes \tilde{V}' \varrho_0 \rangle] - p[\langle \tilde{V}' \varrho_0 \otimes \varrho_0 \tilde{V} \rangle], \end{aligned} \quad (\text{A.9})$$

where \tilde{V} and \tilde{V}' are short forms for the coupling matrices $\tilde{V}(\tau)$ and $\tilde{V}(\tau')$, respectively. The arguments τ and τ' of the coupling matrices are interchanged in the second and fourth term of A_{II} . This does not change the value of the integral of course, but it facilitates to handle common terms in the following considerations.

The integrand A_{II} in eq. (A.9) consists of four terms. These terms will be considered, one after the other. We will always first average the argument of the purity form. Only then we perform the partial traces over subsystem \mathcal{H}_1 , and therefore the final trace over the environment. The averaging is only over the coupling, and it is done by applying two simple rules, as described below.

For the coupling $V_{1,e}$ in the product eigenbasis of H_0 , we use either random Gaussian unitary (GUE) or orthogonal (GOE) matrices. Their statistical properties are completely characterized by the following second moments (for notational ease we ignore the subscript $1,e$ for a moment)

$$\langle V_{ij} V_{kl} \rangle = \delta_{il} \delta_{jk} + \chi_{\text{GOE}} \delta_{ik} \delta_{jl}, \quad (\text{A.10})$$

where $\chi_{\text{GOE}} = 1$ if V is taken from the GOE, while $\chi_{\text{GOE}} = 0$ if V is taken from the GUE. In the interaction picture we then find:

$$\langle \tilde{V}_{ij} \tilde{V}_{kl} \rangle = (\delta_{il} \delta_{jk} e^{-i(E_j - E_i)(\tau - \tau')} + \chi_{\text{GOE}} \delta_{ik} \delta_{jl} e^{-i(E_j - E_i)(\tau + \tau')}) . \quad (\text{A.11})$$

A.2 The GUE case

We now proceed to calculate one by one the contributions.

$p[\mathcal{T}\langle \tilde{V}\tilde{V}' \rangle \varrho_0 \otimes \varrho_0](t)$: We first compute the average

$$\begin{aligned} \mathcal{T}\langle \tilde{V}\tilde{V}' \varrho_0 \otimes \varrho_0 \rangle &= \sum_{ijklmn} |ij\rangle \mathcal{T}\langle \tilde{V}(\tau)_{ij,kl} \tilde{V}(\tau')_{kl,mn} \rangle \langle mn | \varrho_0 \otimes \varrho_0 \\ &= \sum_{ijkl} |ij\rangle e^{-i(E_{kl} - E_{ij})|\tau - \tau'|} \langle ij | \varrho_0 \otimes \varrho_0, \end{aligned} \quad (\text{A.12})$$

where we have used the averaging rule, eq. (A.11), as well as the fact that the time-ordering operator \mathcal{T} requests to exchange τ with τ' whenever $\tau < \tau'$. The indices i, k and m denote basis states in \mathcal{H}_1 , while the indices j, l and n denote basis states in \mathcal{H}_e . We can rewrite that expression in a more compact form by employing the diagonal matrices $C_x(\tau)$, defined in eq. (A.37):

$$\begin{aligned} \mathcal{T}\langle \tilde{V}\tilde{V}' \varrho_0 \otimes \varrho_0 \rangle &= (C_1(|\tau - \tau'|) \otimes C_e(|\tau - \tau'|)) \\ &\quad \times (\rho_1 \otimes |\psi_e\rangle\langle\psi_e|) \otimes (\rho_1 \otimes |\psi_e\rangle\langle\psi_e|) . \end{aligned} \quad (\text{A.13})$$

Now we apply the partial traces over subsystem \mathcal{H}_1

$$\text{tr}_1(\langle \tilde{V}\tilde{V}' \rangle \varrho_0) \text{tr}_1 \varrho_0 = C_1(|\tau - \tau'|) C_e(|\tau - \tau'|) |\psi_e\rangle\langle\psi_e| . \quad (\text{A.14})$$

The final trace over the environment yields

$$p[\mathcal{T}\langle \tilde{V}\tilde{V}' \rangle \varrho_0 \otimes \varrho_0](t) = C_1(|\tau - \tau'|) C_e(|\tau - \tau'|) . \quad (\text{A.15})$$

$p[\langle \tilde{V}' \varrho_0 \tilde{V} \rangle \otimes \varrho_0](t)$: We first compute the average

$$\begin{aligned} \langle \tilde{V}' \varrho_0 \tilde{V} \rangle \otimes \varrho_0 &= \sum_{ijklmnpq} |ij\rangle \langle \tilde{V}'_{ij,kl} \langle kl | \varrho_0 | mn \rangle \tilde{V}_{mn,pq} \rangle \langle pq | \otimes \varrho_0 \\ &= \sum_{ijkl} |ij\rangle e^{-i(E_{ij} - E_{kl})(\tau - \tau')} \langle kl | \varrho_0 | kl \rangle \langle ij | \otimes \varrho_0, \end{aligned} \quad (\text{A.16})$$

where we have used eq. (A.11). We apply the partial traces over subsystem \mathcal{H}_1

$$\begin{aligned} \text{tr}_1 (\langle \tilde{V}' \rho_0 \tilde{V} \rangle) \text{tr}_1 \rho_0 &= \left(\sum_{ik} e^{-i(E_i - E_k)(\tau - \tau')} \langle k | \rho_1 | k \rangle \right) \\ &\quad \times \sum_{jl} |j\rangle e^{-i(E_j - E_l)(\tau - \tau')} \langle l | \psi_e \rangle \langle \psi_e | l \rangle \langle j | \psi_e \rangle \langle \psi_e | \\ &= C_1(\tau - \tau') \sum_{jl} |j\rangle e^{-i(E_j - E_l)(\tau - \tau')} \\ &\quad \times \langle l | \psi_e \rangle \langle \psi_e | l \rangle \langle j | \psi_e \rangle \langle \psi_e |. \end{aligned} \quad (\text{A.17})$$

The final trace over the environment yields

$$\begin{aligned} p[\langle \tilde{V}' \rho_0 \tilde{V} \rangle \otimes \rho_0] &= C_1(\tau - \tau') \sum_{jl} \langle \psi_e | l \rangle e^{iE_l(\tau - \tau')} \langle l | \psi_e \rangle \langle \psi_e | j \rangle e^{-iE_j(\tau - \tau')} \langle j | \psi_e \rangle \\ &= C_1(\tau - \tau') S_e(\tau - \tau'), \end{aligned} \quad (\text{A.18})$$

where $S_x(\tau)$ is defined in eq. (A.39).

$p[\langle \tilde{V} \rho_0 \otimes \tilde{V}' \rho_0 \rangle](t)$: We first compute the average

$$\begin{aligned} \langle \tilde{V} \rho_0 \otimes \tilde{V}' \rho_0 \rangle &= \sum_{ijklmn pq} |ij\rangle \langle \tilde{V}_{ij,kl} \langle kl | \rho_0 \otimes |mn\rangle \tilde{V}_{mn,pq} \rangle \langle pq | \rho_0 \\ &= \sum_{ijkl} |ij\rangle e^{-i(E_{kl} - E_{ij})(\tau - \tau')} \langle kl | \rho_0 \otimes |kl\rangle \langle ij | \rho_0. \end{aligned} \quad (\text{A.19})$$

Then we apply the partial traces over subsystem \mathcal{H}_1

$$\begin{aligned} \langle \text{tr}_1 (\tilde{V} \rho_0) \text{tr}_1 (\tilde{V}' \rho_0) \rangle &= \left(\sum_{ik} e^{-i(E_k - E_i)(\tau - \tau')} \langle k | \rho_1 | i \rangle \langle i | \rho_1 | k \rangle \right) \\ &\quad \times \sum_{jl} |j\rangle e^{-i(E_l - E_j)(\tau - \tau')} \langle l | \psi_e \rangle \langle \psi_e | l \rangle \langle j | \psi_e \rangle \langle \psi_e |. \end{aligned}$$

The final trace over the environment yields

$$p[\langle \tilde{V} \rho_0 \otimes \tilde{V}' \rho_0 \rangle] = S_1(\tau - \tau') S_e(\tau - \tau'). \quad (\text{A.20})$$

$p[\langle \tilde{V}' \rho_0 \otimes \rho_0 \tilde{V} \rangle](t)$: We first compute the average

$$\begin{aligned} \langle \tilde{V}' \rho_0 \otimes \rho_0 \tilde{V} \rangle &= \sum_{ijklmn pq} |ij\rangle \langle \tilde{V}'_{ij,kl} \langle kl | \rho_0 \otimes \rho_0 |mn\rangle \tilde{V}_{mn,pq} \rangle \langle pq | \\ &= \sum_{ijkl} |ij\rangle e^{-i(E_{ij} - E_{kl})(\tau - \tau')} \langle kl | \rho_0 \otimes \rho_0 |kl\rangle \langle ij | \end{aligned} \quad (\text{A.21})$$

We apply the partial traces over subsystem \mathcal{H}_1

$$\begin{aligned} \langle \text{tr}_1 (\tilde{V} \varrho_0) \text{tr}_1 (\varrho_0 \tilde{V}') \rangle &= (\sum_{ik} e^{-i(E_i - E_k)(\tau - \tau')} \langle k | \rho_1 | i \rangle \langle i | \rho_1 | k \rangle) \\ &\quad \times \sum_{jl} |j\rangle e^{-i(E_j - E_l)(\tau - \tau')} \langle l | \psi_e \rangle \langle \psi_e | l \rangle \langle j | . \end{aligned}$$

The final trace over the environment yields

$$p[\langle \tilde{V} \varrho_0 \otimes \varrho_0 \tilde{V}' \rangle] = S_1(\tau - \tau') C_e(\tau - \tau') . \quad (\text{A.22})$$

A.3 The GOE case

In the GOE case, the average over the coupling yields, besides the previously considered GUE-term an additional one; see eq. (A.11). In the following we will redo the calculation of the previous subsection, but consider only that additional term. As a reminder, we add the subscript $_2$ to the brackets which denote the ensemble average.

$p[\mathcal{T} \langle \tilde{V} \tilde{V}' \rangle_2 \varrho_0 \otimes \varrho_0](t)$: We first compute the average

$$\begin{aligned} \mathcal{T} \langle \tilde{V} \tilde{V}' \rangle_2 \varrho_0 \otimes \varrho_0 &= \sum_{ijklmn} |ij\rangle \mathcal{T} \langle \tilde{V}(\tau)_{ij,kl} \tilde{V}'(\tau')_{kl,mn} \rangle_2 \langle mn | \varrho_0 \otimes \varrho_0 \\ &= \sum_{ij} |ij\rangle \langle ij | \varrho_0 \otimes \varrho_0 \end{aligned} \quad (\text{A.23})$$

$$= \varrho_0 \otimes \varrho_0 , \quad (\text{A.24})$$

where we have used the averaging rule, eq. (A.11). Here the time-ordering operator has no effect. Now we apply the partial traces over subsystem \mathcal{H}_1

$$\text{tr}_1 (\langle \tilde{V} \tilde{V}' \rangle_2 \varrho_0) \text{tr}_1 \varrho_0 = |\psi_e\rangle \langle \psi_e | . \quad (\text{A.25})$$

The final trace over the environment yields

$$p[\langle \tilde{V} \tilde{V}' \rangle_2 \varrho_0 \otimes \varrho_0](t) = 1 . \quad (\text{A.26})$$

$p[\langle \tilde{V}' \varrho_0 \tilde{V} \rangle_2 \otimes \varrho_0](t)$: We first compute the average

$$\begin{aligned} \langle \tilde{V}' \varrho_0 \tilde{V} \rangle_2 \otimes \varrho_0 &= \sum_{ijklmn pq} |ij\rangle \left\langle \tilde{V}'_{ij,kl} \langle kl | \varrho_0 | mn \rangle \tilde{V}_{mn,pq} \right\rangle_2 \langle pq | \otimes \varrho_0 \\ &= \sum_{ijkl} |ij\rangle e^{-i(E_{ij} - E_{kl})(\tau + \tau')} \langle kl | \varrho_0 | ij \rangle \langle kl | \otimes \varrho_0 , \end{aligned} \quad (\text{A.27})$$

where we have used eq. (A.11). We apply the partial traces over subsystem \mathcal{H}_1

$$\text{tr}_1 (\langle \tilde{V}' \varrho_0 \tilde{V} \rangle_2) \text{tr}_1 \varrho_0 = \sum_{jl} |j\rangle e^{-i(E_j - E_l)(\tau + \tau')} \langle l | \psi_e \rangle \langle \psi_e | j \rangle \langle l | \psi_e \rangle \langle \psi_e | . \quad (\text{A.28})$$

The final trace over the environment yields

$$\begin{aligned} p[\langle \tilde{V}' \varrho_0 \tilde{V} \rangle \otimes \varrho_0] &= \sum_{jl} \langle l | \psi_e \rangle e^{iE_l(\tau + \tau')} \langle l | \psi_e \rangle \langle \psi_e | j \rangle e^{-iE_j(\tau + \tau')} \langle \psi_e | j \rangle \\ &= S'_e(-\tau - \tau') , \end{aligned} \quad (\text{A.29})$$

where $S'_x(\tau)$ is defined in eq. (A.40).

$p[\langle \tilde{V} \varrho_0 \otimes \tilde{V}' \varrho_0 \rangle_2](t)$: We first compute the average

$$\begin{aligned} \langle \tilde{V} \varrho_0 \otimes \tilde{V}' \varrho_0 \rangle_2 &= \sum_{ijklmn pq} |ij\rangle \langle \tilde{V}_{ij,kl} \langle kl | \varrho_0 \otimes |mn\rangle \tilde{V}_{mn,pq} \rangle_2 \langle pq | \varrho_0 \\ &= \sum_{ijkl} |ij\rangle e^{-i(E_{kl} - E_{ij})(\tau + \tau')} \langle kl | \varrho_0 \otimes |ij\rangle \langle kl | \varrho_0 . \end{aligned} \quad (\text{A.30})$$

Then we apply the partial traces over subsystem \mathcal{H}_1

$$\begin{aligned} \langle \text{tr}_1 (\tilde{V} \varrho_0) \text{tr}_1 (\tilde{V}' \varrho_0) \rangle_2 &= (\sum_{ik} e^{-i(E_k - E_i)(\tau + \tau')} \langle k | \rho_1 | i \rangle \langle k | \rho_1 | i \rangle) \\ &\quad \times \sum_{jl} |j\rangle e^{-i(E_l - E_j)(\tau + \tau')} \langle l | \psi_e \rangle \langle \psi_e | j \rangle \langle l | \psi_e \rangle \langle \psi_e | . \end{aligned} \quad (\text{A.31})$$

The final trace over the environment yields

$$p[\langle \tilde{V} \varrho_0 \otimes \tilde{V}' \varrho_0 \rangle_2] = S'_1(\tau + \tau') S'_e(\tau + \tau') . \quad (\text{A.32})$$

$p[\langle \tilde{V}' \varrho_0 \otimes \varrho_0 \tilde{V} \rangle_2](t)$: We first compute the average

$$\begin{aligned} \langle \tilde{V}' \varrho_0 \otimes \varrho_0 \tilde{V} \rangle_2 &= \sum_{ijklmn pq} |ij\rangle \langle \tilde{V}'_{ij,kl} \langle kl | \varrho_0 \otimes \varrho_0 |mn\rangle \tilde{V}_{mn,pq} \rangle_2 \langle pq | \\ &= \sum_{ijkl} |ij\rangle e^{-i(E_{ij} - E_{kl})(\tau + \tau')} \langle kl | \varrho_0 \otimes \varrho_0 |ij\rangle \langle kl | . \end{aligned} \quad (\text{A.33})$$

We apply the partial traces over subsystem \mathcal{H}_1

$$\begin{aligned} \langle \text{tr}_1 (\tilde{V} \varrho_0) \text{tr}_1 (\varrho_0 \tilde{V}') \rangle_2 &= (\sum_{ik} e^{-i(E_i - E_k)(\tau + \tau')} \langle k | \rho_1 | i \rangle \langle k | \rho_1 | i \rangle) \\ &\quad \times \sum_{jl} |j\rangle e^{-i(E_j - E_l)(\tau + \tau')} \langle l | \psi_e \rangle \langle \psi_e | j \rangle \langle l | . \end{aligned}$$

The final trace over the environment yields

$$p[\langle \tilde{V} \varrho_0 \otimes \varrho_0 \tilde{V}' \rangle_2] = S'_1(-\tau - \tau'). \quad (\text{A.34})$$

A.4 The general solution

If the coupling matrix is taken either from the Gaussian unitary (GUE) or orthogonal (GOE) ensemble, we find

$$\begin{aligned} A_{\text{II}} = & [C_1(|\tau - \tau'|) - S_1(\tau - \tau')] [C_e(|\tau - \tau'|) - S_e(\tau - \tau')] \\ & + \chi_{\text{GOE}} [1 - S'_e(-\tau - \tau') + S'_1(\tau + \tau') S'_e(\tau + \tau') - S'_1(-\tau - \tau')]. \end{aligned} \quad (\text{A.35})$$

These expressions are derived from the previous two sections, for the GUE case in A.2, for the GOE case in A.3. The correlation functions C_x, S_x, C'_x and S'_x with $x \in \{1, e\}$ are defined and discussed in A.5.

If the dimension of the Hilbert space of the environment goes to infinity, the corresponding correlation functions simplify, as discussed in A.5. We are then left with

$$A_{\text{II}} = [C_1(|\tau - \tau'|) - S_1(\tau - \tau')] \bar{C}(|\tau - \tau'|) + \chi_{\text{GOE}} [1 - S'_1(-\tau - \tau')]. \quad (\text{A.36})$$

A.5 Some particular correlation functions

Averaging over the perturbation (*i.e.* the coupling) leads to expressions which may involve the diagonal matrix

$$C_x(\tau) = \sum_{ik} |i\rangle e^{-i(E_k - E_i)\tau} \langle i| \quad x \in 1, e. \quad (\text{A.37})$$

Here, x denotes one of the two subsystems, either the qubit or the environment. Evidently, the energies E_k are the eigenvalues of the corresponding Hamiltonian. In the derivations in this appendix, the expectation value of $C_x(\tau)$ with respect to the initial state $\varrho_0 = \rho_1 \otimes \rho_e$ are of particular importance. These are denoted by

$$C_x(\tau) = \text{tr} (C_x(\tau) \rho_x) \quad x \in 1, e. \quad (\text{A.38})$$

In this work, $\rho_e = |\psi_e\rangle\langle\psi_e|$ is always a pure state.

We will also encounter another type of correlation function, which may be defined as follows

$$S_x(\tau) = \text{tr}_x \left[e^{-iH_x \tau} \rho_x e^{iH_x \tau} \rho_x \right]. \quad (\text{A.39})$$

If the initial state ρ_x is pure, this quantity becomes the return probability. At $\tau = 0$ it gives the purity of ρ_x . In the case of GOE averages, we also encounter the correlation function

$$S'_x(\tau) = \text{tr}_x \left[e^{-iH_x \tau} \rho_x e^{iH_x \tau} \rho_x^T \right]. \quad (\text{A.40})$$

In the main part of this paper, we focus on the limit, where the dimension of the environment(s) becomes infinite. In that case it makes sense to perform an additional spectral average over H_e and/or $H_{e'}$. In the case of $C_e(t)$ this yields

$$\langle C_e(\tau) \rangle = \bar{C}(\tau) \mathbb{1}_e \bar{C}(\tau) = \langle C_e(\tau) \rangle = 1 + \delta(\tau/\tau_H) - b_2^{(\beta)}(\tau/\tau_H), \quad (\text{A.41})$$

where $b_2^{(\beta)}(t)$ is the two-point spectral form factor with time measured in units of the Heisenberg time τ_H for the corresponding spectral ensemble. In the limit of large dimension $N_e = \dim(\mathcal{H}_e)$ we find for the other correlation functions:

$$S_e(\tau) = \text{tr} \left(e^{-iH_e \tau} |\psi_e\rangle\langle\psi_e| e^{iH_e \tau} |\psi_e\rangle\langle\psi_e| \right) \quad (\text{A.42})$$

$$S'_e(\tau) = \text{tr} \left(e^{-iH_e \tau} |\psi_e\rangle\langle\psi_e| e^{iH_e \tau} |\psi_e^*\rangle\langle\psi_e^*| \right). \quad (\text{A.43})$$

For random pure states, as considered in the present work, both correlation functions are at most of order one at $\tau = 0$. For $\tau > 0$ they drop very quickly and soon become of order N_e^{-1} . This happens on the same time scale, where $C_e(\tau)$ drops from values of the order N_e to values of the order one. In that sense we consider these correlation functions to contribute only $O(N_e^{-1})$ corrections to the result given in eq. (A.36).

A single qubit is a two level system. The most general pure initial state is given by $|a\rangle = |1\rangle a_1 + |2\rangle a_2$, with $|a_1|^2 + |a_2|^2 = 1$. The most general mixed state is given by $\rho_1 = \lambda_1 |a\rangle\langle a| + \lambda_2 |b\rangle\langle b|$, with $\lambda_1, \lambda_2 \geq 0$, real, $\lambda_1 + \lambda_2 = 1$, and $|a\rangle, |b\rangle$ arbitrary pure states with $\langle a|b\rangle = 0$. We will now investigate the behaviour of the different correlation functions $\text{Re}C_1(\tau)$, $S_1(\tau)$, and $S'_1(\tau)$ as it depends on the initial state and the Hamiltonian $H_1 = |1\rangle E_1 \langle 1| + |2\rangle E_2 \langle 2|$.

(a) Assume $\rho_1 = |a\rangle\langle a|$. Then

$$C_1(\tau) = \sum_{ik} |a_i|^2 e^{-i(E_k - E_i)\tau} = 1 + \cos \Delta\tau + i(|a_2|^2 - |a_1|^2) \sin \Delta\tau, \quad (\text{A.44})$$

holds, so

$$\text{Re } C_1(\tau) = 1 + \cos \Delta\tau \quad \Delta = E_2 - E_1. \quad (\text{A.45})$$

(b) For $\rho_1 = \lambda_1 |a\rangle\langle a| + \lambda_2 |b\rangle\langle b|$ we still have

$$\text{Re } C_1(\tau) = 1 + \cos \Delta\tau. \quad (\text{A.46})$$

(c) Assume $\rho_1 = |a\rangle\langle a|$. Then we find for $S_1(\tau) = s(|a\rangle; \tau)$

$$S_1(\tau) = \sum_{ik} |a_i|^2 |a_k|^2 e^{-i(E_i - E_k)\tau} = |a_1|^4 + |a_2|^4 + 2|a_1|^2 |a_2|^2 \cos \Delta\tau. \quad (\text{A.47})$$

This expression only depends on the absolute values squared of the coefficients a_1 and a_2 . Therefore we may parametrize them without loss of generality as $a_1 = \cos \phi$ and $a_2 = \sin \phi$. We then find

$$S_1(\tau) = g_\phi + (1 - g_\phi) \cos \Delta\tau \quad g_\phi = |a_1|^4 + |a_2|^4 = 1 - \frac{1}{2} \sin^2 2\phi. \quad (\text{A.48})$$

(d) For a general mixed state $\rho_1 = \lambda_1 |a\rangle\langle a| + \lambda_2 |b\rangle\langle b|$ we find

$$\begin{aligned} S_1(\tau) &= \lambda_1^2 s(|a\rangle; \tau) + \lambda_2^2 s(|b\rangle; \tau) + 2\lambda_1\lambda_2 \sum_{ik} a_i a_k^* b_k b_i^* \cos(E_i - E_k)\tau \\ &= \lambda_1^2 s(|a\rangle; \tau) + \lambda_2^2 s(|b\rangle; \tau) + \\ &\quad 4\lambda_1\lambda_2 |a_1|^2 |b_1|^2 (1 - \cos \Delta\tau), \end{aligned} \quad (\text{A.49})$$

where we have used that $\langle a|b\rangle = a_1 b_1^* + a_2 b_2^* = 0$. Note that the coefficients a_1, a_2, b_1, b_2 may be arranged into a square unitary matrix, and must therefore be of the following general form

$$\begin{pmatrix} a_1 & b_1 \\ a_2 & b_2 \end{pmatrix} = e^{i\theta} \begin{pmatrix} e^{i\xi} \cos \phi & e^{i\chi} \sin \phi \\ -e^{-i\chi} \sin \phi & e^{-i\xi} \cos \phi \end{pmatrix}. \quad (\text{A.50})$$

This shows that $s(|a\rangle; \tau) = s(|b\rangle; \tau) = g_\phi + (1 - g_\phi) \cos \Delta\tau$, and that

$$\begin{aligned} S_1(\tau) &= (\lambda_1^2 + \lambda_2^2) [g_\phi + (1 - g_\phi) \cos \Delta\tau] \\ &\quad + 2\lambda_1\lambda_2 (1 - g_\phi) (1 - \cos \Delta\tau). \end{aligned} \quad (\text{A.51})$$

Since $\lambda_1 + \lambda_2 = 1$ it is convenient to set $\lambda_1 = \cos^2 \theta$ and $\lambda_2 = \sin^2 \theta$ such that we may write $\lambda_1^2 + \lambda_2^2 = g_\theta$ and obtain

$$S_1(\tau) = 1 - g_\theta - g_\phi + 2g_\theta g_\phi + (2g_\theta - 1)(1 - g_\phi) \cos \Delta\tau. \quad (\text{A.52})$$

(e) Assume again that $\rho_1 = |a\rangle\langle a|$. Then we find for $S'_1(\tau) = s'(|a\rangle; \tau)$

$$\begin{aligned} S'_1(\tau) &= |a_1|^4 + |a_2|^4 + a_1^2(a_2^*)^2 e^{i\Delta\tau} + a_2^2(a_1^*)^2 e^{-i\Delta\tau} \\ &= g_\phi + 2|a_1|^2|a_2|^2 \cos(\Delta\tau + 2\eta) \\ &= g_\phi + (1 - g_\phi) \cos(\Delta\tau + 2\eta) \quad \eta = \arg(a_1) - \arg(a_2). \end{aligned} \quad (\text{A.53})$$

However, as discussed in sec. 2.5, a natural symmetry around the y axis (in the Bloch sphere picture) appears for $\Delta = 0$. In that case, using γ as defined in that section, one can prove that

$$1 - S'_1(\tau)|_{\Delta=0} = (1 - g_\phi)[1 - \cos(2\eta)] = \sin^2 \gamma \quad (\text{A.54})$$

using elementary geometric and trigonometric considerations.

(f) For a general mixed state $\rho_1 = \lambda_1 |a\rangle\langle a| + \lambda_2 |b\rangle\langle b|$ we find

$$S'_1(\tau) = \lambda_1^2 s'(|a\rangle; \tau) + \lambda_2^2 s'(|b\rangle; \tau) + 2\lambda_1\lambda_2 \operatorname{Re} \sum_{ik} a_i a_k^* b_k^* b_i e^{-i(E_i - E_k)\tau}. \quad (\text{A.55})$$

It follows from eq. (A.50) that $\arg(b_1) - \arg(b_2) = \arg(a_1) - \arg(a_2) - \pi$, such that the equality $s'(|a\rangle; \tau) = s'(|b\rangle; \tau)$ holds, just as in the case of $S_1(\tau)$. Therefore we may write

$$S'_1(\tau) = g_\theta [g_\phi + (1 - g_\phi) \cos(\Delta\tau + 2\eta)] \quad (\text{A.56})$$

$$\begin{aligned} &+ 2\lambda_1\lambda_2(1 - g_\phi) \operatorname{Re}(1 + e^{i(\Delta\tau + 2\eta - \pi)}) \\ &= 1 - g_\theta - g_\phi + 2g_\theta g_\phi + (2g_\theta - 1)(1 - g_\phi) \cos(\Delta\tau + 2\eta). \end{aligned} \quad (\text{A.57})$$

Note that the only difference to $S(\tau)$ in case (d) is the additional phase 2η in the argument of the cosine function. Using the same angle γ defined with eq. (3.26), in complete analogy with eq. (2.23), and using eq. (A.54) we obtain

$$1 - S'_1(\tau)|_{\Delta=0} = 1 - g_\theta + (2g_\theta - 1) \sin^2 \gamma. \quad (\text{A.58})$$

Appendix B

Implementing the evolution of the KI models

In this appendix we describe how to implement numerically Hamiltonians describing a set of qubits with pairwise variable Ising interaction, and kicked with a periodic, and site dependent, magnetic field. We have used this systems in chapters 5 and 6, the reason being (i) the flexibility of the dynamical model to describe various physical situations, (ii) it has various dynamical regimes, and (iii) it has an efficient implementation making it useful for numerical studies.

Recall eq. (5.5), the Hamiltonian of the system is

$$H = \sum_{j>k=1}^L J_{j,k} \sigma_j^z \sigma_k^z + \delta_1(t) \sum_{j=1}^L \vec{b}_j \cdot \vec{\sigma}_j. \quad (\text{B.1})$$

which gives rise to the Floquet operator $U_{\text{KI}} = U_{\text{Ising}} U_{\text{kick}}$ with

$$U_{\text{Ising}} = \exp \left(-i \sum_{j>k=1}^L J_{j,k} \sigma_j^z \sigma_k^z \right), \quad U_{\text{kick}} = \exp \left(-i \sum_{j=1}^L \vec{b}_j \cdot \vec{\sigma}_j \right). \quad (\text{B.2})$$

However notice that

$$U_{\text{Ising}} = \prod_{j>k=1}^L \exp \left(-i J_{j,k} \sigma_j^z \sigma_k^z \right), \quad U_{\text{kick}} = \prod_{j=1}^L \exp \left(-i \vec{b}_j \cdot \vec{\sigma}_j \right) \quad (\text{B.3})$$

Thus the evolution operator is decomposed trivially into single and two qubit operators that can be efficiently implemented in a computer. Notice

that we do not need to explicitly diagonalize or even store the complete evolution operator thus allowing the implementation of twice as much spins than with brute force diagonalization.

The state can be stored in a complex array with indices ranging from 0 to $2^L - 1$. The state (expressed in the computational basis)

$$|\psi\rangle = \sum_{i_{L-1}, i_{L-2}, \dots, i_0=0}^1 \alpha_{i_{L-1}i_{L-2}\dots i_0} |i_{L-1}i_{L-2}\dots i_0\rangle, \quad (\text{B.4})$$

can be stored in a complex array of dimension 2^L , if in the position $\sum_j i_j 2^j$ we store the value $\alpha_{i_{L-1}i_{L-2}\dots i_0}$. A Fortran 90 routine implementing the Ising interaction with the state stored in this form is the following.

```
subroutine Action_Ising_Interaction(psi,l,m,J)
complex(kind(1d0)),intent(inout)  :: psi(0:)
real(kind(1d0)),intent(in)        :: J
integer,intent(in)                 :: l,m
integer                             :: i
do i=0,size(psi)-1
  If(bttest(i,l).eqv.bttest(i,m)) then
    psi(i)=exp(-(0d0,1d0)*J)*psi(i)
  else
    psi(i)=exp((0d0,1d0)*J)*psi(i)
  end If
end do
end subroutine Action_Ising_Interaction
```

A routine to implement the magnetic kick is now presented.

```
subroutine Application_Of_Kick(psi,b,l)
complex(kind(1d0)),intent(inout)  :: psi(0:)
real(kind(1d0)),intent(in)        :: b(:)
complex(kind(1d0))                 :: Matrix_For_Kick(2,2)
complex(kind(1d0))                 :: z(2)
integer,intent(in)                 :: l
integer                             :: j_left,j_right,left_digit
integer                             :: UpperNumber,LowerNumber
if(sum(b**2).eq.0d0) return
Matrix_For_Kick=Matrix_For_Magnetic_Kick(b)
```



```

do j_left=0,size(psi)/2*(1+1)-1
  left_digit=ishft(j_left,1+1)
  do j_right=0,2**l-1
    LowerNumber=left_digit+j_right
    UpperNumber=IBset(LowerNumber,1)
    z(1)=psi(LowerNumber); z(2)=psi(UpperNumber)
    z=MatMul(Matrix_For_Kick,z)
    psi(LowerNumber)=z(1); psi(UpperNumber)=z(2)
  end do
end do
end subroutine Application_Of_Kick

```

The previous routine uses the following function.

```

function Matrix_For_Magnetic_Kick(b)
  complex(kind(1d0))      :: Matrix_For_Magnetic_Kick(2,2)
  real(kind(1d0)),intent(in) :: b(3)
  real(kind(1d0))         :: n(3),phi,cosphis2,sinphis2
  phi=norma(b);   n=b/phi
  Matrix_For_Magnetic_Kick(1,1)=&
    cos(phi)-(0d0,1d0)*n(1)*sin(phi)
  Matrix_For_Magnetic_Kick(2,2)=&
    conjg(Matrix_For_Magnetic_Kick(1,1))
  Matrix_For_Magnetic_Kick(1,2)=&
    -(n(3)+(0d0,1d0)*n(2))*sin(phi)
  Matrix_For_Magnetic_Kick(2,1)=&
    -conjg(Matrix_For_Magnetic_Kick(1,2))
end function Matrix_For_Magnetic_Kick

```


Appendix C

The exponentiation

The linear response formulae for purity derived throughout the thesis are expected to work for high purities or, equivalently, when the first two terms in the series eq. (2.9) approximate the echo operator well; it is of obvious interest to extend them to cover a larger range. The exact solution for fidelity decay has, in some cases, been possible with some effort, using super-symmetry techniques. This has been partly due to the simple structure of fidelity, but trying to use this approach for a more complicated object such as purity seems to be out of reach for the time being. Exponentiating the formulae obtained from the linear response formalism has proved to be in good agreement with the exact super-symmetric and numerical results for fidelity, if the perturbation is not too big. The exponentiation of the linear response formulae for purity can be compared with Monte Carlo simulations in order to prove its validity. We wish to explain the details required to implement this procedure in this appendix.

Given a linear response formula $P_{\text{LR}}(t)$ [for which $P(0) = 1$], and an expected asymptotic value for infinite time P_∞ , the exponentiation reads

$$P_{\text{ELR}}(t) = P_\infty + (1 - P_\infty) \exp \left[-\frac{1 - P_{\text{LR}}(t)}{1 - P_\infty} \right]. \quad (\text{C.1})$$

This particular form guaranties that

$$P_{\text{ELR}}(t) \approx P_{\text{LR}}(t) \quad (\text{C.2})$$

for short times, and that

$$\lim_{t \rightarrow \infty} P_{\text{ELR}}(t) = P_\infty. \quad (\text{C.3})$$

The particular value of P_∞ will depend on the physical situation; in our case it will depend on the configuration and on the initial condition. We now turn to an estimation of this quantity for the spectator configuration, under some very general assumptions.

Let us write the initial condition in the qubits as

$$|\psi_{12}(\theta)\rangle = \cos\theta|\tilde{0}_1\tilde{0}_2\rangle + \sin\theta|\tilde{1}_1\tilde{1}_2\rangle \quad (\text{C.4})$$

for some rotated qubits $|\tilde{0}_i\rangle, |\tilde{1}_i\rangle$. We assume that for long enough times, decoherence is described for the uncoupled qubit by the following channel:

$$\mathcal{E}_{\text{td}}[\rho] = \frac{\mathbf{1}}{2} = \frac{1}{4}(\sigma_x\rho\sigma_x + \sigma_y\rho\sigma_y + \sigma_z\rho\sigma_z + \rho). \quad (\text{C.5})$$

This is the depolarizing channel with full strength [NC00]. This channel is unital. We now evaluate $\mathcal{E}_{\text{td}} \otimes \mathbf{1}[|\psi_{12}(\theta)\rangle\langle\psi_{12}(\theta)|]$. Note that $\mathcal{E}_{\text{td}} \otimes \mathbf{1}[|00\rangle\langle 00|] = \mathbf{1} \otimes |0\rangle\langle 0|/2$ and $\mathcal{E}_{\text{td}} \otimes \mathbf{1}[|11\rangle\langle 11|] = \mathbf{1} \otimes |1\rangle\langle 1|/2$. For the cross terms we obtain:

$$\mathcal{E}_{\text{td}} \otimes \mathbf{1}[|00\rangle\langle 11|] = \frac{|10\rangle\langle 01| - |10\rangle\langle 01| - |00\rangle\langle 11| + |00\rangle\langle 11|}{4} = 0, \quad (\text{C.6})$$

and also $\mathcal{E}_{\text{td}} \otimes \mathbf{1}[|11\rangle\langle 00|] = 0$. Using the linearity of the channel and the results found, we see that

$$\mathcal{E}_{\text{td}} \otimes \mathbf{1}[|\psi_{12}(\theta)\rangle\langle\psi_{12}(\theta)|] = \frac{1}{2} \begin{pmatrix} \cos^2\theta & 0 & 0 & 0 \\ 0 & \cos^2\theta & 0 & 0 \\ 0 & 0 & \sin^2\theta & 0 \\ 0 & 0 & 0 & \sin^2\theta \end{pmatrix}. \quad (\text{C.7})$$

In the end, we estimate the asymptotic value of purity as

$$P_\infty = \frac{\cos^4\theta + \sin^4\theta}{2} = \frac{g_\theta}{2}, \quad (\text{C.8})$$

where g_θ was defined in eq. (2.17).

For both the joint and the separate environment configuration we use the value

$$P_\infty = P(\mathcal{E}_d \otimes \mathcal{E}_d[|\psi_{12}(\theta)\rangle\langle\psi_{12}(\theta)|]) = \frac{1}{4}. \quad (\text{C.9})$$

Good agreement is found with Monte Carlo simulations for moderate and strong couplings. Obtaining the value of P_∞ for weak coupling should be possible using perturbation theory on the eigenvectors. This calculation is still missing.

Appendix D

Entanglement

Here we want to discuss or comment on some technical aspects that do not need to be in the introduction. We prefer to include them in an appendix to ease the reading of the main part of the text.

Recall from eq. (1.1) that a pure state of a bipartite system is separable if it is the tensor product of states in the individual systems. The generalization for multipartite systems is straightforward. Let us have n particles, each in a Hilbert space \mathcal{H}_i , $i = 1, \dots, n$. A state $|\psi\rangle$ is said to be separable if it can be written as

$$|\psi\rangle = \bigotimes_{i=1}^n |\psi_i\rangle, \quad (|\psi_i\rangle \in \mathcal{H}_i), \quad (\text{D.1})$$

compare with eq. (1.1). Otherwise it is called entangled. A mixed, bipartite system in state ρ is said to be separable if it can be written as a convex combination of separable states. That is, if

$$\rho = \sum_i p_i \rho_i^{(A)} \otimes \rho_i^{(B)} \quad (\text{D.2})$$

where $p_i > 0$ and $\rho_i^{(A)}$ ($\rho_i^{(B)}$) are density matrices of system A (B). Though this definition is simpler from a conceptual point of view, often a more comfortable formulation in terms of pure states is obtained expressing the density matrices in terms of projectors. Thus a bipartite mixed state ρ is said to be separable if it can be written as

$$\rho = \sum_i p_i |\psi_i^{(A)}\rangle\langle\psi_i^{(A)}| \otimes |\psi_i^{(B)}\rangle\langle\psi_i^{(B)}| \quad (\text{D.3})$$

with $|\psi_A\rangle \in \mathcal{H}_A$, $|\psi_B\rangle \in \mathcal{H}_B$ and p_i real and positive. For the multipartite case one should require, instead of eq. (D.2), that

$$\rho = \sum_i p_i \otimes_{k=1}^n \rho_i^{(k)} \quad (\text{D.4})$$

with $\rho_i^{(k)}$ being a density matrix of space \mathcal{H}_k and the p_i s probabilities (*i.e.* still a convex combination of separable states).

D.1 Quantifying two qubit entanglement

Here we want to present the entanglement of formation, and its relation to concurrence.

Let us first define the entanglement of formation. The entanglement of formation E_F measures the number of Bell pairs needed to create an ensemble of pure states representing the state to be studied [HW97]. We define E_F by stages. The entanglement of formation for a pure state is the von Neumann entropy of the reduced density matrix. Given $|\psi\rangle$ with Schmidt coefficients λ_1 and $\lambda_2 = \sqrt{1 - \lambda_1^2}$, $E_F(|\psi\rangle\langle\psi|) = -\lambda_1 \log_2 \lambda_1 - \lambda_2 \log_2 \lambda_2$ ¹. For mixed states we have

$$E_F(\rho) = \min_{\{p_i, |\psi_i\rangle\}} \sum_i p_i E_F(|\psi_i\rangle\langle\psi_i|) \quad \text{such that} \quad \rho = \sum_i p_i |\psi_i\rangle\langle\psi_i| \quad (\text{D.5})$$

and the p_i s are positive. This represents the minimum amount of entanglement needed to create an ensemble that reproduces ρ . All the requirements discussed above are fulfilled.

Concurrence C is defined via the entanglement formation:

$$E_F(\rho) = h\left(\frac{1 + \sqrt{1 - C(\rho)^2}}{2}\right); \quad h(x) = -x \log_2(x) - (1 - x) \log_2(1 - x). \quad (\text{D.6})$$

This weird definition is inspired in the fact that a simple and close formula for $C(\rho)$ was obtained.

¹Notice the close relation with the classical entropy.

D.2 Some generalizations

Two possible generalizations for the entanglement measures would be desirable: (i) Allow qudits instead of qubits (*i.e.* having more than 2 levels). Furthermore one could like to quantify the entanglement in systems with infinite or a continuous number of levels. (ii) Allow the Hilbert space of the system to have a more complicated partition, namely let $\mathcal{H} = \otimes_{k=1}^n \mathcal{H}_k$ with n being bigger than 2; for example if one wants to examine the entanglement between three particles, $n = 3$. The cases in which the state representing the system is pure are again much simpler than when the state is mixed.

For both cases the concept of entanglement is easy to define. A relevant review of entanglement measures for qudits is [PV07]. Some measures of entanglement, for the multipartite case, are discussed in [MCKB05]. As the reader can find, these generalizations are not simple, unique or easy to calculate.

Appendix E

RMT: various aspects

In this appendix we wish to discuss some technicalities about the random matrix ensembles used in this thesis. It includes a small discussion about the ensembles with/without time reversal symmetry, the construction of the ensembles, and concepts as the Heisenberg time, level density, and form factor.

We start by discussing the difference between the unitary ensembles (GUE and CUE) and the orthogonal ensembles (GOE and COE). We first describe the GOE. This is an ensemble of Hermitian matrices with the special property of being real. As we know, any Hamiltonian describing a system with an anti-unitary symmetry (as time reversal) can be represented as a real matrix *without diagonalizing it*. The COE corresponds to the unitary version of this ensemble, for each H in the GOE, a corresponding $\exp(iH)$ is found in the COE. On the other hand, when the physical system has no underlying anti-unitary symmetry, it must be described by arbitrary Hermitian matrices. The GUE is the appropriate ensemble as it has no anti-unitary symmetry. The set corresponding to this ensemble is the set of all Hermitian matrices. The CUE is the unitary version of this ensemble. The most common example of this distinction involves a particle in a chaotic billiard. With/without a magnetic field the level statistics resemble those of the GUE/GOE. Numerical [BGdS95] and experimental [SAOO95, DDG⁺03] confirmation has been reported.

We now turn our attention to the construction of the ensembles used in this thesis. The neatest way to perform that construction is using the arguments of least information (see [Bal68, Dys62] or, for a more modern

view, [Mel95] section 2). We wish to recall that an ensemble is a set and a probability distribution, which can be regarded as a measure. The set shall be no problem to define, but the measure is more delicate.

We start by defining the entropy of a distribution of matrices (objects) A . Let $P(A)$ be a probability distribution on a set matrices A (or of anything). The information of the ensemble is measured via the information entropy [Sha48]:

$$I[P(A)] = - \int P(A) \log P(A) dA \quad (\text{E.1})$$

Notice that we need an *a priori* measure dA . This measure, in all the cases considered here, is an invariant (under a suitable operation) measure. If there is a group structure underling (like for the GOE and GUE with matrix addition and the CUE with matrix multiplication) this measure coincides with the Haar measure. Otherwise (for the COE), it is slightly more complicated. For details see [Car35, Meh91]. The information entropy, for a given $P(A)$, can be interpreted in a number of ways [Sha48]. For example, it measures the amount of information in a given member of the ensemble. For bigger entropy, the information in each member is smaller (*i.e.* its members are closer to the anonymity).

Let us start by constructing the CUE, which stands for circular unitary ensemble. This is an ensemble of unitary matrices of given dimension. The distribution that we use for the ensemble is simply the homogeneous one, $P(A) = \text{constant}$. Intuitively it is clear that, for this set, it is the ensemble with greatest information entropy, see eq. (E.1). We can do an analogous treatment for orthogonal matrices to obtain the circular orthogonal ensemble (COE), using a uniform “probability” for all orthogonal matrices.

For Hermitian operators, as compared to the unitary ones, the situation is more complicated. Think of Hermitian 1×1 operators (real numbers). Its Haar measure is simply the usual Lebesgue measure. The whole set has an unbounded measure hence it cannot be normalized; working naively with $P(A) \propto 1$ results in diverging integrals. Moreover, for the real line (and using the usual measure) there does not exist such a thing as a uniform distribution. Similar problems result for larger matrices due to the non-compactness of the set under consideration. However one can create a least information ensemble if one is willing to postulate an additional condition. We shall require that the average of $\text{tr } H^2$ (the “strength” of the operator) is some fixed number. Its particular value is irrelevant and will only impose some normalization condition in the ensemble. Notice that this condition is basis independent. One can solve the problem of max-

imizing the entropy constrained to the condition above, using Lagrange multipliers. The solution is

$$P(H) \propto e^{-\lambda \text{tr} H^2} \quad (\text{E.2})$$

with λ a real (ensemble dependent) number.

In all the cases (COE, CUE, GOE, and GUE) we can see that the distribution is invariant under unitary (for the CUE and GUE) or orthogonal (for the COE and GOE) transformations, e. g. for the GUE, $P(H) = P(U^{-1}HU)$ for any unitary operator U , as the only condition we imposed is basis independent. The invariance properties of the ensemble will be used heavily to simplify the problem under consideration and group together equivalent cases during the thesis.

A practical way to realize the Gaussian ensembles (G*E) is to choose the matrix elements as Gaussian random variables with a given standard deviation σ . Consider the independent elements of a Hermitian matrix H . We have that $\text{tr} H^2 = \sum_i H_{ii}^2 + 2 \sum_{i<j} H_{ij}H_{ji}$ and then the distribution eq. (E.2) can be factorized as

$$P(H) \propto \prod_{i<j=1}^N e^{-2\lambda H_{ij}H_{ji}} \prod_{i=1}^N e^{-\lambda H_{ii}^2}. \quad (\text{E.3})$$

For the GOE (of fixed dimension N) we choose: the diagonal elements as real variables with $\sigma^2 = 1$ (forget about the global, unimportant normalization constant); for the elements above the diagonal, real variables with $\sigma^2 = 2$; and the others (below the diagonal) are chosen to make the matrix symmetric. The matrix elements average like

$$\overline{V_{ij}} = 0, \overline{V_{ij}V_{kl}} = \delta_{il}\delta_{jk} + \delta_{ik}\delta_{jl}. \quad (\text{E.4})$$

Of course the matrix elements can be multiplied by a convenient (possibly N dependent) factor to achieve certain particular condition. Under similar considerations one can show that a typical GUE element is obtained as follows. Choose the diagonal elements from a real Gaussian ensemble with $\sigma = 1$. The upper triangle of the matrix are complex numbers; the real and imaginary parts are chosen independently from a real Gaussian ensemble with $\sigma = 1/\sqrt{2}$. The lower elements are chosen to make the matrix Hermitian. Its matrix elements average as

$$\overline{V_{ij}} = 0, \overline{V_{ij}V_{kl}} = \delta_{il}\delta_{jk}. \quad (\text{E.5})$$

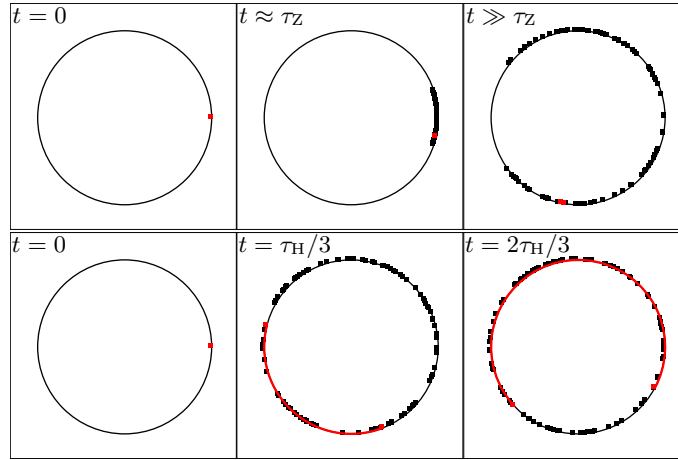


Figure E.1: Visualization of the Zeno time (above) and the Heisenberg time (below). Eigenvalues E are plotted in the unit circle as dots as time passes, using $\exp(-iEt/\hbar)$. An arc between 2 particular adjacent eigenvalues is shown in red. The Zeno time τ_Z is close to the first time chosen all eigenvalues cover the unit circle. Heisenberg time τ_H is the *average* time when adjacent eigenvalues cross in the unit circle. 100 Poissonian eigenvalues were used for these plots.

At this point we want to introduce the concept of level density, sometimes also called density of states. This is the number of levels per unit interval. The level density is a particular feature of each system, even of chaotic ones. Random matrices have their own level density. The circular ensembles have a constant level density (within the interval $[0, 2\pi)$) whereas the Gaussian ensembles have an ellipsoidal level density (often referred to as circular). In the large dimension limit it is given by

$$\rho(E) = \frac{\sqrt{N}}{\pi} \sqrt{1 - \frac{E^2}{4N}}. \quad (\text{E.6})$$

for the normalization previously proposed, see fig. E.2. Other concept closely related to the level density is the Heisenberg time τ_H . This is the typical time in which two neighboring levels cross in the unit circle (*i.e.* when $(E_{i+1} - E_i)t/\hbar \approx 2\pi$). Of course if the level density is not uniform, the Heisenberg time is also not uniform. Sometimes it is convenient to have a uniform Heisenberg time. This amounts to have constant density of states throughout the spectrum. If one uses the circular ensembles this

is automatically granted. Otherwise, the constant density can be achieved using the unfolding procedure. Normally it requires adjusting an average density but, since for the GUE and GOE we know the average density, we can calculate its cumulative function [GMGW98], and use that to unfold the spectrum. Let E_c be the smallest expected energy (eigenvalue) of your spectrum. The unfolded energy ϕ_i corresponding to the original eigenvalue E_i is

$$\phi_i = \frac{N}{\pi} \left(\sin^{-1} e_i + e_i \sqrt{1 - e_i^2} \right), \quad e_i = \frac{E_i}{E_c}. \quad (\text{E.7})$$

Another important time scale is the Zeno time τ_Z . It is the time the eigenvalues are far from the origin, but are still much smaller than 2π . Both concepts are sketched in fig. E.1.

An important characteristic of the RMT spectra are its correlations. We can use the form factor

$$K_2(t) := \frac{1}{N} \left| \sum_{j=1}^N e^{itE_j} \right|^2 \quad (\text{E.8})$$

to quantify this correlation. In the large dimension limit we have that

$$\overline{K_2(t)} = K_2^{(\beta)}(t) = 1 + \delta \left(\frac{t}{\tau_H} \right) - b_2^{(\beta)} \left(\frac{t}{\tau_H} \right). \quad (\text{E.9})$$

The index β characterizes the ensemble, $\beta = 1$ for the GOE (and COE) and $\beta = 2$ for the GUE (and CUE). The functions $b_2^{(\beta)}$ are given by

$$b_2^{(1)}(t) = \begin{cases} 1 - 2|t| + |t| \ln(2|t| + 1) & \text{if } |t| \leq 1, \\ -1 + |t| \ln \frac{2|t|+1}{2|t|-1} & \text{if } |t| > 1 \end{cases} \quad (\text{E.10})$$

and

$$b_2^{(2)}(t) = \begin{cases} 1 - |t| & \text{if } |t| \leq 1, \\ 0 & \text{if } |t| > 1 \end{cases}, \quad (\text{E.11})$$

see fig. E.2.

A characteristic features of the GOE and GUE spectra is the hole in the correlation function (for a random spectra, $K_2(t) = 1 + \delta(t/\tau_H)$). This hole has been shown to induce a certain stability in fidelity decay. In this work it will also display some enhancement of stability though not as spectacular as for fidelity decay.

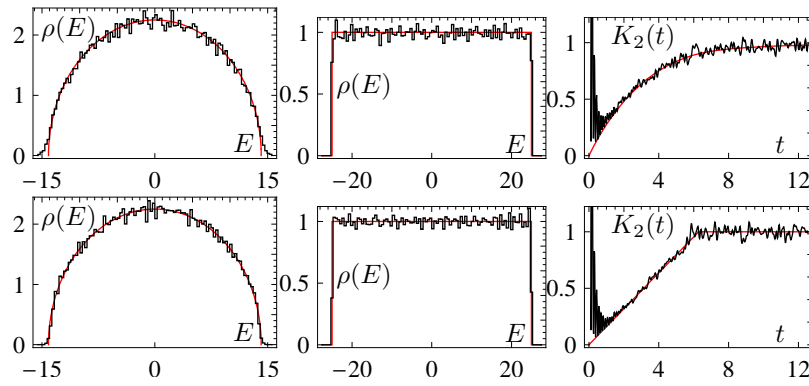


Figure E.2: We see here the level density of an ensemble of 800 elements, of the GOE (top) and GUE (bottom) with $N = 50$. We show, from left to right, the level density eq. (E.6), the unfolded level density (see eq. (E.7)) and the form factor K_2 Eqs. E.10 and E.11.

Appendix F

On the numerics of RMT and quantum information

We now describe some tricks to implement some aspects of RMT. We also include some of the routines useful for quantum information simulation. All routines are for Fortran 90. $\text{pi} = \pi$ and $\text{I} = i$.

F.1 Random matrices

To build the random matrices, as noted in Appendix E, one can use random Gaussian variables. Most low level languages provide homogeneous distributions in the unit interval $[0,1)$. A transformation from this distribution (characterizing variables u and v), to a complex Gaussian one (characterizing variable z) of width σ and centered at x_0 is provided by

$$z = \sigma e^{2\pi i v} \sqrt{-2 \log u} + x_0 \quad (\text{F.1})$$

Its implementation is straightforward, however if $u = 0$ (which occurs numerically with very small, but finite probability) the routine could crash. If instead of selecting $u \in [0,1)$ we select $1 - u \in [0,1)$, the problem is fixed. The routine is called `RandomGaussian`. Its first argument is σ and the second one x_0 .

In view of the considerations of the Appendix E, to build a GUE matrix, one has to choose the diagonal elements real and with $\sigma^2 = 1$ whereas for

114 Appendix F. On the numerics of RMT and quantum information

the off diagonal elements $\sigma^2 = 1/2$. The routine to build the GUE matrix is:

```
subroutine generate_GUE_matrix(matrix)
  implicit none
  integer :: nsize, j1, j2
  complex(kind(1d0)), intent(out) :: matrix(:, :)
  nsize=size(matrix(1,:))
  do j1=1,nsize
    matrix(j1,j1)=real(RandomGaussian(1d0,0d0))
    do j2=j1+1,nsize
      matrix(j1,j2)=RandomGaussian(1/sqrt(2d0),0d0)
      matrix(j2,j1)=conjg(matrix(j1,j2))
    end do
  end do
end subroutine generate_GUE_matrix
```

A routine to generate a GOE matrix is

```
subroutine generate_GOE_matrix(matrix)
  implicit none
  integer :: nsize, j1, j2
  real(kind(1d0)), intent(out) :: matrix(:, :)
  nsize=size(matrix(1,:))
  do j1=1,nsize
    matrix(j1,j1)=&
      real(RandomGaussian(sqrt(2d0),0d0),kind(1d0))
    do j2=j1+1,nsize
      matrix(j1,j2)=real(RandomGaussian(),kind(1d0))
      matrix(j2,j1)=matrix(j1,j2)
    end do
  end do
end subroutine generate_GOE_matrix
```

The normalization is such that eq. (E.4) holds. To obtain the spectrum of such matrices one must diagonalize numerically a dense matrix. The LAPACK90 package provides this routines conveniently packed for Fortran 90.

Most RMT results refer to the center of the spectrum, where the density of states is constant. To have better agreement of the numerics with the

theory one can unfold the spectrum, *i.e.* force an approximate constant level density. Given a density $\rho(E)$, the function $\eta(e) = \int_{\min\{E\}}^e dE \rho(E)$ maps E to an “unfolded” energy e . Since

$$\int_{-1}^e \frac{2N}{\pi} \sqrt{1-E^2} = \frac{N}{\pi} \left(e\sqrt{1-e^2} + \pi - \sin^{-2} e \right) \quad (\text{F.2})$$

(which would assume an spectrum with ranging roughly from ± 1), the following routine gives an unfolded spectrum, ranging from 0 to N .

```
function approxcumulative(Energy,size_spectrum)
  real(kind(1d0))                :: approxcumulative
  real(kind(1d0)), intent(in)    :: energy
  integer, intent(in)           :: size_spectrum
  real(kind(1d0))                :: rescaled_energy
  rescaled_energy=Energy*sqrt(pi)/size_spectrum
  if (rescaled_energy <= -1D0) approxcumulative=0d0
  if (rescaled_energy >= 1D0) approxcumulative=pi
  if ((-1d0<rescaled_energy).and.(rescaled_energy<1d0)) &
    approxcumulative=(asin(rescaled_energy)+ &
    rescaled_energy*sqrt(1-rescaled_energy**2)+pi/2)
  approxcumulative=(approxcumulative-pi/2)*size_spectrum/pi
end function approxcumulative
```

We assume in this function that the spectrum ranges from $\pm N/\sqrt{\pi}$. The unfolding procedure can also work with the same routine presented above as the level density is again a semicircle.

F.2 Quantum information

During the numerical implementation of the ideas exposed in the thesis, we have to do operations that involve tensor product of states [as in eq. (2.4)], like

$$|\psi\rangle = |\psi_A\rangle \otimes |\psi_B\rangle \quad (\text{F.3})$$

with $|\psi_A\rangle \in \mathcal{H}_A$ and $|\psi_B\rangle \in \mathcal{H}_B$. We shall assume that both \mathcal{H}_A and \mathcal{H}_B are spaces of one or more qubits. This allows to take advantage of the bitwise operations available in all programming languages.

In order to explain the implementation of tensor products its better to use an example. We restrict our selfs to tensor products of qubit spaces.

Consider an space composed of L qubits, numbered from 0 to $L - 1$: $\mathcal{H} = \mathcal{H}_{L-1} \otimes \cdots \otimes \mathcal{H}_0$. Now consider the two subspaces $\mathcal{H}_A = \mathcal{H}_{a_{A-1}} \otimes \cdots \otimes \mathcal{H}_{a_0}$ of dimension 2^A and $\mathcal{H}_B = \mathcal{H}_{b_{B-1}} \otimes \cdots \otimes \mathcal{H}_{b_0}$ of dimension 2^B such that $\mathcal{H} = \mathcal{H}_A \otimes \mathcal{H}_B$. Assume that $L = 7$, \mathcal{H}_A is the subspace of qubits 0, 3 and 5 and thus \mathcal{H}_B is the subspace of qubits 1, 2, 4, 6. One can label unambiguously \mathcal{H}_A with a number $n_A = \sum_i 2^{a_i}$. In our case, $n_a = 2^0 + 2^3 + 2^5 = 41$. Analogously one can label \mathcal{H}_B with $n_b = 2^1 + 2^2 + 2^4 + 2^6 = 86$ (notice that $n_a + n_b = 2^L - 1$ and thus are not independent). Using tensor notation, one can associate an single index μ of \mathcal{H} with two indices, one in \mathcal{H}_A and one in \mathcal{H}_B . If one uses the notation explained in Appendix B one must combine the binary bits of index μ with the bits of the numbers representing each space (say i_A in \mathcal{H}_A and i_B in \mathcal{H}_B). As an example assume that $\mu = 55$. One obtains $n_a = 5$ and $n_b = 7$, as shows the following table.

qubit number	6	5	4	3	2	1	0
$\mu = 55$	0	1	1	0	1	1	1
$n_a = 41$	0	1	0	1	0	0	1
$i_A = 5$		1		0			1
$n_b = 86$	1	0	1	0	1	1	0
$i_B = 7$	0		1		1	1	

A routine implementing the procedure is

```

subroutine exdig(number_in,L,n1out,n2out,nwhich)
  implicit none
  integer, intent(in)  :: L,nwhich,number_in
  integer, intent(out) :: n1out,n2out
  integer              :: j,numin, L1,L2
  n1out=0
  n2out=0
  numin=number_in
  L1=bits_on_one(nwhich)
  L2=L-L1
  do j=0,L-1
    if (btest(nwhich,j)) then
      if (btest(numin,0)) n1out=ibset(n1out,0)
      n1out=ishftc(n1out,-1,L1)
    else
      if (btest(numin,0)) n2out=ibset(n2out,0)

```

```

        n2out=ishftc(n2out,-1,L2)
    endif
    numin=ishftc(numin,-1,L)
end do
return
end subroutine exdig

```

Here $\text{number_in} = \mu$, $L = L$, $n1\text{out} = i_A$, $n2\text{out} = i_B$, and $n\text{which} = n_a$. A routine to calculate tensor products of real matrices, that takes advantage of the previous routine is the following.

```

subroutine TensorProduct_real_routine(H_a,H_b,nwhich,H_out)
integer, intent(in)          :: nwhich
real(kind(1d0)), intent(in) :: H_a(0:,0:),H_b(0:,0:)
real(kind(1d0)), intent(out):: H_out(0:,0:)
integer                      :: total_size, j1, j2, &
                             j1a, j1b, j2a, j2b, qubits
total_size=size(H_a,1)*size(H_b,1)
qubits=IntegerLogBase2(total_size)
do j1=0,total_size-1
  do j2=0,total_size-1
    call exdig(j1,qubits,j1a,j1b,nwhich)
    call exdig(j2,qubits,j2a,j2b,nwhich)
    H_out(j1,j2)=H_a(j1a,j2a)*H_b(j1b,j2b)
  enddo
enddo

```

The function `IntegerLogBase2` calculates the integer logarithm in base 2, of its argument (it must be a power of 2). Again $n\text{which} = n_a$, H_A (H_B) is the operator acting in \mathcal{H}_A (\mathcal{H}_B).

The last routine that we wish to document is one for performing partial traces. This routine calculates the partial trace over \mathcal{H}_B of a pure state $\rho = \text{tr}_B |\psi\rangle\langle\psi|$. The input parameters are the state $|\psi\rangle$ (`statin`) and n_a (`nwhich`). The output parameter `rho` is ρ .

```

subroutine safe_PartialTrace(statin,rho,nwhich)
implicit none
complex(kind(1d0))          :: statin(:)
complex(kind(1d0))          :: rho(0:,0:)

```

```

integer, intent(in)          :: nwhich
integer                      :: &
                             err(3), n_final, j1, j2, qubits
complex(kind(1d0)), pointer :: &
                             staout(:, :), st1(:), st2(:)
qubits=IntegerLogBase2(size(statin))
n_final=bits_on_one(nwhich)
allocate (staout(0:2**(qubits-n_final)-1,0:2**n_final-1), &
         stat=err(2))
allocate (st1(0:2**(qubits-n_final)-1), &
         st2(0:2**(qubits-n_final)-1), stat=err(3))
if (any(err /= 0)) then
  print*, "error en PartialTrace"
  stop
endif
call unmsta(statin, staout, nwhich, qubits)
do j1=0, 2**n_final-1
  do j2=0, 2**n_final-1
    rho(j1, j2)=dot_product(staout(:, j2), staout(:, j1))
  enddo
enddo
deallocate(staout, st1, st2, stat=err(1))
return
contains
  subroutine unmsta(statin, staout, nwhich, qubits)
    implicit none
    integer, intent(in)          :: nwhich, qubits
    complex(kind(1d0)), intent(in) :: statin(:)
    complex(kind(1d0)), intent(out) :: staout(:, :)
    integer                      :: j, ncol, nrow
    staout=0d0
    do j=0, size(statin)-1
      call exdig(j, qubits, ncol, nrow, nwhich)
      staout(nrow+1, ncol+1)=statin(j+1)
    enddo
    return
  end subroutine unmsta
end subroutine safe_PartialTrace

```

The function `bits_on_one` counts the number of bits of its argument, set

to 1. The subroutine `unmsta` reorganizes the input state as a matrix, to be able to express the partial trace as a dot product of the vectors composing this matrix. All the programs, and routines are available upon explicit request to the author.

Appendix G

Two minor technicalities

G.1 The Form Factor

We define the spectral form factor as

$$K(t) = \frac{1}{N} \sum_{i=1}^N e^{itE_i}. \quad (\text{G.1})$$

Some authors rescale the energy (or, equivalently the time). The factor in front is used to obtain an asymptotic average value of one for most spectra. This quantity has been studied extensively in the context of quantum chaos [GMGW98, JPA]

We want to evaluate a double integral of the two-level form factor for the GUE case:

$$B_2^{\beta=2}(t) := \int_0^t d\tau \int_0^\tau d\tau' b_2^{\beta=2} \left(\frac{\tau' - \tau}{\tau_H} \right) = \int_0^t d\tau \int_0^\tau d\tau' b_2^2 \left(\frac{\tau'}{\tau_H} \right) \quad (\text{G.2})$$

Let us suppose first that $0 < t < \tau_H$, and thus replace b_2^2 by a linear expression:

$$B_2^2(t) = \int_0^t d\tau \int_0^\tau d\tau' b_2^{\beta=2} \left(\frac{\tau' - \tau}{\tau_H} \right) \quad (\text{G.3})$$

$$= \int_0^t d\tau \int_0^\tau d\tau' \left(1 - \frac{\tau'}{\tau_H} \right) \quad (\text{G.4})$$

$$= \frac{t^2}{2} - \frac{t^3}{6\tau_H}. \quad (\text{G.5})$$

If $t > \tau_H$ the expression must be strictly linear since $b_2^2(t \geq \tau_H) = 0$, and with slope given by $\int_0^{\tau_H} b_2^2(t/\tau_H) = \tau_H/2$. Furthermore, since $B_2^2(t)$ must be continuous, we also have the y intercept of the linear function. This leave us with the result

$$B_2^2(t) = \begin{cases} \frac{t^2}{2} - \frac{t^3}{6\tau_H} & \text{if } 0 \leq t < \tau_H \\ \frac{t\tau_H}{2} - \frac{\tau_H^2}{6} & \text{if } t \geq \tau_H \end{cases}. \quad (\text{G.6})$$

G.2 A small proof of the Born expansion

Consider the Hamiltonian $H_\lambda = H_0 + \lambda W$. The definition of the state ket in the interaction picture is [Sak94]

$$|\psi(t)\rangle_I = U_0^\dagger(t)U_\lambda(t)|\psi(0)\rangle \quad (\text{G.7})$$

where $U_\lambda(t) = \exp(itH_\lambda)$. Consider the equation of motion of the ket in the interaction picture [Sak94]:

$$i\frac{d|\psi(t)\rangle_I}{dt} = \lambda\tilde{W}|\psi(t)\rangle_I \quad (\text{G.8})$$

with $\tilde{W}(t) = U_0^\dagger(t)WU_0(t)$. Formal integration leads to

$$|\psi(t)\rangle_I = |\psi(0)\rangle - i\lambda \int_0^t d\tau \tilde{W}(\tau)|\psi(\tau)\rangle_I. \quad (\text{G.9})$$

Solving the integral by iteration we obtain

$$|\psi(t)\rangle_I = \left(\mathbf{1} + (-i\lambda) \int_0^t d\tau \tilde{W}(\tau) + (-i\lambda)^2 \int_0^t d\tau \int_0^\tau d\tau' \tilde{W}(\tau') + \dots \right) |\psi(0)\rangle. \quad (\text{G.10})$$

Comparing (G.7) and (G.10) we obtain the Born expansion:

$$U_0^\dagger(t)U_\lambda(t) = \mathbf{1} + (-i\lambda) \int_0^t d\tau \tilde{W}(\tau) + (-i\lambda)^2 \int_0^t d\tau \int_0^\tau d\tau' \tilde{W}(\tau)\tilde{W}(\tau') + \dots \quad (\text{G.11})$$

Bibliography

- [Alb92] A. Albrecht. Investigating decoherence in a simple system. *Phys. Rev. D*, 46(12):5504–5520, Dec 1992.
- [Alb93] A. Albrecht. Following a “collapsing” wave function. *Phys. Rev. D*, 48(8):3768–3778, Oct 1993.
- [ALKH02] D. Ahn, J. Lee, M. S. Kim, and S. W. Hwang. Self-consistent non-markovian theory of a quantum-state evolution for quantum-information processing. *Phys. Rev. A*, 66(1):012302, Jul 2002.
- [AV07] R. F. Abreu and R. O. Vallejos. Statistical bounds on the dynamical production of entanglement. March 2007, quant-ph/0703057.
- [Bal68] R. Balian. Random matrices and information theory. *Il Nuovo Cimento B*, (57):183, 1968.
- [BBC⁺93] C. H. Bennett, G. Brassard, C. Crépeau, R. Jozsa, A. Peres, and W. K. Wootters. Teleporting an unknown quantum state via dual classical and einstein-podolsky-rosen channels. *Phys. Rev. Lett.*, 70(13):1895–1899, Mar 1993.
- [BFF⁺81] T. A. Brody, J. Flores, J. B. French, P. A. Mello, A. Pandey, and S. S. M. Wong. Random matrix physics: Spectrum and strength fluctuations. *Rev. Mod. Phys.*, 53:385–479, 1981.
- [BGdS95] O. Bohigas, M.-J. Giannoni, A. M. O. de Almeida, and C. Schmit. Chaotic dynamics and the GOE-GUE transition. *Nonlinearity*, 8:203–221, March 1995.
- [BGS84] O. Bohigas, M. J. Giannoni, and C. Schmit. Characterization of chaotic quantum spectra and universality of level fluctuation laws. *Phys. Rev. Lett.*, 52(1):1–4, Jan 1984.

- [BMM05] J. P. Barjaktarevic, G. J. Milburn, and Ross H. McKenzie. Fast simulation of a quantum phase transition in an ion-trap realizable unitary map. *Phys. Rev. A*, 71(1):012335, 2005.
- [Bra06] D. Braun. Decoherence in a system of many two-level atoms. *Phys. Rev. Lett.*, 96(23):230502, 2006.
- [Bro73] T. A. Brody. *Lett. Nuovo Cimento*, 7:482, 1973.
- [Car35] É. Cartan. Quasi composition algebras. *Abh. Math. Sem. Hamburg*, 11:116, 1935.
- [CDPZ03] F. M. Cucchietti, D. A. R. Dalvit, J. P. Paz, and W. H. Zurek. Decoherence and the Loschmidt Echo. *Phys. Rev. Lett.*, 91(21):210403, 2003.
- [CdRF⁺05] C. W. Chou, H. de Riedmatten, D. Felinto, S. V. Polyakov, S. J. van Enk, and H. J. Kimble. Measurement-induced entanglement for excitation stored in remote atomic ensembles. *Nature*, 438:828–832, Dec 2005.
- [CGVG80] G. Casati, I. Guarneri, and F. Valz-Gris. On the connection between quantization of nonintegrable systems and statistical theory of spectra. *Lett. Nuovo Cimento Soc. Ital. Fis.*, 28:279, 1980.
- [CL83] A. O. Caldeira and A. J. Leggett. Path integral approach to quantum Brownian motion. *Physica A*, 121:587–616, September 1983.
- [CMJ⁺05] T. Chaneliere, D. N. Matsukevich, S. D. Jenkins, S. Y. Lan, T. A. B. Kennedy, and A. Kuzmich. Storage and retrieval of single photons transmitted between remote quantum memories. *Nature*, 438:833–836, Dec 2005.
- [CPW02] F. M. Cucchietti, H. M. Pastawski, and D. A. Wisniacki. Decoherence as decay of the Loschmidt echo in a Lorentz gas. *Phys. Rev. E*, 65(4):045206, 2002.
- [CPŽ05] G. L. Celardo, C. Pineda, and M. Žnidarič. Stability of quantum Fourier transformation on Ising quantum computer. *Int. J. Quantum Inf.*, 3(3):441, 2005, quant-ph/0310163.
- [DDG⁺03] C. Dembowski, B. Dietz, H.-D. Gräf, A. Heine, F. Leyvraz, M. Miski-Oglu, A. Richter, and T. H. Seligman. Phase Shift Experiments Identifying Kramers Doublets in a Chaotic Superconducting Microwave Billiard of Threefold Sym-

- metry. *Phys. Rev. Lett.*, 90(1):014102–+, January 2003, arXiv:nlin/0211033.
- [DDZ00] D. A. R. Dalvit, J. Dziarmaga, and W. H. Zurek. Decoherence in bose-einstein condensates: Towards bigger and better schrödinger cats. *Phys. Rev. A*, 62(1):013607, Jun 2000.
- [DRS91] F.-M. Dittes, I. Rotter, and T. H. Seligman. Chaotic behaviour of scattering induced by strong external coupling. *Phys. Lett. A*, 158:14–18, August 1991.
- [dSDS03a] R. de Sousa and S. Das Sarma. Electron spin coherence in semiconductors: considerations for a spin-based solid-state quantum computer architecture. *Phys. Rev. B*, 67(3):033301, Jan 2003.
- [dSDS03b] R. de Sousa and S. Das Sarma. Theory of nuclear-induced spectral diffusion: Spin decoherence of phosphorus donors in si and gaas quantum dots. *Phys. Rev. B*, 68(11):115322, Sep 2003.
- [Dys62] F. J. Dyson. A Brownian-motion model for the eigenvalues of a random matrix. *J. Math. Phys.*, 3(6):1191–1198, November/December 1962.
- [EAM⁺05] M. D. Eisaman, A. Andre, F. Massou, M. Fleischhauer, A. S. Zibrov, and M. D. Lukin. Electromagnetically induced transparency with tunable single-photon pulses. *Nature*, 438:837–841, Dec 2005.
- [ELPC04] J. Emerson, S. Lloyd, D. Poulin, and D. Cory. Estimation of the local density of states on a quantum computer. *Phys. Rev. A*, 69(5):050305, 2004.
- [Eve57] H. Everett. “Relative State” formulation of quantum mechanics. *Rev. Mod. Phys.*, 29(3):454–462, Jul 1957.
- [EWS⁺03] J. Emerson, Y. S. Weinstein, M. Saraceno, S. Lloyd, and D. G. Cory. Pseudo-Random Unitary Operators for Quantum Information Processing. *Science*, 302(5653):2098–2100, 2003.
- [FFP04] L. Fedichkin, A. Fedorov, and V. Privman. Additivity of decoherence measures for multiqubit quantum systems. *Phys. Lett. A*, 328:87–93, Jul 2004.
- [FFS04] K. M. Frahm, R. Fleckinger, and D. L. Shepelyansky. Quantum chaos and random matrix theory for fidelity decay

- in quantum computations with static imperfections. *Eur. Phys. J. D*, 29:139–155, 2004, quant-ph/0312120.
- [Ged06] Z. Gedik. Spin bath decoherence of quantum entanglement. *Solid State Commun.*, 138:82, 2006.
- [GKP⁺06] T. Gorin, H. Kohler, T. Prosen, T. H. Seligman, H.-J. Stöckmann, and M. Žnidarič. Anomalous slow fidelity decay for symmetry-breaking perturbations. *Phys. Rev. Lett.*, 96(24):244105, 2006.
- [GLM04] V. Giovannetti, S. Lloyd, and L. Maccone. Quantum-Enhanced Measurements: Beating the Standard Quantum Limit. *Science*, 306(5700):1330–1336, 2004.
- [GLM06] V. Giovannetti, S. Lloyd, and L. Maccone. Quantum metrology. *Phys. Rev. Lett.*, 96(1):010401, 2006.
- [GMCMB07] I. Garcia-Mata, A. R. R. Carvalho, F. Mintert, and A. Buchleitner. Entanglement screening by nonlinear resonances. *Phys. Rev. Lett.*, 98(12):120504, 2007.
- [GMGW98] T. Guhr, A. Müller-Groeling, and H. A. Weidenmüller. Random matrix theories in quantum physics: Common concepts. *Phys. Rep.*, 299(4):189–425, June 1998, cond-mat/9707301.
- [GPS04] T. Gorin, T. Prosen, and T. H. Seligman. A random matrix formulation of fidelity decay. *New J. Phys.*, 6:20, 2004.
- [GPS07] T. Gorin, C. Pineda, and T. H. Seligman. Decoherence of an n -qubit quantum memory. 2007, quant-ph/0703190. Accepted in *Phys. Rev. Lett.*
- [GPSS04] T. Gorin, T. Prosen, T. H. Seligman, and W. T. Strunz. Connection between decoherence and fidelity decay in echo dynamics. *Phys. Rev. A*, 70(4):042105, 2004.
- [GPSŽ06] T. Gorin, T. Prosen, T. H. Seligman, and M. Žnidarič. Dynamics of Loschmidt echoes and fidelity decay. *Phys. Rep.*, 435:33, 2006, quant-ph/0607050.
- [GS02] T. Gorin and T. H. Seligman. A random matrix approach to decoherence. *J. Opt. B*, 4(4):S386, 2002.
- [GS03] T. Gorin and T. H. Seligman. Decoherence in chaotic and integrable systems: a random matrix approach. *Phys. Lett.*

- A*, 309:61–67, Mar 2003.
- [GSW06] T. Gorin, T. H. Seligman, and R. L. Weaver. Scattering fidelity in elastodynamics. *Phys. Rev. E*, 73(1):015202(R), 2006.
- [Haa01] F. Haake. *Quantum Signatures of Chaos, II ed.* Springer, Berlin, 2001.
- [HHR⁺05] H. Häffner, W. Hänsel, C. F. Roos, J. Benhelm, D. Chekalkar, M. Chwalla, T. Körber, U. D. Rapol, M. Riebe, P. O. Schmidt, C. Becher, O. Gühne, W. Dür, and R. Blatt. Scalable multiparticle entanglement of trapped ions. *Nature*, 438:643, December 2005, quant-ph/0603217.
- [HSKH⁺05] H. Häffner, F. Schmidt-Kaler, W. Hänsel, C. F. Roos, T. Körber, M. Chwalla, M. Riebe, J. Benhelm, U. D. Rapol, C. Becher, and R. Blatt. Robust entanglement. *Applied Physics B: Lasers and Optics*, 81:151, Jul 2005.
- [HW97] S. Hill and W. K. Wootters. Entanglement of a pair of quantum bits. *Phys. Rev. Lett.*, 78(26):5022, 1997.
- [JL03] R. Jozsa and N. Linden. On the role of entanglement in quantum computational speed-up. *Proc. R. Soc. London, Ser. A*, 459:2011–2032, June 2003.
- [JPA] *J. Phys A* 36 No. 12 (2003).
- [JSC⁺04] B. Julsgaard, J. Sherson, J. I. Cirac, J. Fiurasek, and E. S. Polzik. Experimental demonstration of quantum memory for light. *Nature*, 432:482–486, Nov 2004.
- [KA06] O. Kern and G. Alber. Selective recoupling and stochastic dynamical decoupling. *Phys. Rev. A*, 73(6):062302, 2006.
- [KAS05] O. Kern, G. Alber, and D. L. Shepelyansky. Quantum error correction of coherent errors by randomization. *The European Physical Journal D - Atomic, Molecular, Optical and Plasma Physics*, 32:153–156, Jan 2005. 10.1140/epjd/e2004-00196-9.
- [KD98] A. Krämer and S. Doniach. Superinsulator phase of two-dimensional superconductors. *Phys. Rev. Lett.*, 81(16):3523–3526, Oct 1998.
- [Key02] M. Keyl. Fundamentals of quantum information theory. *Phys. Rev.*, 369:431–548, Oct 2002.
- [KJZ02] Z. P. Karkuszewski, C. Jarzynski, and W. H. Zurek. Quan-

- tum chaotic environments, the butterfly effect, and decoherence. *Phys. Rev. Lett.*, 89(17):170405, Oct 2002.
- [KS04] H. G. Krojanski and D. Suter. Scaling of decoherence in wide nmr quantum registers. *Phys. Rev. Lett.*, 93(9):090501, 2004.
- [KS06] H. G. Krojanski and D. Suter. Decoherence in large nmr quantum registers. *Phys. Rev. A*, 74(6):062319, 2006.
- [LDK⁺05] J. Lages, V. V. Dobrovitski, M. I. Katsnelson, H. A. De Raedt, and B. N. Harmon. Decoherence by a chaotic many-spin bath. *Phys. Rev. E*, 72(2):026225, 2005.
- [LKA⁺04] J. Lee, I. Kim, D. Ahn, H. McAneney, and M. S. Kim. Completely positive non-markovian decoherence. *Phys. Rev. A*, 70(2):024301, 2004.
- [LS05] A. Lakshminarayan and V. Subrahmanyam. Multipartite entanglement in a one-dimensional time-dependent ising model. *Phys. Rev. A*, 71(6):062334, 2005.
- [MCKB05] F. Mintert, A. R. R. Carvalho, M. Kuś, and Andres. Buchleitner. Measures and dynamics of entangled states. *Phys. Rep.*, 415(4):207, 2005.
- [Meh91] M. L. Mehta. *Random Matrices*. Academic Press, San Diego, California, second edition, 1991.
- [Mel95] P. A. Mello. Theory of random matrices: spectral statistics and scattering problems in mesoscopic quantum physics. In E. Akkermans, G. Montambaux, and J.-L. Pichard, editors, *Mesoscopic Quantum Physics*. Elsevier Science B.V., Amsterdam, 1995. Proceedings of the Les Houches Summer School, Session LXI.
- [MJWK01] W. J. Munro, D. F. V. James, A. G. White, and P. G. Kwiat. Maximizing the entanglement of two mixed qubits. *Phys. Rev. A*, 64(3):030302, 2001.
- [MPK88] P. A. Mello, P. Pereyra, and N. Kumar. A soluble random-matrix model for relaxation in quantum systems. *J. Stat. Phys.*, 51:77–94, Apr 1988. 10.1007/BF01015321.
- [NC00] M. A. Nielsen and I. L. Chuang. *Quantum Computation and Quantum Information*. Cambridge University Press, Cambridge, U.K., 2000.

- [PF02] T. B. Pittman and J. D. Franson. Cyclical quantum memory for photonic qubits. *Phys. Rev. A*, 66(6):062302, Dec 2002.
- [PFL⁺04] A. Poppe, A. Fedrizzi, T. Loruenser, O. Maurhardt, R. Ursin, H. R. Boehm, M. Peev, M. Suda, C. Kurtsiefer, H. Weinfurter, T. Jennewein, and A. Zeilinger. Practical Quantum Key Distribution with Polarization-Entangled Photons. *Optics Express*, 12(16):3865–3871, 2004, quant-ph/0404115.
- [PGS07] C. Pineda, T. Gorin, and T. H. Seligman. Decoherence of two-qubit systems: a random matrix description. *New J. Phys.*, 9(4):106, April 2007, quant-ph/0702161.
- [PP07] C. Pineda and T. Prosen. Non-universal level statistics in a chaotic quantum spin chain. February 2007, quant-ph/0702164. Accepted in *Phys. Rev. E*.
- [Pro00] T. Prosen. Exact time-correlation functions of quantum ising chain in a kicking transversal magnetic field. *Prog. Theor. Phys. Suppl.*, 139:191–203, 2000.
- [Pro02] T. Prosen. General relation between quantum ergodicity and fidelity of quantum dynamics. *Phys. Rev. E*, 65(3):036208, 2002.
- [PS02] T. Prosen and T. H. Seligman. Decoherence of spin echoes. *J. Phys. A*, 35(22):4707, 2002.
- [PS06] C. Pineda and T. H. Seligman. Evolution of pairwise entanglement in a coupled n -body system. *Phys. Rev. A*, 73(1):012305, 2006.
- [PS07] C. Pineda and T. H. Seligman. Bell pair in a generic random matrix environment. *Phys. Rev. A*, 75(1):012106, 2007.
- [PSPS06] C. Pineda, R. Schäfer, T. Prosen, and T. H. Seligman. Verification of generic fidelity recovery in a dynamical system. *Phys. Rev. E*, 73(6):066120, 2006.
- [PSW01] T. Prosen, T. H. Seligman, and H. A. Weidenmüller. Random matrix ensembles for semi-separable systems. *Europhys. Lett.*, 55(1):12–18, 2001.
- [PSŽ03] T. Prosen, T. H. Seligman, and M. Žnidarič. Estimation of purity in terms of correlation functions. *Phys. Rev. A*, 67(6):062108, 2003.

- [PV07] M. B. Plenio and S. Virmani. An introduction to entanglement measures. *Quant. Inf. Comp.*, 7:1, 2007.
- [PZ01] T. Prosen and M. Žnidarič. Can quantum chaos enhance the stability of quantum computation? *J. Phys. A*, 34(47):L681–L687, 2001.
- [PŽ02] T. Prosen and Marko Žnidarič. Stability of quantum motion and correlation decay. *J. Phys. A*, 35(6):1455, 2002.
- [Sak94] J. J. Sakurai. *Modern Quantum Mechanics*. Addison-Wesley Publishing Company, Reading, MA, Revised edition, 1994.
- [SAOO95] Paul So, Steven M. Anlage, Edward Ott, and Robert N. Oerter. Wave chaos experiments with and without time reversal symmetry: Gue and goe statistics. *Phys. Rev. Lett.*, 74(14):2662–2665, Apr 1995.
- [Sch07] Erhard Schmidt. Zur theorie der linearen und nichtlinearen integralgleichungen. *Math. Ann.*, 63:433–476, Dec 1907. 10.1007/BF01449770.
- [SGSS05] R. Schäfer, T. Gorin, T. H. Seligman, and H.-J. Stöckmann. Fidelity amplitude of the scattering matrix in microwave cavities. *New J. Phys.*, 7:152, 2005.
- [Sha48] C. E. Shannon. A mathematical theory of communication. *The Bell System Technical Journal*, 27:379–423, 623–656, july, october 1948.
- [SKK⁺00] C. A. Sackett, D. Kielpinski, B. E. King, C. Langer, V. Meyer, C. J. Myatt, M. Rowe, Q. A. Turchette, W. M. Itano, D. J. Wineland, and C. Monroe. Experimental entanglement of four particles. *Nature*, 404:256, Mar 2000.
- [SLH⁺04] R. W. Simmonds, K. M. Lang, D. A. Hite, S. Nam, D. P. Pappas, and J. M. Martinis. Decoherence in Josephson phase qubits from junction resonators. *Phys. Rev. Lett.*, 93(7):077003, 2004.
- [SS05] H.-J. Stöckmann and R. Schäfer. Fidelity recovery in chaotic systems and the Debye-Waller factor. *Phys. Rev. Lett.*, 94(24):244101, June 2005.
- [SSGS05] R. Schäfer, H.-J. Stöckmann, T. Gorin, and T. H. Seligman. Experimental verification of fidelity decay: From perturbative to Fermi golden rule regime. *Phys. Rev. Lett.*,

- 95(18):184102, 2005.
- [ste] S. Mossmann, private communication, 2007.
- [VADM01] F. Verstraete, K. Audenaert, J. Dehaene, and B. De Moor. A comparison of the entanglement measures negativity and concurrence. *J. Phys. A*, 34(47):10327–10332, 2001.
- [vN55] J. von Neumann. *Mathematical Foundations of Quantum Mechanics*. Princeton University Press, 1955.
- [WFL02] T. J. Walls, T. V. Filippov, and K. K. Likharev. Quantum fluctuations in Josephson junction comparators. *Phys. Rev. Lett.*, 89(21):217004, Nov 2002.
- [Wig51] E. P. Wigner. On a class of analytic functions from the quantum theory of collisions. *Ann. Math.*, 53:36, 1951.
- [Wig55] E. P. Wigner. Characteristic vectors of bordered matrices with infinite dimensions. *Ann. Math.*, 62:548, 1955.
- [Wis28] J. Wishart. The generalized product moment distribution in samples from a normal multivariate population. *Biometrika*, A20:32–52, 1928.
- [WNG⁺03] T.-C. Wei, K. Nemoto, P. M. Goldbart, P. G. Kwiat, W. J. Munro, and F. Verstraete. Maximal entanglement versus entropy for mixed quantum states. *Phys. Rev. A*, 67(2):022110, 2003.
- [YE02] T. Yu and J. H. Eberly. Phonon decoherence of quantum entanglement: Robust and fragile states. *Phys. Rev. B*, 66(19):193306, 2002.
- [YE03] T. Yu and J. H. Eberly. Qubit disentanglement and decoherence via dephasing. *Phys. Rev. B*, 68(16):165322, Oct 2003.
- [YE04] T. Yu and J. H. Eberly. Finite-time disentanglement via spontaneous emission. *Phys. Rev. Lett.*, 93(14):140404, 2004.
- [ZB05] M. Ziman and V. Buzek. Concurrence versus purity: Influence of local channels on bell states of two qubits. *Phys. Rev. A*, 72(5):052325, 2005.
- [ZCP⁺07] A. Zazunov, M. Creux, E. Paladino, A. Crepieux, and T. Martin. Detection of finite frequency current moments with a dissipative resonant circuit. 2007, cond-mat/0702247.

- [ZCZ⁺04] Z. Zhao, Y.-A. Chen, A.-N. Zhang, T. Yang, H. J. Briegel, and J.-W. Pan. Experimental demonstration of five-photon entanglement and open-destination teleportation. *Nature*, 430:54, Jul 2004.
- [Zur91] W.H. Zurek. Decoherence and the transition from quantum to classical. *Phys. Today*, 44(10):36, 1991, quant-ph/0306072.
- [Zur03] W. H. Zurek. Decoherence, einselection, and the quantum origins of the classical. *Rev. Mod. Phys.*, 75(3):715, May 2003.